

Review

A Review of Rheological Modeling of Cement Slurry in Oil Well Applications

Chengcheng Tao, Barbara G. Kutchko, Eilis Rosenbaum and Mehrdad Massoudi * 

U.S. Department of Energy, National Energy Technology Laboratory (NETL), Pittsburgh, PA 15236, USA; Chengcheng.Tao@netl.doe.gov (C.T.); Barbara.Kutchko@netl.doe.gov (B.G.K.); Eilis.Rosenbaum@netl.doe.gov (E.R.)

* Correspondence: Mehrdad.Massoudi@netl.doe.gov; Tel.: +1-412-386-4975

Received: 25 November 2019; Accepted: 21 January 2020; Published: 24 January 2020



Abstract: The rheological behavior of cement slurries is important in trying to prevent and eliminate gas-migration related problems in oil well applications. In this paper, we review the constitutive modeling of cement slurries/pastes. Cement slurries, in general, behave as complex non-linear fluids with the possibility of exhibiting viscoelasticity, thixotropy, yield stress, shear-thinning effects, etc. The shear viscosity and the yield stress are two of the most important rheological characteristics of cement; these have been studied extensively and a review of these studies is provided in this paper. We discuss the importance of changing the concentration of cement particles, water-to-cement ratio, additives/admixtures, shear rate, temperature and pressure, mixing methods, and the thixotropic behavior of cement on the stress tensor. In the concluding remarks, we propose a new constitutive model for cement slurry, considering the basic non-Newtonian nature of the different models.

Keywords: cement slurries; non-Newtonian fluids; rheology; constitutive relations; viscosity; yield stress; thixotropy

1. Introduction

In oil well cementing applications, cement slurries are placed in the annulus space between the well casing and the geological formations surrounding the wellbore; this is done primarily to provide zonal isolation from the surrounding fluid flow and to prevent the corrosion to the casing for the life of the well [1,2]. Figure 1 shows a typical schematic of an oil well cementing operation. The space must be filled before the cement begins to harden [3]. Failure of the zonal isolation and flow of the formation fluids penetrating the cement can cause disasters, financial loss, and other serious consequences. Thus, understanding the behavior of the cement is one of the key factors in designing a gas resistant cement column [4]. Cement, in general, is mixed on the rig before being pumped into the well [5]. Gas migration caused by the fluid flow in the wellbore requires expensive remedial techniques [6,7]. Studying rheological properties of cement slurry plays an important role in understanding the factors that can prevent or eliminate the gas migration. In the early stages of cement hydration, cement changes from a fluid to a solid-like material and develops compressible strength. Gelation during the cementing process is the buildup of the gel strength, or the premature increase in the cement viscosity. Early gelation is a serious problem in petroleum industry, but it is desired that the cement gel quickly once placed [8]. Static gel strength (SGS) [9] is the yield point showing the phase change; this is related to the safety of cement jobs and the gas migration problem [10].

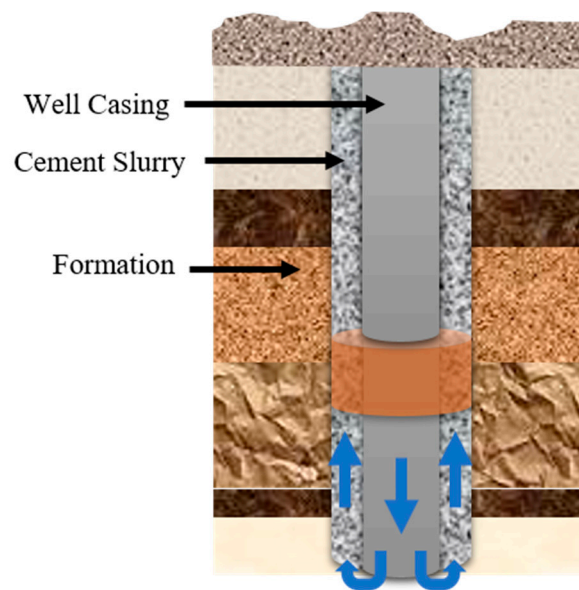


Figure 1. Schematic of an oil well cementing operation [11].

According to the U.S. Department of Transportation, Type I/II ordinary Portland cement provides adequate strength and durability for common applications [12]. However, more specific performance criteria are required for cementing around the steel casing of gas and oil wells. Wells with an average depth of up to 8000 feet below the mud line [13] can require handling cement slurries under high temperature and high pressure conditions (200 °C and 150 MPa in deep wells) [14]. For oil and gas wells, cement should not set too early so that it can be pumped during the placement and the setting time should not be too long once placed to prevent fluids from penetrating the cement barrier. Cement requires a high level of consistency, related to the minimum quantity of water required to initiate the chemical reactions between water and cement. The API Class G and H cements are two common forms of cements used today [15]. Cements ground too fine (Blaine fineness > 9000 cm²/gm) are not suitable for oil well cementing because of insufficient compressive strength to hold the casing and inadequate sulphate resistance. However, the microfine cements are good for oil well repairing of small cracks [16].

In cementing operations, different cement slurries including “lead” slurries at the upper section and “tail” slurries at the lower section are pumped into the wellbore, as shown in Figure 2. The tail slurries, under higher pressures and temperatures, usually have higher density and higher strength than the lead slurries and are pumped after the lead slurries [17]. Portland cement is widely used in the oil well and construction industries because of its flexibility and widespread availability of its constituent materials [18]. It is produced from the grinding of clinker, which is produced by the calcination of limestone and other raw materials in a cement rotary kiln. After the cement is mixed with water, a series of exothermal chemical reactions occur which results in strength development and cement hardening. Cement slurries are reactive systems, changing continuously chemically and physically [19].

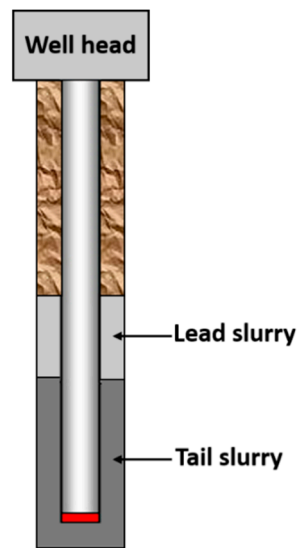


Figure 2. Different types of cement slurry in an oil well.

The first few hours (after mixing the cement and water) is a dormant period for the reactions. The slurry is in a fresh state, after which the setting is initiated, and the cement begins to harden. The fresh cement slurry should be pumpable into the wellbore, where it would harden soon after placement [20]. The design of the cementing operation requires a comprehensive understanding of the mechanical and rheological behavior of cement slurries [21]. Flowability and stability of cement slurries are two important factors for successful oil well cementing [22]. Retarders are usually applied to control the duration of the fresh state, providing a safety time for the pumping operations. Many researchers have put considerable effort to understand the mechanisms for fluid migration during cementing, using experimental and computational models. To monitor the conditions of cement slurry in real-time, wireless sensor network-based monitoring systems can be used [23–26]. In many cases, computational fluid dynamics (CFD) applications can also be used (see Appendix C). Table 1 shows the general cement properties.

Table 1. Cement properties [27–29].

Cement Properties	Value
Cement Powder Density	3.15 g/cm ³
Cement Slurry Density	1.38 g/cm ³ –2.28 g/cm ³
Cement Particle Size	0.1 to 100 μm
Compressive Strength	20–40 Mpa
Maximum Solid Concentration Packing	0.65 (spherical particles)
β in the Krieger and Dougherty's relation	1.5–2
Viscosity of the Continuous Phase (Base Fluid)	1 cP for water at 20 °C
Reynolds Number	2716–3971

The objective of this paper is to review the existing constitutive equations for cement slurries, used in oil well applications; specifically, we look at the relationships suggested for the yield stress and the viscosity of the cement as functions of parameters such as: volume fraction, cement surface, shear rate, cement chemistry, mineralogical composition, concentration of additives, temperature and pressure variations, mixing conditions, etc. In the next sections, we review different constitutive models for cement slurries. In Appendix A, a discussion of the chemistry of cement is provided. In Appendix B, we present the governing equations for a single phase approach and the multi-phase approach to the flow of cement slurry. In Appendix C, we provide a short review of the various CFD studies related to cement slurries.

2. Constitutive Modeling of Cement Slurries

Constitutive modeling and mathematical modeling of cement present challenging opportunities in research. Beginning as a (1) powder, (2) becoming a paste (when mixed with water), (3) flowing as a slurry (suspension), and then (4) hardening to become a solid-like material, cement can be modeled and studied as (1) granular materials (powder), (2) visco-plastic fluids with a yield stress (paste), (3) viscoelastic (non-Newtonian fluids, slurry), and (4) a poro-elastic solid. Cement as a paste or as a suspension, can be modeled mathematically using different approaches. For example, it can be considered as a multi-component material composed of water and cement particles, and other additives or it can be considered as a non-homogeneous (single component) fluid that behaves in a non-linear fashion. In this review report, we are basically interested in the latter approach. As such, the cement paste or cement slurry behave as complex fluids exhibiting certain non-linear characteristics such as thixotropy, viscoelasticity, yield stress, presence of normal stress effects, shear-rate dependent viscosity, etc., (see [30–33]).

Fresh cement paste/slurries are suspensions with a high concentration of particles. The size of cement particles is between 0.1 μm and 100 μm . Cement, in general, behaves as a thixotropic material with a yield stress; after the hydration process, it begins to behave as a solid-like material [34]. The rheological studies of cement reveal various phenomena [2]: (1) Rapid formation of gel at rest; (2) failure of gel under a critical value of stress, which is dependent on the interparticle forces; (3) destruction of gel at some shear rate, resulting in a shear-thinning behavior; (4) reconstructions at higher shear rates and jamming, etc.

In the petroleum industry, we need to know the rheological properties of cement in order to evaluate the displacement and the flow rates for optimal mud removal and cement placement before setting [2]. The cement and concrete industries prefer high performance cement with high impermeability, high density, and high strength for structures, which are related to the cement composites [35]. The quality of the concrete structure depends on the behavior of fresh cement during its placement into formwork at the jobsite [36]. The sustained-casing-pressure (SCP) tests in the drilling industry test the solid cement after hydration though gas migration occurs in cement slurries and mud. In general, non-Newtonian fluids models should be taken into consideration when studying cement slurries and muds. Yield stress effects and thixotropy should also be taken into consideration in these studies.

Some of the basic issues in studying cement rheology are (1) lack of reliable experimental data along with inaccurate experimental procedures and difficulties to reproduce the measurements; (2) complex flow behavior of cement affected by various physical and chemical factors; (3) complex cement hydration and setting process. If cement behaves as a viscoplastic fluid, then the yield stress and the plastic viscosity also need to be measured and studied [37]. These properties can depend on different factors [35,38–40] such as:

1. *Physical factors*, such as water-to-cement ratio, geometry of the cement grain (specific surface of cement particles) [38];
2. *Chemical and mineralogical factors*, such as the cement type, its chemical composition, additive types, cement particle concentration in the mix, structural modifications after hydration [41];
3. *Mixing conditions*, such as the type of blender/grinding condition, hydration time, storage/transport condition, curing temperature, stirrer rate, and time [38];
4. *Measurement conditions* (experimental equipment and procedures).

For oil well applications, these properties can also depend on temperature, water-to-cement ratio, and the type of additives used.

The basic governing equations for flow of cement are given in Appendix B. For a purely mechanical case, i.e., where thermo-chemical and electro-magnetic effects are ignored, the constitutive parameter of interest is the stress tensor T . In a sense, we think the rheological response of the cement can be described through constitutive modeling of the stress tensor. As we will discuss, it is well-known that cement, in general, exhibits visco-elastic behavior, along with a yield stress. Some researchers focus on

the modeling of the yield stress, T_y , and some on the viscous stress, T_v , and some on the total stress, T . In general, we can assume

$$T = T_v + T_y \quad (1)$$

In the remainder of this report, we provide reviews related to these three approaches.

The shear viscosity, in general, can be measured using a coaxial cylinder viscometer. Based on the shear rate vs. shear stress curves, it can be seen that cement paste exhibits both thixotropic and rheopectic behavior at different times [35,39,42,43]. The experimental procedure, sometimes, can affect these measurements. For example, an apparent wall slip or sedimentation of some particles in the coaxial viscometers could cause error. The Bingham plastic model and the power-law models are the two most commonly used models for cement slurries. In this section, we review some of the mathematical models used for cement slurries.

2.1. Models for the Total Stress Tensor T

The Bingham fluid model [44] is widely used to describe the relationship between the shear stress and the shear rate for cement slurries at low shear rates. It also is one of the simplest models to describe the visco-plastic nature of some non-Newtonian fluids, where

$$\tau = \tau_y + \eta_p \dot{\gamma} \quad (2)$$

where τ is the shear stress, τ_y is the constant yield stress, η_p is the plastic viscosity, and $\dot{\gamma}$ is the shear rate. The *total* viscosity of the material can be defined as:

$$\eta = \frac{\tau}{\dot{\gamma}} = \eta_p + \frac{\tau_y}{\dot{\gamma}} \quad (3)$$

The (one-dimensional) model given in Equation (2) indicates a linear relationship after the initial yield stress is reached. However, this is not an accurate model for the non-linear behavior of many of the cement slurries [45]; in some cases, there is no clear relationship between the shear rate and the volumetric flow rate inside the pipe or annulus [46].

The three-dimensional tensorial form of the Bingham model is given by in the books, for example, Macosko [47] (p. 93), Lootens et al. [48] for cement:

$$T = \left[\tau_y / \left(\frac{1}{2} D : D \right)^{1/2} + \eta_p \right] D \quad (4)$$

where T is the total stress tensor, $D = \dot{\gamma}$ is the symmetric part of the velocity gradient, τ_y is the yield stress, and η_p is the plastic viscosity, and where “:” indicates the inner (scalar) product of two tensors, $\dot{\gamma} = (2D_{ij}D_{ij})^{1/2} = (\Pi)^2$, $D = \frac{1}{2}(L + L^T)$, $L = \text{grad}v$, $\Pi = 2\text{tr}D^2$. Later, we will also use the following notation: $A_1 = 2D$. Oldroyd (1947) derived a proper (frame invariant) 3-D form for the Bingham fluid by assuming that the material behaves as a linear elastic solid below the yield stress; he used the von Mises criterion for the yield surface. Thus

$$T = \begin{cases} \left[\eta_p + \frac{\tau_y}{\sqrt{\frac{1}{2}\Pi A_1}} \right] A_1 & \text{when } \left[\frac{1}{2} T : T \right] \geq \tau_y^2 \\ T = GE & \text{when } \left[\frac{1}{2} T : T \right] < \tau_y^2 \end{cases} \quad (5)$$

where G is the shear modulus, indicating that below the yield stress, the material behaves as a linear elastic solid, obeying the Hooke's Law, and where

$$\begin{aligned} \Pi_{A_1} &\equiv A_1 : A_1 \\ A_1 &= \text{grad } \mathbf{v} + (\text{grad } \mathbf{v})^T \\ \mathbf{E} &: \text{strain tensor} \end{aligned} \quad (6)$$

As Denn [49] indicates, if the material is assumed to be inelastic prior to yielding, then $G \rightarrow \infty$, and Equation (5) is replaced by

$$A_1 = 0 \quad \left[\frac{1}{2} \mathbf{T} : \mathbf{T} \right] < \tau_y^2 \quad (7)$$

Macosko [31] (p. 96) mentions that for many fluids with a yield stress, there is a lower *Newtonian* regime rather than a *Hookean* one, and thus one can use a two-viscosity (bi-viscous) model, such as

$$\mathbf{T} = 2 \begin{cases} \eta_p \mathbf{D} & \text{for } \Pi_{2D}^{1/2} \leq \dot{\gamma}_c \\ \left[\frac{\tau_y}{\Pi_{2D}^{1/2}} + K |\Pi_{2D}|^{\frac{n-1}{2}} \right] \mathbf{D} & \text{for } \Pi_{2D}^{1/2} > \dot{\gamma}_c \end{cases} \quad (8)$$

where K is the consistency factor and n is the power-law exponent; when $n = 1$, the fluid is Newtonian; when $n > 1$, the fluid is shear-thickening, and when $n < 1$, the fluid is shear-thinning. In this formulation, one uses a critical shear rate instead of a yield criterion and this makes the numerical solution easier. For additional and interesting applications of the flow of a Bingham-type fluid, see White [50], and Lipscomb and Denn [51]. Mendes and Dutra [52] provide further insight into the viscosity of a shear-thinning (yield stress) fluids.

Herschel and Bulkley [53] generalized the Bingham model by introducing a three-parameter model where:

$$\tau = \tau_y + K \dot{\gamma}^n \quad (9)$$

where τ_y , K , and n are constants. According to Banfill [3], K could be chosen as 2.5 or 0.25 and n as 0.75 or 1.25 for cement. Jones and Taylor [54] and Atzeni [45] have used this model to study cement. This model has been found to describe the rheological behavior for the sealing cement slurries used in drilling technologies [55].

The power-law model, also known as the Ostwald-de Waele model [56] is one of the most popular models in describing the pseudoplastic fluids without yield stress. Here,

$$\tau = K \dot{\gamma}^n \quad (10)$$

where K is the consistency factor, n is the flow behavior index (the power-law exponent), measuring the degree of non-Newtonian behavior, and $\dot{\gamma}$ is the shear rate.

Williamson's model [57] was used by Lapasin [58] to describe the fresh cement pastes, where

$$\tau = \eta_\infty \dot{\gamma} + \tau_y \frac{\dot{\gamma}}{\dot{\gamma} + \Gamma} \quad (11)$$

where η_∞ is the viscosity at infinite shear rate and Γ is a parameter indicating the deviation from the Bingham behavior.

The Eyring model [59] was applied to Portland cement pastes by Atzeni et al. [45]; this is suitable for suspensions with dispersed particles:

$$\tau = \sum_{i=1}^n a_i \sinh^{-1}(\dot{\gamma} b_i) \quad (12)$$

where a_i and b_i are constants, and n is the number of flow units. For the simplest case $n = 2$, where there is one Newtonian fluid and one non-Newtonian fluid. This model does not have a yield stress component and is more suitable for non-Newtonian behavior at high shear rates.

Sisko's model [60], applied by Papo [61] to cement pastes, does not include a yield stress term:

$$\tau = a\dot{\gamma} + b\dot{\gamma}^c \quad (13)$$

where a is related to the infinite shear rate viscosity η_∞ , and b and c are adjustable parameters with $c < 1$.

The Casson equation [62], applied to cement pastes by Atzeni et al. [45] is given by:

$$\sqrt{\tau} = \sqrt{\tau_y} + \sqrt{\eta_p \dot{\gamma}} \quad (14)$$

where the yield stress τ_y is constant and η_p is the plastic viscosity. According to Kok and Karakaya [63], the Casson model is considered to be one of the most accurate and useful models describing the rheological properties of cement slurries.

Shangraw–Grim–Mattocks model [64] was used by Papo (1988) to study cement, with a constant yield stress:

$$\tau = \tau_y + \eta_\infty \dot{\gamma} + \alpha_1 [1 - \exp(-\alpha_2 \dot{\gamma})] \quad (15)$$

where η_∞ is the viscosity at infinite shear rate, α_1 and α_2 are adjustable parameters.

The Ellis's model (1965), applied to cement by Atzeni et al. [45] is given by:

$$\dot{\gamma} = a\tau + b\tau^c \quad (16)$$

where a is a function of the initial viscosity η_0 , b is related to the shear stress τ , and c is a constant with the value 2.

Robertson and Stiff [46] proposed a three-parameter model for a yield-pseudoplastic fluid where:

$$\tau = a(\dot{\gamma} + b)^c \quad (17)$$

where a , b , and c are constants. The values for these constants, suggested by Banfill [3] are: 20, 1.5, and 0.35. By adjusting these three parameters, the model can predict the behavior of Newtonian fluids, the Bingham plastic, and the power-law models. However, Beirute and Flumerfelt [65] indicated that the Robertson–Stiff model is not able to describe the yield stress and is limited to the fluids with no yield stress.

According to Batra and Parthasarathy [66], the Robertson–Stiff fluid model can be rewritten as

$$\dot{\gamma}_{ij} = \frac{2A^{1/n} \Pi_T^{1/2}}{\Pi_T^{1/2n} - \tau_y^{1/n}} e_{ij} \quad (18)$$

where $\dot{\gamma}_{ij}$ and e_{ij} are the shear rate and the strain rate tensors, respectively, A and n are constants, Π_T is the second invariant of the stress tensor and τ_y is the yield stress. The equation is satisfied when $\sqrt{\Pi_T} \geq \tau_y$.

The Vom Berg model [67] is given by

$$\tau = \tau_y + a \sin h^{-1}(b\dot{\gamma}) \quad (19)$$

where a and b are constants, and for cement, their values were given to be 26.5 and 0.1, respectively (see Banfill [3]). The model considers yield stress, τ_y , explicitly, describing the flow behavior of cement at shear rates up to 380 s^{-1} , and it also describes the yield behavior at zero shear rate. This model seems to be effective in describing shear-dependent behavior of cement pastes [45,58].

Lapasin et al. [68] suggested the following model:

$$\tau = \tau_{\infty} + (\tau_0 - \tau_{\infty}) \exp(-bt_s) \quad (20)$$

where τ is the shear stress at time t , τ_0 and τ_{∞} are the shear stresses at the initial and the equilibrium states, b is the thixotropic exponent and t_s is the shear time. This model neglects the flocculation process. In this model, there is no yield stress.

The initial shear stress is also known as the gel strength at rest, which is a measure of the electrochemical forces within the fluid under static conditions. The relation between the shear stress and the resting time is given by [69]:

$$\tau_0 = \tau_{r0} + ct^m \quad (21)$$

where τ_{r0} is the initial gel strength, t is the resting time, c is the recovery coefficient, m is the gel exponent.

Quemada's model [70] was reviewed by Banfill [3] and applied to cement slurries, where:

$$\tau = \left(\frac{1 + \sqrt{(a\dot{\gamma})}}{b + c\sqrt{(a\dot{\gamma})}} \right)^2 \dot{\gamma} \quad (22)$$

where a , b , and c are material parameters, with the values of 0.14, 10^{-4} , and 0.14 for cement [3]. This model does not include a yield stress term.

Azteni [45] and Banfill [3] applied a modified form of the Casson's model to study cement pastes:

$$\dot{\gamma} = a + b\tau^{1/2} + c\tau \quad (23)$$

where a , b , and c are functions of the viscosity, concentration, and other flow parameters such as the aggregation of solid particles. This model considers interaction forces among the particles; however, it is not accurate when predicting the behavior of suspensions with high particle concentration.

Azteni et al. [45] reviewed the models proposed by Ellis, Casson, Eyring, and Vom Berg for fresh cement pastes and proposed a new model with a constant yield stress, where:

$$\tau = \tau_y + a\dot{\gamma} + \sinh^{-1}(\dot{\gamma}/c) \quad (24)$$

where a and c are the constants.

Lapasin et al. [58] proposed a 6-parameter equation for fresh cement paste by combining the Vom Berg, the Shangraw–Grim–Mattocks, and the Williamson models, where:

$$\tau = \tau_y + \left[A_0 + (A_1 - A_0) \exp\left\{ -\frac{\dot{\gamma}}{a + b\dot{\gamma}} t \right\} \right] \sinh^{-1} \frac{\dot{\gamma}}{c} \quad (25)$$

where the yield stress τ_y is independent of the structural parameter λ , $\eta_0 = A_0/C$ and $\eta_1 = A_1/C$ are the dynamic viscosities at $\dot{\gamma} = 0$ when the structural parameter λ is 0 and 1. Equation (25) was checked and compared with experimental data and it was found to be a reasonable model to describe the behavior of different cements. For the Portland cement PTL 425 with water-to-cement ratio 0.40, the following values are suggested: $\tau_y = 12.1$ Pa, $A_0 = 43.6$ Pa, $A_1 - A_0 = 87.6$ Pa, $a = 2100$, $b = 9.45$, and $c = 56.1$ [58].

Using experimental data, Lapasin et al. [58] proposed an equation describing the effects of specific surface S_{vB} and volume concentration of cement particles ϕ on the dynamic viscosities η_0 and η_1 and the yield stress τ_y :

$$\eta_0 = (1.1 \times 10^{-3} e^{13.2\phi}) S_{vB}^{4.2} \quad (26)$$

$$\eta_1 = (8.6 \times 10^{-5} e^{20.9\phi}) S_{vB}^{6.3} \quad (27)$$

$$\tau_y = (2.1 \times 10^{-3} e^{19.2\phi}) S_{vB}^{2.5} \quad (28)$$

De Kee and Chan Man Fong [71] suggested a three-parameter model for structured fluids such as hydrolyzed polyacrylamide solutions; their model was used by Yahia and Khayat to study cement grout [72]:

$$\tau = \tau_y + \eta_p \dot{\gamma} e^{-a\dot{\gamma}} \quad (29)$$

where η_p is the plastic viscosity, $\dot{\gamma}$ is the shear rate, and a is a time-dependent parameter, with the value 10^{-3} for cement [3]. This model can predict shear-thinning behavior at lower shear rates and shear-thickening behavior at higher shear rates.

Yahia and Khayat [73] suggested a modified Bingham model for cement by adding a second order term:

$$\tau = \tau_y + \eta_p \dot{\gamma} + c \dot{\gamma}^2 \quad (30)$$

where c is a parameter for capturing the second order effects, with the value of -0.0035 for cement [3].

Additionally, Yahia and Khayat [73] developed a new model for cement grouts with pseudoplastic or shear-thinning behavior, by combining the Casson and the De Kee–Chan Man Fong models:

$$\tau = \tau_y + 2(\sqrt{\tau_y \eta_p}) \sqrt{\dot{\gamma} e^{-a\dot{\gamma}}} \quad (31)$$

where a is a time-dependent parameter, which allows for the shear-thinning behavior (positive) or shear-thickening behavior (negative) of the cement grouts, which is equal to 10^{-3} according to Banfill [3].

Vipulanandan et al. [74] proposed a new model for cement slurry:

$$\tau = \tau_y + \frac{\dot{\gamma}}{a + b\dot{\gamma}} \quad (32)$$

where a and b are model parameters fitted with experimental data. For oil well cement slurry with the water-to-cement ratio 0.44 and temperature 85°C , the following values can be used: $\tau_y = 40$ Pa, $a = 1.38$, $b = 0.004$ [74]. This model has a maximum shear stress limit at relatively high rate of shear strains.

Yuan et al. [75] substituted Equation (21) into (20) for an improved thixotropy model:

$$\tau = \tau_\infty + (\tau_{r0} + ct^m - \tau_\infty) \exp(-bt_s) \quad (33)$$

where τ_{r0} and τ_∞ are the shear stresses at the initial and the equilibrium states, t is the resting time, c is the recovery coefficient, m is the gel exponent, b is the thixotropic exponent, and t_s is the shear time.

Papo [61] found that the Herschel–Bulkley model, the Sisko model, and the Robertson–Stiff model can all match reasonably well with the experimental data of cement pastes; he recommended the Herschel–Bulkley model mostly because of its ability to describe the yield behavior. Table 2 provides a summary of the existing constitutive relations for cement. The parameters used in various constitutive relations for cement are listed in Table 3. Figure 3 shows the stress vs. shear rate curves for different constitutive relations with the parameters listed in Table 3.

Table 2. Summary of constitutive relations for cement.

Author(s)	Model	Equation No.
Bingham (1922)	$\tau = \tau_y + \eta_p \dot{\gamma}$	(2)
Bingham (tensor form)	$T = \left[\tau_y / \left(\frac{1}{2} D : D \right)^{1/2} \right] + \eta_p D$	(4)
Herschel–Bulkley (1926)	$\tau = \tau_y + K \dot{\gamma}^n$	(9)
Power-Law (1929)	$\tau = K \dot{\gamma}^n$	(10)
Williamson (1929)	$\tau = \eta_\infty \dot{\gamma} + \tau_y \frac{\dot{\gamma}}{\dot{\gamma} + \Gamma}$	(11)
Eyring (1936)	$\tau = \sum_{i=1}^n a_i \sinh^{-1}(\dot{\gamma} b_i)$	(12)
Sisko (1958)	$\tau = a \dot{\gamma} + b \dot{\gamma}^c$	(13)
Casson (1959)	$\sqrt{\tau} = \sqrt{\tau_y} + \sqrt{\eta \dot{\gamma}}$	(14)
Shangraw–Grim–Mattocks	$\tau = \tau_y + \eta_\infty \dot{\gamma} + \alpha_1 [1 - \exp(-\alpha_2 \dot{\gamma})]$	(15)
Ellis (1965)	$\dot{\gamma} = a \tau + b \tau^c$	(16)
Robertson and Stiff (1976)	$\tau = a(\dot{\gamma} + b)^c$	(17)
Robertson and Stiff (tensor form)	$\dot{\gamma}_{ij} = \frac{2A^{1/n} \Gamma^{1/2}}{\Gamma^{1/2n} - \tau^{1/n}} e_{ij}$	(18)
Vom Berg (1979)	$\tau = \tau_y + a \sinh^{-1}(b \dot{\gamma})$	(19)
Lapasin (1979)	$\tau = \tau_\infty + (\tau_0 - \tau_\infty) \exp(-bt_s)$	(20)
Quemada (1984)	$\tau = \left(\frac{1 + \sqrt{(a\dot{\gamma})}}{b + c \sqrt{(a\dot{\gamma})}} \right)^2 \dot{\gamma}$	(22)
Modified Casson (1985)	$\dot{\gamma} = a + b \tau^{1/2} + c \tau$	(23)
Atzeni (1985)	$\tau = \tau_y + a \dot{\gamma} + \sinh^{-1}(\dot{\gamma}/c)$	(24)
Lapasin (1983)	$\tau = \tau_y + \left[A_0 + (A_1 - A_0) \exp\left\{ -\frac{\dot{\gamma}}{a + b\dot{\gamma}} t \right\} \right] \sinh^{-1} \frac{\dot{\gamma}}{C}$	(25)
De Kee (1994)	$\tau = \tau_y + \eta_p \dot{\gamma} e^{-a\dot{\gamma}}$	(29)
Modified Bingham (2001)	$\tau = \tau_y + \eta_p \dot{\gamma} + c \dot{\gamma}^2$	(30)
Yahia and Khayat (2001)	$\tau = \tau_y + 2(\sqrt{\tau_y \eta_p}) \sqrt{\dot{\gamma} e^{-a\dot{\gamma}}}$	(31)
Vipulanandan (2014)	$\tau = \tau_y + \frac{\dot{\gamma}}{a + b\dot{\gamma}}$	(32)
Yuan (2015)	$\tau = \tau_\infty + (\tau_{r0} + ct^m - \tau_\infty) \exp(-bt_s)$	(33)

Table 3. Parameters for various models

Equation	τ_y (Pa)	η_p (Pa·s)	K	n	a	b	c	A_0 (Pa)	$A_1 - A_0$ (Pa)
Bingham (1922)	20	0.8	-	-	-	-	-	-	-
Herschel–Bulkley (1926)	20	-	2.5	0.75	-	-	-	-	-
Power-Law (1929)	-	-	0.25	1.25	-	-	-	-	-
Casson (1959)	20	0.31	2.5	0.75	-	-	-	-	-
Robertson and Stiff (1976)	-	-	-	-	20	1.5	0.35	-	-
Vom Berg (1979)	20	-	-	-	26.5	0.1	-	-	-
Quemada (1984)	-	-	-	-	0.14	10 ⁻⁴	0.14	-	-
Lapasin (1983)	12.1	-	-	-	2100	9.45	56.1	43.6	87.6
De Kee (1994)	20	0.89	-	-	10 ⁻³	-	-	-	-
Modified Bingham (2001)	20	1.15	-	-	-	-	-0.0035	-	-
Yahia and Khayat (2001)	20	0.9	-	-	10 ⁻³	-	-	-	-
Vipulanandan (2014)	40	-	-	-	1.38	0.004	-	-	-

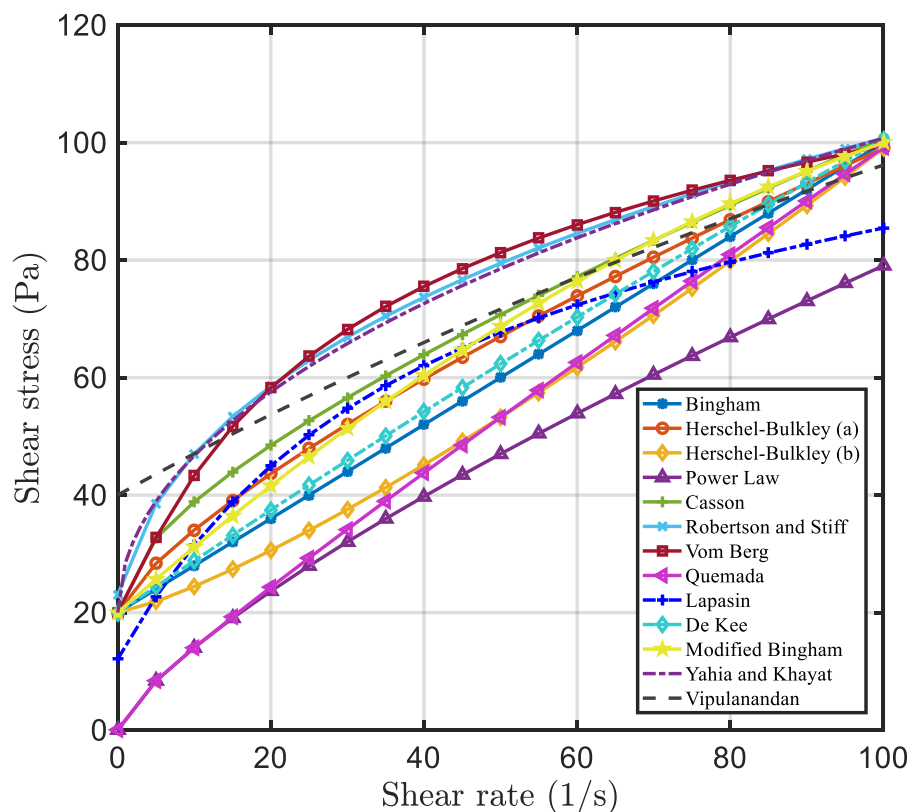


Figure 3. Stress vs. shear rate curves for various models for cement.

A look at Tables 2 and 3 and Figure 3 reveals that almost all the constitutive relationships given for the stress tensor of the cement, other than the Bingham model and the Herschel–Bulkley model, are given in 1-dimensional form where the (shear) stress τ is related to the shear rate $\dot{\gamma}$, a component of the velocity gradient tensor. In general, most problems of interests are 3-dimensional and as a result, constitutive relations are needed for the stress tensor T (with nine components).

2.2. The Importance of Yield Stress and Viscosity

In the previous section, we focused on the constitutive models available for the (total) stress tensor T for cement. Many researchers have looked at the yield stress T_y and the viscous stress T_v separately, and they have also looked at the factors and the parameters that can affect T_y and T_v . In this section we will focus on these issues. For example, it is known that the range of yield stress for a cement paste/slurry/grout is 10–100 N/m² and the range of plastic viscosity is 0.01–1 Ns/m² [3]. It has been shown that both of these parameters increase when finer cement particles are used [67]; this is mostly due to water and cement interaction. The effect of particle size is related to the surface area in the fine-grained pastes, rather than the volume of the coarse grains. Some of the variables which can affect the rheological properties of cement are: time, shear rate, concentration (volume fraction of the solid particles and the water-to-cement ratio), cement composition (Portland cement), fineness, flyash, silica fume, slags, chemical admixtures, age and temperature, pressure etc., [3,76].

In Section 2.2.1, we review some important yield stress models and in Section 2.2.2, we provide a review of various viscosity correlations, while looking at the different effects.

2.2.1. Yield Stress Models

The idea of fluids with yield stress perhaps can be traced back to Bingham ([44]). However, with all the successes of this model and the subsequent generalizations of it, Barnes and Walter [77] and Barnes [78] have questioned the concept or the reality of fluids with yield stress (see also Barnes [79]).

With the publications of [77], a series of interesting exchanges among different scientists started. Hartnett and Hu [80] responded to [77] with a new paper titled “The Yield stress—An engineering reality,” which was followed by other papers Astarita [81], and Evans [82]. For additional and more recent and important discussions on the status of yield stress fluids, we refer the reader to Papanastasiou [83], Bonn and Denn [84], and Denn and Bonn [85]. Moller et al. [86] provide an excellent discussion on the relationship between thixotropic fluids and fluids with yield stress. For a historical survey of the yield stress fluids, see [79], and for a comprehensive review of the flow of visco-plastic materials, see [87].

The yield stress, to a large extent, determines the transition between or the point at which the solid-like behavior changes to a fluid-like behavior. It is one of the most important and difficult properties of the fluid to measure, which in theory, can be obtained at low shear rate tests. Møller et al. [88] discuss some of the difficulties of measuring the yield stress. Dinkgreve et al. [89] talk about the various ways of measuring the yield stress. Nguyen and Boger [90] provide a detailed review of the flow properties of yield stress fluids, and Coussot [91] provides a recent review of the experimental data in yield stress fluids. Different methods to measure the yield stress have been suggested [92]. Unlike ideal yield stress fluids, concentrated colloidal fluids stop flowing abruptly at a critical stress and begin to flow with a high velocity at another critical stress, which increases with the duration of the preliminary rest (a period of rest after pre-shearing over a larger number of applied stresses) [92]. When the shear stress reaches a critical value, the shear rate changes from zero to a critical shear rate abruptly [93]; the critical values of shear rate and the shear stress are considered intrinsic material parameters and independent of flow condition. Below the yield stress, fresh cement behaves as a poro-elastic solid. After the yield stress is reached, the slurry exhibits plastic strains [35].

Roussel et al. [94] identified two different critical strains in fresh cement pastes, while studying the origins of the thixotropy and the mechanism of yielding: (1) the largest critical strain (of the order of a few %), is the strain at the yield point obtained from measurements [95,96]. This strain is related to the network breakage of the colloidal interactions between cement particles (e.g., C-S-H particles) shortly after mixing. It takes only a couple of seconds to form the network; (2) the smallest critical strain (of the order of a few hundredths of %), is the strain when the shear modulus drops significantly [97,98]. This strain is related to the breakage of the early hydrates, which are caused by the contact of flocculated cement grains. Short-term thixotropy is related to colloidal flocculation and long-term thixotropy is related to the ongoing hydrates nucleation. According to the two different critical strains mentioned above, the static yield stress measurement is either determined by the strength of the C-S-H bonds at the rigid critical strain at long times or determined by the C-S-H nucleation at the colloidal critical strain at short times. Perrot et al. [99] analyzed the effects of three parameters on the yield stress and the stability of fresh cement pastes: (1) Brownian motion, depending on temperature; (2) colloidal attractive forces, depending on the average distance between the interacting particles; (3) gravity, depending on the grain size. According to the Perrot et al. [99], cement displays yield stress when the colloidal attractive forces dominate the Brownian motion, while no yield stress is observed if the Brownian motion dominates the colloidal attractive forces. A cement suspension is stable and homogenous without bleeding (cement grains unstably suspended in water) if the colloidal attractive forces dominate gravity, while cement particles settle if gravity dominates the colloidal attractive forces. These forces are time driven and are affected by the interstitial fluid viscosity.

Because of thixotropy, there is more than one state of flocculation for the yield stress measurement: the dynamic yield stress measured through the flow curve at zero shear rate (equilibrium state) and the static yield stress needed to initiate flow before the structure is broken down. The dynamic and the static yield stresses of fresh cement are usually measured in a rotational rheometer with a vane [100,101]. Qian and Kawashima [101] measured the yield stress through shear-rate-controlled and shear-stress-controlled tests. The authors detected a negative slope in the equilibrium flow curve (torque vs. angular velocity) at steady-state condition, shear banding, and stick-slip in the shear-rate-controlled test. They also detected viscosity bifurcation and considered the creep stress as

the static yield stress based on the stress-controlled test [101]. Michaux and Defosse [102] reported that the yield stress of cement slurries exhibited a peak value at low dispersant (such as the sodium salt of Polynaphthalene Sulphonate) concentration and decreased to zero at high concentration. The dispersant seemed to break the structure through attractive interparticle forces.

In this section, we review the existing models for the yield stress for cement considering different effects such as volume fraction, water-to-cement ratio, additives and damage.

Effect of Concentration on the Yield Stress

From the experimental data by Lapasin [58] it can be noticed that the yield stress τ_y (see Equation (25)) increases with increasing the specific surface area of cement and with decreasing the water-to-cement ratio as well as water film thickness [103]. Larger cement solid concentration and flocculation result in larger yield stress [104].

Legrand [105] proposed a relationship between the yield stress and the concentration

$$\tau_y = A_0 \alpha^{(\phi-0.5)} \quad (34)$$

where A_0 and α are related to the particle size and the shape, and ϕ is the concentration of the cement particles. This relationship is valid when ϕ is in the range of [0.475–0.677], corresponding to the w/c range [0.15–0.35] [106].

Sybertz and Reick [107] suggested an equation showing the influence of concentration of cement particles on the yield stress:

$$\tau_y = P_1 \cdot e^{P_2 \cdot \phi} \quad (35)$$

where P_n ($n = 1, 2$) are material parameters obtained from experiment, where $P_1 = 2.31 \times 10^{-3}$ and 4.75×10^{-3} and $P_2 = 20.7$ and 19.1 for different types of cement.

Zhou et al. [108] proposed a yield stress model for concentrated flocculated suspensions with different size particles, using the yield stress of individual components in the suspension:

$$\tau_y = \left(\sum \phi_{vi} \tau_{yi}^{1/2} \right)^2 \quad (36)$$

where ϕ_{vi} is the volume fraction of i th component.

Zhou et al. [108] and Flatt and Bowen [109] suggested a yield stress function of the type:

$$\tau_{y,max} = K \left(\frac{\phi}{1-\phi} \right)^c \frac{1}{d^2} \quad (37)$$

$$K = \frac{3.1Ab}{24\pi h_0}$$

where A is the Hamaker constant [110] of colloidal material (5.3×10^{-20} J), b and c are fitting parameters ranging from 0.1 to 0.53, h_0 is the distance between the two particles (2.4 nm) and d is the particle diameter.

Flatt and Bowen [111] proposed a yield stress model (YODEL) that depends on the volume fraction:

$$\tau_y = m_1 \frac{\phi^2 (\phi - \phi_{perc})}{\phi_m (\phi_m - \phi)} \quad (38)$$

where ϕ_m is the maximum packing volume fraction (equal to 0.57 [111]), ϕ_{perc} is the percolation threshold (equal to 0.026 [111]), and m_1 is given by:

$$m_1 = \frac{1.8}{\pi^4} \left(\frac{G_{max}}{R_{v,50}} \right) F_{\sigma, \Delta} \quad (39)$$

where G_{max} is the maximum attractive force between the particles, $R_{v,50}$ is the median particle radius and $F_{\sigma, \Delta}$ is a function of coordination number related to the contacts between particles. Figure 4 shows

the yield stress versus volume fraction for various samples. Equation (38) from YODEL [111] is applied to fit Zhou et al. [108] experimental data.

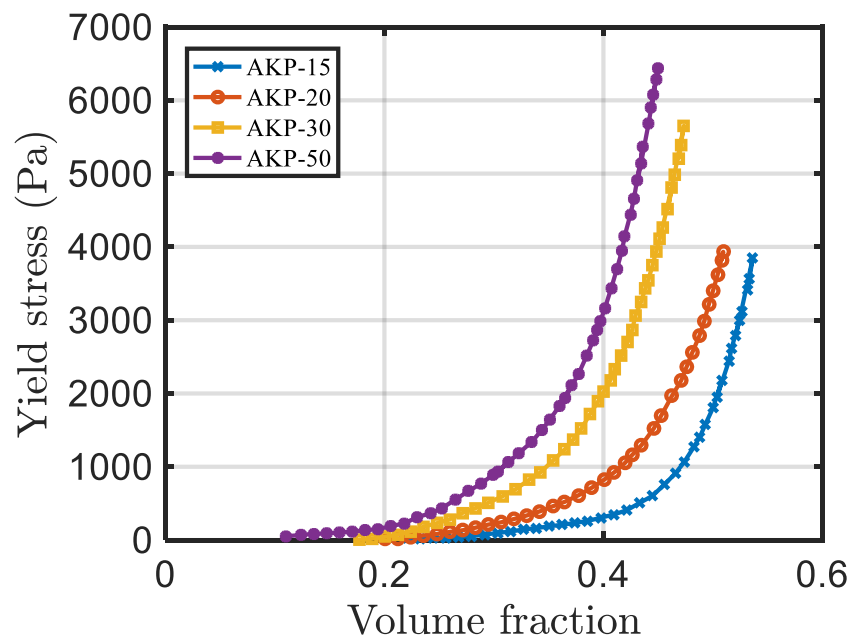


Figure 4. Yield stress vs. volume fraction for concentrated suspensions. YODEL [111] is applied to fit the experimental data of Zhou et al. [108], where AKP-15, 20, 30, and 50 are different alumina particulate samples.

Based on YODEL, Ma and Kawashima [112] related the yield stress to the hydration degree $\alpha(t)$ by assuming $\phi = \phi_0(1 + \chi\alpha(t))$:

$$\tau_y = m_1 \frac{(\phi_0(1 + \chi\alpha(t)))^2 (\phi_0(1 + \chi\alpha(t)) - \phi_{perc})}{\phi_m(\phi_m - \phi_0(1 + \chi\alpha(t)))} \quad (40)$$

where χ is an expansion parameter obtained from experiment, related to the density difference between unhydrated cement clinkers and the hydration products. For neat cement pastes (cement without sand or aggregate), $\phi_{perc} = 0.37$ and $\phi_m = 0.59$, $\phi_0 = 0.425$ for cement with water-to-cement ratio of 0.43, $\alpha(t) = 1 - e^{-kt^n}$, where $k = 6.73 \times 10^{-10}$ and $n = 2.85$ [112].

Mahaut et al. [95] used the Chateau–Ovarlez–Trung yield stress model [113] to describe the behavior of a thixotropic cement paste:

$$\frac{\tau_y(\phi)}{\tau_y(0)} = \sqrt{\frac{1 - \phi}{(1 - \phi/\phi_m)^{2.5\phi_m}}} \quad (41)$$

where $\frac{\tau_y(\phi)}{\tau_y(0)}$ is the dimensionless yield stress of a monodisperse suspension, where $\phi_m = 0.56$. This equation is suitable for yield stress fluids consisting of rigid spherical non-colloidal particles with no interactions between the particles and the paste. Figure 5 shows the fit for the Chateau–Ovarlez–Trung yield stress model for cement.

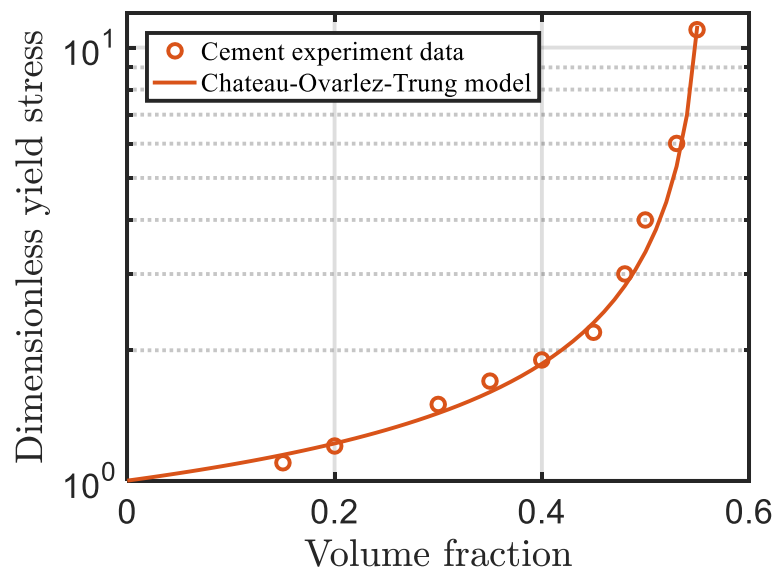


Figure 5. Dimensionless yield stress $\frac{\tau_y(\phi)}{\tau_y(0)}$ vs. volume fraction of cement: comparing the experimental data and the Chateau–Ovarlez–Trung yield stress model [108].

Chougnnet et al. [114] also proposed a correlation for the dynamic yield stress, which is the shear stress at the zero limit of shear rate, as a function of the volume fraction

$$\tau_y^{dyn} = \frac{F}{a^2} \left(\frac{\phi}{\phi_m} \right)^{\frac{1}{m(3-f)}} \quad (42)$$

where F is the adhesion force necessary to separate the particles from each other, a is the particle radius, m and f are material parameters.

Based on the experimental data, Lapasin et al. [58] proposed a correlation for the yield stress τ_y describing the effect of cement specific surface S_{vB} and concentration of cement particles ϕ :

$$\tau_y = 2.1 \times 10^{-3} e^{19.2 \cdot \phi} \cdot S_{vB}^{2.5} \quad (43)$$

Effect of Water-to-Cement Ratio on the Yield Stress

Ivanov and Roshavelov [115] found that the yield stress decreases when the water-to-cement ratio increases. Rosquoët et al. [116] suggested a coefficient K in the power-law relation [56] (see Equation (10)), where K is a function of w/c :

$$\tau = K \left(\frac{\dot{\gamma}}{\dot{\gamma}_0} \right)^n = (-175w/c + 137) \left(\frac{\dot{\gamma}}{\dot{\gamma}_0} \right)^{0.6} \quad (44)$$

where $\dot{\gamma}_0$ is the reference shear rate with a value of 1000 s^{-1} [116]. Figure 6 shows the shear stress vs. the shear rate curves for various values of water-to-cement ratio.

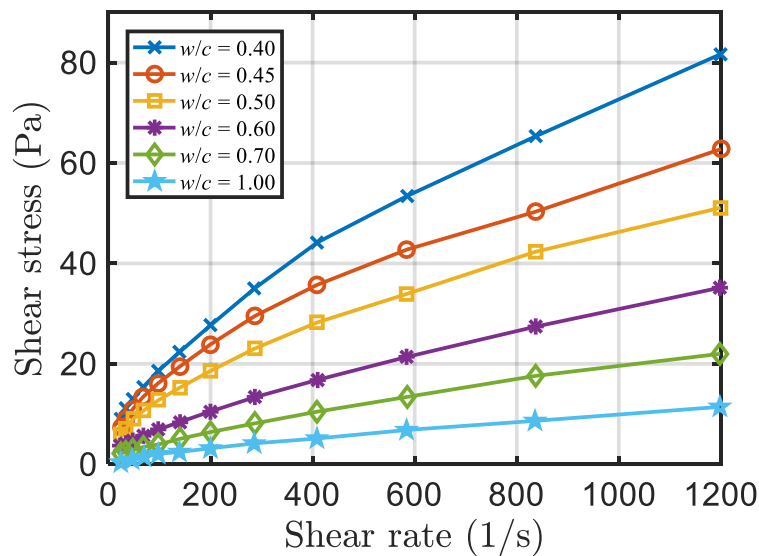


Figure 6. Shear stress vs. shear rate for different w/c [116].

Lapasin et al. [68] found that the yield stress increases linearly when the specific surface bearing (SSB) obtained from Blaine permeability apparatus increases,

$$\tau_y = K(SSB - 2000) \tag{45}$$

where K depends on the water-to-cement ratio (w/c) and it decreases while the w/c increases. Figure 7 shows the effect of water-to-cement ratio on the yield stress, reported by Banfill [3] from various published experimental data of cement. From Figure 7, we can see that there is a reverse log-linear relationship between the yield stress and the water-to-cement ratio.

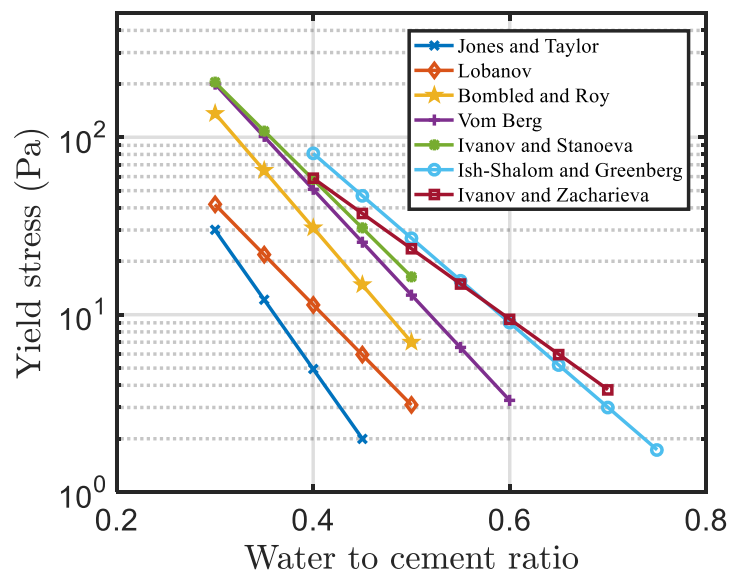


Figure 7. Effect of water-to-cement ratio on the yield stress of cement [3]. Data are from different published experimental data [39,42,54,67,117–121].

Effect of Additives/Admixtures on the Yield Stress

Ivanov and Roshavelov [115] proposed a polynomial equation, based on the experimental data fitted with a regression analysis, describing the effect of each clinker component on the yield stress (with units Pa):

$$\begin{aligned} \tau_y = & -118.5 - 72.3X_1 - 104.8X_2 + 103.6X_3 - 46.1X_4 - 48.7X_5 + 75.4X_1X_2 - \\ & 77.4X_1X_3 + 38X_1X_4 + 42.4X_1X_5 - 107X_2X_3 + 39.9X_2X_4 + 41.6X_2X_5 - \\ & 54.5X_3X_4 - 50.7X_3X_5 + 21.5X_1^2 + 19.3X_2^2 + 158.7X_3^2 + 38.9X_4^2 + 37.1X_5^2 \end{aligned} \quad (46)$$

where X_1 , X_2 , X_3 , X_4 , and X_5 are parameters indicating the contributions of the water-to-cement ratio (w/c), concentration of superplasticizer, condensed silica fume (CSF), tricalcium aluminate (C_3A), and SO_3 , respectively. Equation (46) indicates that CSF has the strongest influence on the behavior of the cement; as indicated by Ivanov and Roshavelov [115] τ_y initially decreases when CSF increases to a certain value, and then it begins to increase when the CSF is in the range 7.5–15%.

Sybertz and Reick [107] studied the effect of fly ash on the behavior of cement paste and suggested the following equation:

$$\tau_y = P_1 \cdot e^{P_2 \cdot \phi} \cdot (1 - \phi_f) + P_3 \cdot e^{P_4 \cdot \phi} \cdot \phi_f \quad (47)$$

where ϕ_f is the fly ash content and P_n , Q_n ($n = 1, 2, 3, 4$) are the experimental fitting parameters, where $P_1 = 2.31 \times 10^{-3}$ (Fly Ash I) and 4.75×10^{-3} (Fly Ash II), $P_2 = 20.7$ (Fly Ash I) and 19.1 (Fly Ash II), $P_3 = 7.96 \times 10^{-5}$ (Fly Ash I) and 1.29×10^{-5} (Fly Ash II), $P_4 = 17.0$ (Fly Ash I) and 18.9 (Fly Ash II). Figure 8 shows the effect of different types of fly ash on the yield stress. Both Fly Ash I and Fly Ash II lower the value of the yield stress.

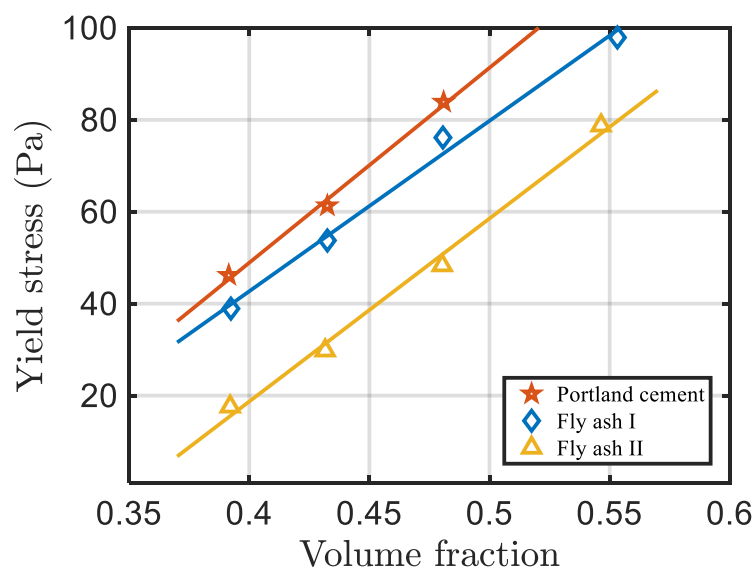


Figure 8. Effect of fly ash additives on yield stress [107].

Effect of Damage on the Yield Stress

Chen et al. [122] suggested a strain rate-dependent constitutive equation for the stress, including the effect of damage because of the dynamical experiment of measuring the mechanical properties of cement-based materials:

$$\tau = [1 - (D_1 + D_0 \dot{\gamma}_d^\xi) \gamma] \cdot \left[A_0 + A_1 \left(\frac{\dot{\gamma}_d}{\dot{\gamma}_s} \right)^B \right] \gamma \quad (48)$$

where $\xi = \lambda - 1$, and D_0 , D_1 , and λ are constants or parameters related to damage; A_0 , A_1 , and B are constants or parameters related to the shear rate, and $\dot{\gamma}_d$ and $\dot{\gamma}_s$ are the dynamic strain rate and

static strain rate, respectively, and γ is the strain. Figure 9 shows the stress–strain curves for cement at various strain rates (104/s and 134/s).

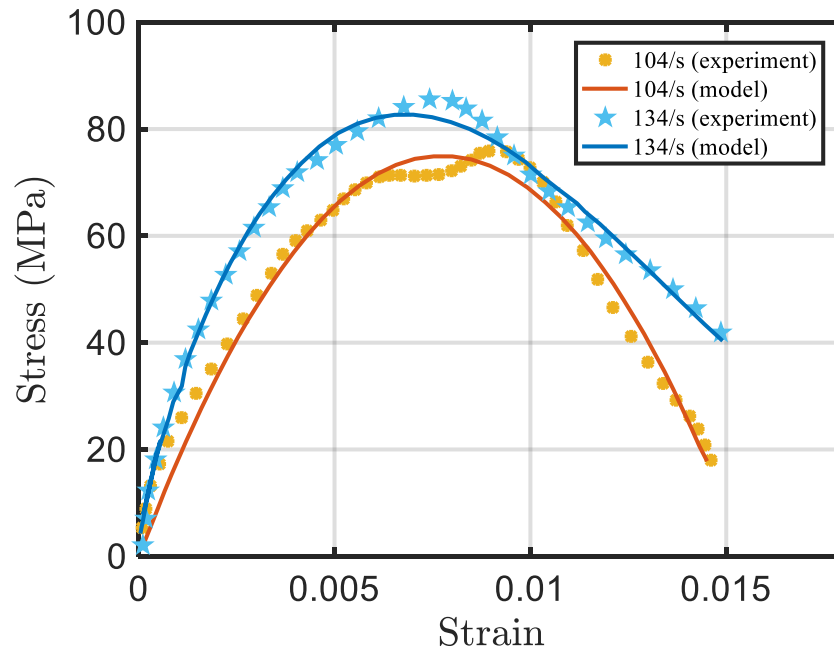


Figure 9. The stress–strain curves for cement using experiments and the damage-based model [122].

We summarize the yield stress models for cement in Table 4:

Table 4. Summary of the yield stress models for cement.

Effect	Author(s)	Model	Equation No.
Effect of concentration	Legrand (1970)	$\tau_y = A_0\alpha^{(\phi-0.5)}$	(34)
	Sybertz and Reick (1991)	$\tau_y = P_1 \cdot e^{P_2 \cdot \phi}$	(35)
	Zhou et al. (1999)	$\tau_y = \left(\sum \phi_{vi} \tau_{yi}^{1/2} \right)^2$	(36)
	Zhou et al. (1999)	$\tau_{y,max} = K \left(\frac{\phi}{1-\phi} \right)^c \frac{1}{d^2}$	(37)
	Flatt and Bowen (2006)	$\tau_y = m_1 \frac{\phi^2 (\phi - \phi_{perc})}{\phi_{max} (\phi_{max} - \phi)}$	(38)
	Ma and Kawashima (2019)	$\tau_y = m_1 \frac{(\phi_0(1+\chi\alpha(t)))^2 (\phi_0(1+\chi\alpha(t)) - \phi_{perc})}{\phi_{max} (\phi_{max} - \phi_0(1+\chi\alpha(t)))}$	(40)
	Chateau–Ovarlez–Trung (2008)	$\frac{\tau_y(\phi)}{\tau_y(0)} = \sqrt{\frac{1-\phi}{(1-\phi/\phi_m)^{2.5\phi_m}}}$	(41)
	Chougnat (2008)	$\tau_y^{dyn} = \frac{F}{d^2} \left(\frac{\phi}{\phi_{max}} \right)^{\frac{1}{m(3-f)}}$	(42)
	Lapasin et al. (1983)	$\tau_y = 2.1 \times 10^{-3} e^{19.2 \cdot \phi} \cdot S_{vB}^{2.5}$	(43)
Effect of water-to-cement ratio	Rosquoët et al. (2003)	$\tau = (-175w/c + 137) \left(\frac{\dot{\gamma}}{\dot{\gamma}_0} \right)^{0.6}$	(44)
	Lapasin et al. (1979)	$\tau_y = K(w/c)(SSB - 2000)$	(45)
Effect of additives/admixtures	Ivanov and Roshavelov (1990)	$\tau_y = -118.5 - 72.3X_1 - 104.8X_2 + 103.6X_3 - 46.1X_4 - 48.7X_5 + 75.4X_1X_2 - 77.4X_1X_3 + 38X_1X_4 + 42.4X_1X_5 - 107X_2X_3 + 39.9X_2X_4 + 41.6X_2X_5 - 54.5X_3X_4 - 50.7X_3X_5 + 21.5X_1^2 + 19.3X_2^2 + 158.7X_3^2 + 38.9X_4^2 + 37.1X_5^2$	(46)
	Sybertz and Reick (1991)	$\tau_y = P_1 \cdot e^{P_2 \cdot \phi} \cdot (1 - \phi_f) + P_3 \cdot e^{P_4 \cdot \phi} \cdot \phi_f$	(47)
Effect of damage	Chen et al. (2013)	$\tau = [1 - (D_1 + D_0 \dot{\gamma}_d^\xi) \gamma] \cdot \left[A_0 + A_1 \left(\frac{\dot{\gamma}_d}{\dot{\gamma}_s} \right)^B \right] \gamma$	(48)

2.2.2. Viscosity Relationships

The non-linear time-dependent response of complex fluids such as cement slurries constitutes an important area of mathematical modeling of non-Newtonian fluids. In general, for many complex fluids such as cement slurries, or drilling fluids, the shear viscosity can be a function of one or all of the following [123]:

- Shear rate $\dot{\gamma}$
- Volume Fraction ϕ
- Temperature θ
- Pressure P
- Thixotropic behavior (structural parameter $\lambda(t)$)
- Water-to-cement ratio w/c
- Additives (Superplasticiser)
- Mixing method
- Electric field
- Magnetic field
- ...

For certain materials or under certain conditions, the dependence of viscosity on some of these can be dropped. In this section, we look at the effects of some of these parameters on the viscosity.

Effect of Shear Rate on the Viscosity

Recall that according to the power-law (the Ostwald-de Waele) model [56,124], shown in Section 2.1, the shear viscosity η , can be defined as

$$\eta = \frac{\tau}{\dot{\gamma}} = K\dot{\gamma}^{n-1} \quad (49)$$

For pseudoplastic (or shear-thinning) fluids $n < 1$; in this case, the viscosity decreases when the shear rate increases. For Newtonian fluids $n = 1$, where the viscosity is independent of the shear rate. For dilatant (or shear-thickening) fluids $n > 1$, the viscosity increases with the shear rate [see Figure 10]. Equation (49) provides an explicit relationship between the shear rate and the shear stress; however, it is not suitable for fluids with yield stress.

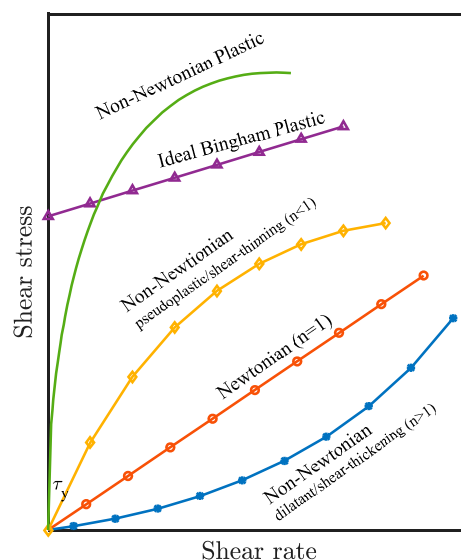


Figure 10. Shear stress vs. shear rate for different types of fluids [125].

Based on the Robertson and Stiff model [46] shown in Section 2.1, the effective viscosity for cement slurries can be written as

$$\eta_{eff} = \frac{A(\dot{\gamma}_R + C)^B}{\dot{\gamma}_R} \quad (50)$$

where η_{eff} is the effective viscosity and $\dot{\gamma}_R$ is the value of the shear rate at the pipe or the annulus wall.

As shown in Section 2.1, the Casson model [62] is widely used for shear-thinning non-Newtonian fluids. According to this model, the viscosity is:

$$\eta = \frac{1}{\dot{\gamma}} \left[k_0 + k_1 \sqrt{\dot{\gamma}} \right]^2 \quad (51)$$

where k_0 and k_1 are material parameters obtained from experiment.

From the Carreau–Yasuda model [33], viscosity approaches a lower limit when the shear rate is close to zero and approaches an upper limit when the shear rate is close to infinity. According to this model, the relation between viscosity and the shear rate is:

$$\eta = \eta_\infty + (\eta_0 - \eta_\infty) \frac{1 + \ln(1 + k\dot{\gamma})}{1 + k\dot{\gamma}} \quad (52)$$

where η_0 and η_∞ are the lower and the upper viscosities when the shear rate is close to zero and infinity, respectively, and k is the shear-thinning parameter. These parameters are obtained from experimental measurements.

Effect of Volume Fraction on the Viscosity

Experiments indicate that the viscosity increases with higher particle concentration and larger cement specific surface [104].

Einstein [126] first presented the simplest mathematical expression for the effects of concentration on the (dimensionless) viscosity, commonly referred as *relative viscosity* of a fluid containing very small number of rigid spheres (low concentration or dilute limit):

$$\eta_r = \frac{\eta}{\eta_0} = 1 + \alpha\phi \quad (53)$$

where η is the viscosity of the suspension, η_0 is the viscosity of the pure liquid (no particles) (1cP for water at 20 °C), $\alpha = 2.5$ for rigid spheres, and ϕ is the concentration. At higher concentrations, the viscosity reaches an infinite value, and this equation is no longer applicable. The Einstein equation has been applied to cement suspensions by Roussel et al. [127].

For spheres of different sizes, Roscoe [128] suggested:

$$\eta_r = \frac{\eta}{\eta_0} = (1 - \phi)^{-2.5} \quad (54)$$

Mooney [129] proposed an equation for densely packed particles:

$$\eta_r = \frac{\eta}{\eta_0} = e^{\left[\frac{\alpha\phi}{(1 - \frac{\phi}{\phi_m})} \right]} \quad (55)$$

where η is the apparent viscosity (the applied shear stress divided by the shear rate, i.e., $\eta = \frac{\tau}{\dot{\gamma}}$) of the suspension, η_0 is the apparent viscosity of the continuous/liquid phase without any particles, ϕ is the concentration, α is a parameter depending on particle shape (2.5 for spheres), and ϕ_m is the maximum solid concentration, depending on the particle size distribution and the shape. However, Mooney's equation does not seem to fit the measured data at high concentrations [104].

Roscoe [128] also suggested an expression for the viscosity of concentrated suspensions considering non-uniform particle size:

$$\eta_r = \frac{\eta}{\eta_0} = (1 - 1.35\phi)^{-2.5} \quad (56)$$

Figure 11 shows the dimensionless viscosity versus volume fraction using various relationships.

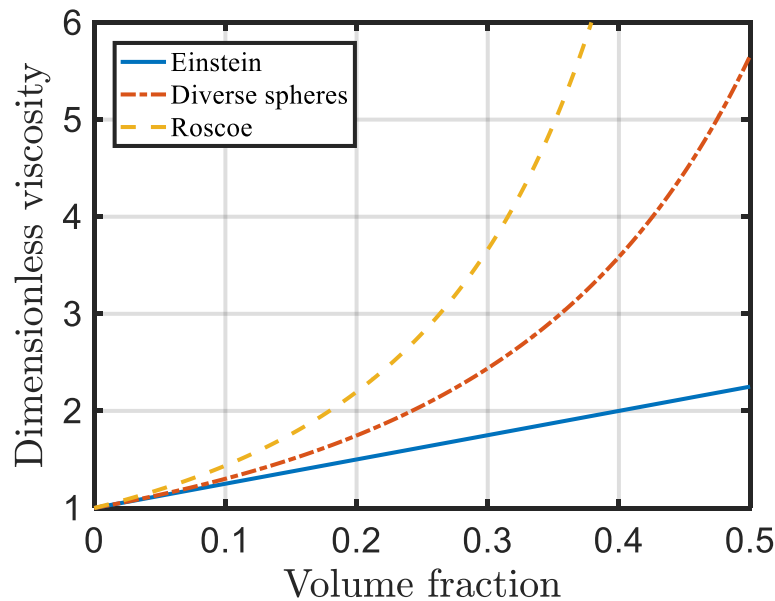


Figure 11. Dimensionless viscosity vs. volume fraction [128].

Krieger and Dougherty [130] provided an equation that is widely applied in cement industry [103, 104,127,131–139]. They suggested,

$$\eta_r = \frac{\eta}{\eta_0} = \left(1 - \frac{\phi}{\phi_m}\right)^{-\alpha\phi_m} \quad (57)$$

For dispersed cement pastes, $\phi_m \cong 0.7$, $\alpha \cong 5$, which increases at higher shear rates. Cement pastes that are not dispersed have higher viscosity and lower ϕ_m [104]. Cement pastes at lower concentrations (higher w/c) exhibit Newtonian behavior, while at higher concentrations (lower w/c) they show pseudo-plastic or plastic behavior. Table 5 shows the Krieger–Dougherty parameters for various types of cements for different strain rates (25 1/s and 500 1/s) [104]. Figure 12 shows the Krieger–Dougherty curves for dimensionless viscosity versus volume fraction using the parameters in Table 5.

Table 5. Krieger–Dougherty parameters for cement [104].

Cement Type	Strain Rate (1/s)	ϕ_m	α
Type I, dispersed	25	0.64	5.1
	500	0.76	6.2
Type I, flocculated	500	0.64	6.3
White cement, dispersed	25	0.67	5.7
	500	0.80	6.8
Type V, dispersed	25	0.68	4.5
	500	0.75	5.2

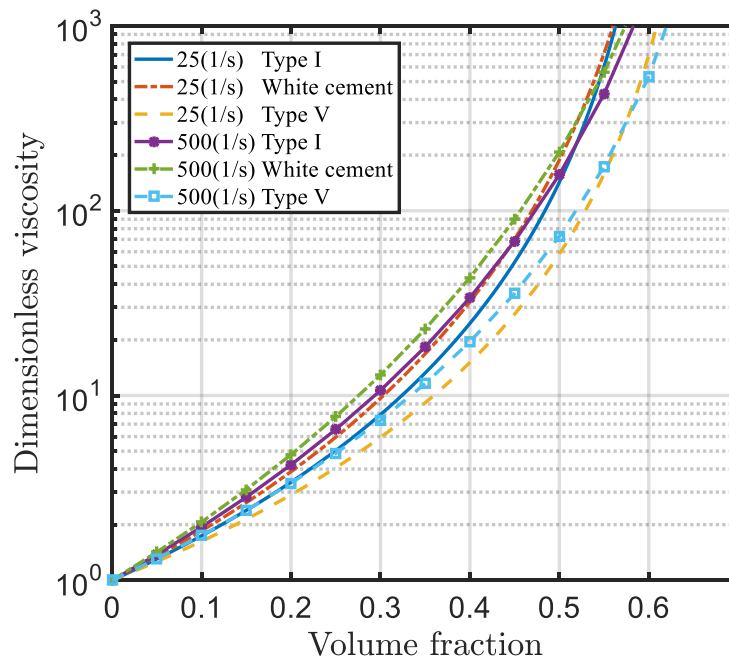


Figure 12. Krieger–Dougherty curves for various types of cements at various strain rates [104].

Chen and Lin [140] combined the Krieger–Dougherty equation with the fitting curves of apparent viscosity measured from a vibrational viscometer and suggested the following equation:

$$\eta_r = \left(1 - \frac{\phi}{\phi_m}\right)^{-2.78} e^{0.073t} \quad (58)$$

where t is the hydration time, $\phi_m = 0.635$ for monodisperse systems. Equation (58) describes the relationship between the viscosity, the volume fraction and the hydration time. It shows that the viscosity increases with the hydration time within 20 min.

Murata and Kikukawa [141] proposed an exponential expression for viscosity; their equation was used by Asaga and Roy to study cement slurry [39]:

$$\eta_r = B_0 e^{(K_1 \phi + K_2)} \quad (59)$$

where B_0 , K_1 , and K_2 are constants obtained from experiments.

Sybertz and Reick [107] suggested an equation showing the effect of concentration of cement particles on the initial viscosity:

$$\eta_0 = Q_1 \cdot e^{Q_2 \cdot \phi} \quad (60)$$

where ϕ is concentration of cement particles and Q_n ($n = 1, 2$) are parameters that can be obtained from experiments, where $Q_1 = 8.97 \times 10^{-5}$ and 4.04×10^{-5} and $Q_2 = 17.1$ and 19.0 for different types of cement.

Chougnnet et al. [114] used Mills [142] viscosity correlation to look at the effect of particle aggregation on viscosity.

$$\eta_r = \frac{\eta}{\eta_0} = \frac{(1 - \phi)}{\left(1 - \frac{\phi}{\phi_m}\right)^2} \quad (61)$$

where $\phi_m = 4/7$ for randomly packed monodispersed spheres.

Liu [143] proposed a dimensionless viscosity relationship for cement pastes that was reviewed by Bentz et al. [137]:

$$\eta_r = \frac{\eta}{\eta_0} = [a(\phi - \phi_m)]^{-n} \quad (62)$$

where a and n are fitting parameters with values 0.95 and 2.14.

Chong et al. [144] proposed a dimensionless viscosity relationship for cement pastes which was also reviewed by Bentz et al. [137]:

$$\eta_r = \frac{\eta}{\eta_0} = \left(1 + \frac{0.75 \frac{\phi}{\phi_m}}{1 - \frac{\phi}{\phi_m}} \right)^2 \quad (63)$$

According to Bentz et al. [137], Liu's model predicts the experimental results better than Chong et al.'s model.

Effects of Temperature and Pressure on the Viscosity

Temperature can play an important role in (oil well) cement operations, especially, in the early stages, when the yield stress increases; its effect on the viscosity is not that obvious because of the decrease of water viscosity (base fluid) at higher temperatures (with increasing rate 0.027 °C/m) [112,145]. With the increase of temperature in deep wells, the viscosity tends to decrease because of thermal thinning [146]. Cement slurries experience different pressure conditions when pumped into the wells. Ma and Kawashima [112] found that the high pressure in deep wellbores (with increasing rate 9.8 kPa/m) increases the yield stress and the viscosity; high pressure seems to accelerate the hydration process without affecting the water viscosity. Kim et al. [147] found that pressure causes the yield stress to decrease by 15% at lower water-to-cement ratios (<0.4), while the effect is not obvious at higher water-to-cement ratios. High pressure also changes the microstructure of the cement, causing deflocculation while increasing the dispersion of cement particles, resulting in a decrease in the yield stress. Figure 13 shows the shear stress versus shear rate curves for different water-to-cement ratios at different temperatures.

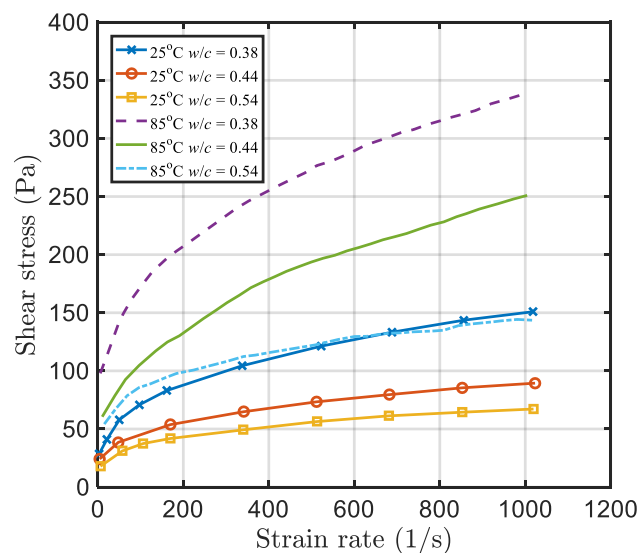


Figure 13. Shear stress vs. shear rate for cement for different water-to-cement ratios at different temperatures (25 °C and 85 °C) [146].

The microscopic and macroscopic properties (e.g., rheometric behavior, mechanical characteristics) of hydration products including calcium silicate hydrate (CSH) and calcium hydroxide (CH) are found to be sensitive to the curing temperature. Vlachou and Piau [19] found that cement particles are more spherical-like at lower temperatures (20 °C) while they are more rod-like at higher temperatures (60 °C), as shown in Figure 14. Temperature seems to accelerate the hydration process. Some studies indicate that both the yield stress and the viscosity decrease when the temperature increases [148]. In

some applications, pressure seems to have negligible effects on the flow of cement slurries; at lower water-to-cement ratios, cement slurries become more sensitive to pressure [22].

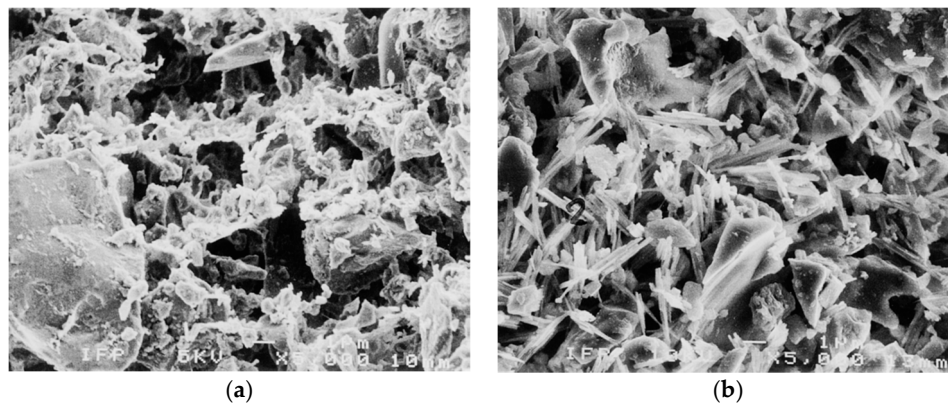


Figure 14. Morphology of cement particle under SEM (a) at 20 °C; (b) at 60 °C [19].

Sercombe et al. [149] suggested an equation showing the temperature effect on the viscosity for long-term creep behavior of cementitious material:

$$\frac{1}{\eta_{\theta}} = \frac{1}{\eta_{\theta,0}} e^{[-\frac{U}{R}(\frac{1}{\theta} - \frac{1}{\bar{\theta}})]} \quad (64)$$

where U is the activation energy of long-term creep, R is the universal gas constant, $U/R = 2700 \text{ K}$ [150], $\bar{\theta}$ is the reference temperature (20 °C in their study), $\eta_{\theta,0}$ is the value of η_{θ} when $\theta = \bar{\theta}$.

The effects of temperature and pressure could also be implemented through the active hydration process, which suggests that the viscosity is related to a fixed hydration reaction rate. Some researchers [149,151] use an Arrhenius-type equation for the hydration kinetics process with some knowledge of chemoplasticity of cement and concrete. The chemical affinity \tilde{A} is expressed as:

$$\tilde{A}(\xi) = \dot{\xi} e^{\left(\frac{E_a}{R\theta}\right)} \quad (65)$$

where $E_a/R \approx 4000\text{K}$, $\dot{\xi}$ is the hydration degree, which is estimated from the evolution of compressive strength depending on the temperature θ .

Scherer et al. [14] assumed that the viscosity of cement slurry is related to the degree of cement hydration and suggested an equation showing the effect of temperature and pressure on the hydration process. From the Avrami–Cahn model [152], the degree of hydration reaction is given by:

$$X \approx \frac{\pi}{3} O_v^B I_B G^3 t^4 \quad (66)$$

where X is the volume fraction of the transformed reactant, O_v^B is the boundary area, I_B is the nucleation rate on the boundary, G is the linear growth rate of the product and t is the time, and I_B and G are functions of temperature θ and pressure p , where:

$$G(\theta, p) \approx G_0 e^{\left(-\frac{\Delta E_G + p\Delta V_G}{R\theta}\right)} \quad (67)$$

$$I_B(\theta, p) \approx I_0 e^{\left(-\frac{\Delta E_I + p\Delta V_I}{R\theta}\right)} \quad (68)$$

where ΔE_G and ΔE_I are the activation energy for growth and nucleation, ΔV_G and ΔV_I are activation volumes for growth and nucleation and G_0 and I_0 are constants.

Pang et al. [153] developed a simple scale factor connecting the degree of hydration to temperature and pressure:

$$\dot{\xi}(t) = \dot{\xi}_r(C(\theta, P), t) \quad (69)$$

where $\dot{\xi}_r$ is the degree of hydration at reference temperature θ_r and pressure P_r . The scale factor C is given by:

$$C = e^{\left[\frac{E_a}{R\left(\frac{1}{\theta_r} - \frac{1}{\theta}\right)} + \frac{\Delta^\ddagger}{R}\left(\frac{P_r}{\theta} - \frac{P}{\theta}\right)\right]} \quad (70)$$

where R is the gas constant, Δ^\ddagger is the activation volume and E_a is the activation energy.

Wu et al. [154] studied the effect of temperature and cement hydration on viscosity and suggested two viscosity equations for temperature effect [155] and cement hydration effect [156],

$$\eta_c = \eta_r \cdot e^{\left[\frac{E}{R\theta_c}\right]} \quad (71)$$

$$\eta_c = \eta_{c0} + (1000 - \eta_{c0}) \cdot (t/t_v)^n \quad (72)$$

$$\eta_c = \eta_r \cdot e^{\left[\frac{E}{R\theta_{c0}}\right]} + \left(1000 - \eta_r \cdot e^{\left[\frac{E}{R\theta_{c0}}\right]}\right) \cdot (t/t_v)^n \quad (73)$$

Equation (71) shows the influence of temperature, where θ_c and θ_r are the temperatures of fresh cement slurry and reference temperature, η_c and η_r are viscosities at temperature θ_c and θ_r , respectively. Equation (72) shows the cement hydration effect, where η_{c0} is the initial viscosity of the fresh cement slurry and n is a parameter related to cement hydration kinetics, t_v is the time needed to reach a very high viscosity (e.g., 1000 Pa·s). According to Papo and Caufin [156], t_v is a function of water-to-cement ratio:

$$t_v = t_{v0} + X[w/c - (w/c)_0]^Y \quad (74)$$

where t_{v0} and $(w/c)_0$ are the initial values of t_v and w/c , and X and Y are parameters obtained from experiment. Equation (73) combines Equations (71) and (72), where θ_{c0} is the initial temperature of fresh cement slurry.

Effect of Additives/Admixtures on the Viscosity

Chemical additives/admixtures have the following functions: (1) To disperse the cement particles; (2) to modify the kinetics of the hydration process; (3) to react with the hydration subproducts; (4) to add binders to cement [157]. Additives are applied to either retard or accelerate the curing process of the cement slurries; they could also be used as viscosifiers or dispersant.

Superplasticizing admixtures could make the cementations materials denser, more impermeable and more durable. A superplasticizer provides better dispersibility. As the amount of the superplasticizer increases, the slurry behavior changes from Newtonian to non-Newtonian and finally back to Newtonian, where the mixture is well dispersed [158]. Figure 15 shows the mechanism of how a superplasticizer works. Flocculated cement particles are dispersed because of the negatively charged superplasticizer and the motion of the entrapped water. A superplasticizer generally improves the flow behavior of cement slurries and provides highly amorphous hydrates [159]. It is observed that increasing the amount of a superplasticizer admixture increases the cement gelation threshold [160], while decreasing the yield stress and viscosity and delaying the cement hydration process [161–164]. These effects are not that obvious when the admixture concentration is higher than 0.75% or when the shear rate is high (>128 rpm). In general, the cement slurry seems to behave as a dilatant/shear-thickening fluid with admixture concentrations higher than 0.75% [165,166]. Effects of ultrafine particles on the superplasticizer is to decrease the flow resistance and viscosity [167–169]. Researchers [170,171] have found that the polycarboxylate (PC) superplasticiser admixture reduces the yield stress and the plastic viscosity by 70%; this reduction is thought to be related to the interconnected flocs or the weak cohesive forces.

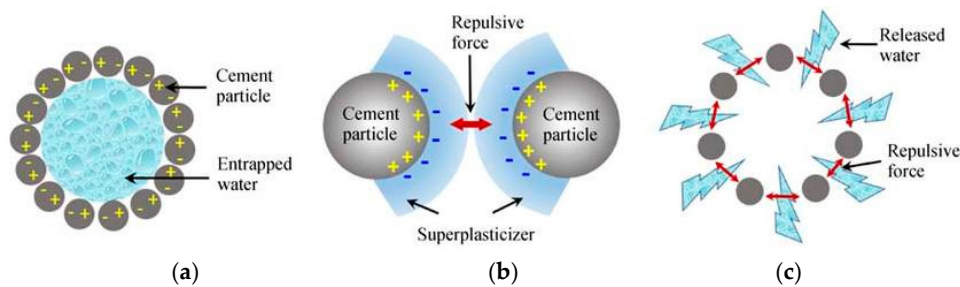


Figure 15. Effect of superplasticizer on cement particles [159]. (a) Flocculated cement particles; (b) dispersing cement particles by repulsive force; (c) release of entrapped water releasing.

Condensed silica fume (CSF), considered as an effective microfiller as superplasticizer, has a significant effect on the viscosity and the yield stress of the cement pastes. Ivanov and Roshavelov [115] proposed a polynomial equation fitted with regression analysis using the experimental data, while describing the effect of each clinker component on the apparent viscosity (mPa·s):

$$\begin{aligned} \eta = & -300.8 - 357.6X_1 - 553.4X_2 + 575.4X_3 - 80.8X_4 - 22.4X_5 + \\ & 293.7X_1X_2 - 329.4X_1X_3 + 14.7X_1X_4 + 57X_1X_5 - 528.4X_2X_3 + 48.9X_2X_4 + \\ & 21.2X_2X_5 - 151.1X_3X_4 - 29.3X_3X_5 + 175.2X_4X_5 + 114.4X_1^2 + 152.8X_2^2 + \\ & 664.6X_3^2 + 159.2X_4^2 + 213X_5^2 \end{aligned} \quad (75)$$

where X_1 , X_2 , X_3 , X_4 , and X_5 are the parameters related to the amount of water-to-cement ratio (w/c), concentration of superplasticizer, condensed silica fume (CSF), tricalcium aluminate (C_3A), and SO_3 , respectively. Equation (75) indicates that CSF has the strongest influence on the viscosity of the cement; it is observed that η initially decreases when CSF increases and reaches a certain value, and then it begins to increase when the CSF is in the range 7.5–15%. Wong and Kwan [172] indicated that the addition of CSF to cement causes an increase in the packing density and the flowability in the lower ranges (<15%) and lower w/c while causing a decrease in the packing density at the higher ranges (>15%). They also mention that the addition of pulverized fuel ash (PFA) increases the packing density and flowability of cement paste. The influences of C_3A and SO_3 are much less than other factors.

Glycerin, as a viscosifier, when added to the cement slurry, can increase the viscosity and accelerate the hydration process at about 26% volume content [17]. The effect of glycerin on viscosity is more obvious at larger shear rates. The shear-thinning behavior is reduced, and the slurry begins to be more Bingham-like with the increase of glycerin content. Another viscosifying agent, hydroxypropylmethylcellulose (HPMC) increases the plastic viscosity, while decreasing the fluid loss, increasing the thickening time, and increasing the compressive strength of cement slurries [173]. This is very suitable for oil well cementing under high temperature conditions.

In general, adding these modifying admixtures can increase the yield stress and the viscosity of cement whereas high-range water reducers can decrease the viscosity at low shear rates much more when compared to the viscosity at high shear rates [165]. A combination of these two additives can increase the performance of cement.

Ultra-fine admixtures (UA), including blast furnace slag (BFS), silica fume (SF), fly ash (FA), limestone (LS), and anhydrous gypsum (AG), also can influence the rheological properties of cement paste. It has been observed that the yield stress decreases with an increase in the UA content and the viscosity decreases with addition of ultra-fine LS, SF, FA, and slag while it increases with AG [174–180]. The effect of ultra-fine slag is more obvious when the UA content is more than 15%. The spherical shape of fly ash particles is found to reduce the viscosity and the yield stress of fresh cement pastes [181,182]. Sybertz and Reick [107] studied the effect of fly ash on the rheological behavior of cement paste and suggested an equation showing the influence of fly ash content on the initial viscosity:

$$\eta_0 = Q_1 \cdot e^{Q_2 \cdot \phi} \cdot (1 - \phi_f) + Q_3 \cdot e^{Q_4 \cdot \phi} \cdot \phi_f \quad (76)$$

where ϕ_f is the fly ash content and Q_1 , Q_2 , Q_3 , and Q_4 are experimental fitting parameters, where $Q_1 = 8.97 \times 10^{-5}$ (Fly Ash I) and 4.04×10^{-5} (Fly Ash II), $Q_2 = 17.1$ (Fly Ash I) and 19.0 (Fly Ash II), $Q_3 = 6.25 \times 10^{-5}$ (Fly Ash I) and 0.54×10^{-5} (Fly Ash II), $Q_4 = 18.4$ (Fly Ash I) and 20.9 (Fly Ash II). Figure 16 shows the effect of different types of fly ash on the initial viscosity. Fly Ash I slightly increases the initial viscosity while Fly Ash II decreases the initial viscosity significantly.

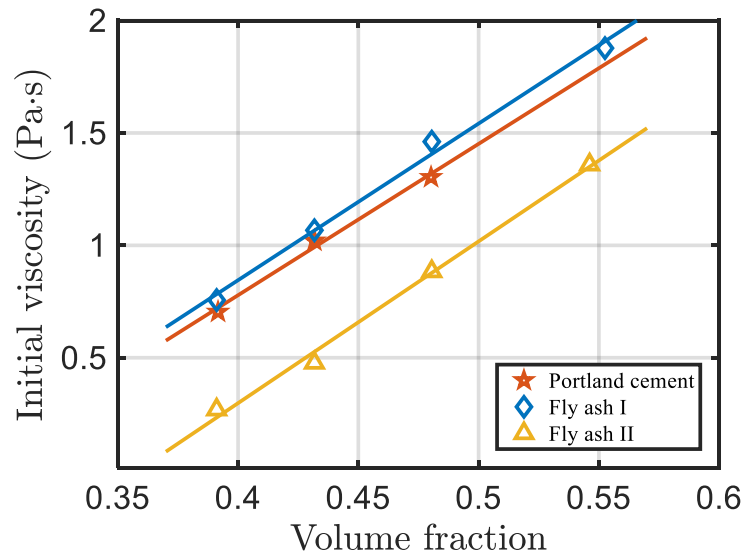


Figure 16. Effect of fly ash additives on the initial viscosity [107].

Hou and Liu [183] found that the addition of synthesizing dispersant extended the thickening time and improved the mobility of the cement slurry. Nehdi [184] noticed that the carbonate filler containing magnesium (MgO) impeded the particle dispersion while accelerating the C_3S hydration, resulting in a rapid increase in the viscosity and the loss of workability for the cement placement.

Sometimes silica flour is added to cement slurries in oil well applications when the temperature exceeds 120°C , in order to prevent decrease in the compressive strength. This additive increases the slurry viscosity and decreases the thickening time [185].

Addition of ultrafine particles to the cement slurry can decrease the yield stress and the plastic viscosity [186]. Application of high content limestone powder to cement seems to improve the fluidity; this can also reduce the amount of the superplasticizer, and reduce the viscosity and the water-to-cement ratio [187]. The addition of nano-additives including nano- SiO_2 (nS) and nano- TiO_2 (nT) can increase the yield stress, the plastic viscosity, and the torque significantly [188]. The addition of Fe_2O_3 nanoparticles can improve the performance of wellbore cement slurries by increasing the viscosity, the elastic properties after early hydration and the suspending ability of cement particles while decreasing the free water, fluid loss, the compressive strength and the thickening time [189]. The addition of cellulose nanofibers (CNF) increases the yield stress, the degree of hydration, and the flexural strength of the cement slurry [190,191]. According to Colombo et al. [192], the addition of softwood calcium lignosulfonate seems to decrease the yield stress and the viscosity of cement pastes. However, it is reported that the application of densified microsilica or nano-silica may have a negative effect on the rheological properties of cement slurry, e.g., inadequate gel strength and stability, poor zonal isolation [193,194]. For a recent numerical study of the cement sheath and wellbore integrity, see Wang and Taleghani [195].

Phan et al. [196] compared the effect of high range water reducing admixture (HRWRA), (changing the granular phase configuration) and viscosity modifying admixture (VMA) (changing the aqueous solution) by applying the Krieger–Dougherty equation (see Equation (57)). It was found that the HRWRA had a bigger influence on the properties (namely, the viscosity increased) than the VMA. The Krieger–Dougherty equation indicates that the viscosity depends more on the configurational skeleton

than on the fluid phase. Emoto and Bier [197] stated that MF 2651 as a plasticizer reduced the viscosity of cement slurry without delaying the hydration process when compared with other plasticizers.

Lu et al. [198] studied the effect of thermo-sensitive viscosity controller (TVC), consisting of inorganic and organic polymeric materials. The cement slurries with TVC become thermally more stable with little thermal thinning between 20 to 120 °C. Velayati et al. [199] investigated the effect of Cassia fistula dry extract on wellbore cement and found that this additive exhibits a retardation property by increasing the thickening time with high efficiency and low costs. Wang et al. [200] studied the effect of chloride additives for cements at low temperatures and found that some chlorides such as LiCl effectively shorten the thickening time and decrease the transition time for static gel strength, while improving the stability of the cement slurry and accelerating the hydration process.

Effect of Water-to-Cement Ratio on the Viscosity

Lapasin et al. [68] showed that the water-to-cement ratio affects the flow behavior of cement slurries. This ratio is defined as the ratio of the weight of water to the weight of cement. From the definition, there is a reverse correlation between volume fraction of cement and water-to-cement ratio. Cements with larger w/c have a smaller concentration. At early stages, w/c has little effect on cement hydration while it has a bigger effect on the physical properties such as strength development, and the setting time [201,202]. The viscosity was found to decrease when the water-to-cement ratio increased [98,115,116,145], shown in Figure 17. It is necessary to increase the w/c of cement slurries for the minimum flow resistances and appropriate injection time when sealing the casing pipes in wellbores [203]. At $w/c = 0.4$, the effect of superplasticizer on rheological properties is not obvious [39]. Massidda and Sanna [204] observed that cement exhibits thixotropic behavior at $w/c = 0.35$ while anti-thixotropic behavior at $w/c > 0.40$. Larger rigidity of slurries (lower w/c and longer hydration time) causes thixotropic behavior while smaller rigidity (higher w/c and shorter hydration time) results in reversible and anti-thixotropic behavior.

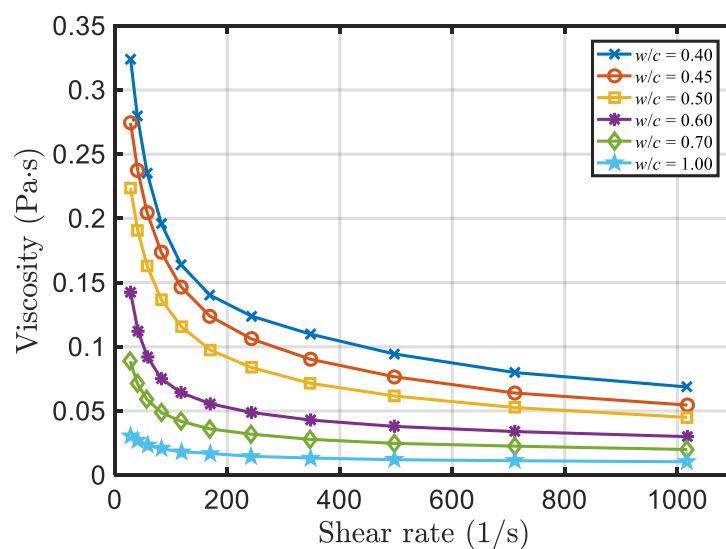


Figure 17. Effect of water-to-cement ratio on the viscosity [116].

Effect of Mixing Method and the Wall Slip on the Viscosity

Yang and Jennings [205] studied the influence of mixing method on the properties of cement paste and found the rheological behavior of cement pastes during the first two hours were significantly affected by the mixing method. Cement pastes have higher peak stresses with hand or paddle mixing than with blender mixing. Williams et al. [206] also noticed that the shear rate during mixing can significantly affect the rheological properties of fresh cement. Orban et al. [207] observed that the plastic viscosity of cement slurries decreases with increasing shear rate. The Yard mixer was found to

increase the plastic viscosity and the yield point significantly [208]. ASTM C1738 protocol increases the plastic viscosity by increasing the volume fraction or the content of polycarboxylate superplasticizer (SP) in cement paste [209]. Increasing the mixing rate can also accelerate the cement hydration process and increase the overall heat in this process [210]. High shear rate of mixing can break down the cement agglomerates before adding water; this is called “irreversible structural breakdown” [5,76].

In oil well cementing, cement slurries are pumped through the annular spaces. Particle migration in cement slurries can cause slip at the walls during shearing, similar to the paper pulp flow inside a transparent pulp. Rubio–Hernández [37] found slippage at the walls or the pipe surface can be a problem during the measurement in a rheometer. This can cause an error in the rheological test. This “slip” is usually caused by particle migration. A clear water layer is detected adjacent to the walls, where the fluid has lower viscosity, resulting in a pseudo wall slip. This is caused by a thin film of liquid less than 1 μm , lubricating the walls of the viscometer [211]. Application of vane methods could eliminate the effect of wall slip [212].

Bannister [213] studied the slip effect in a rotational viscometer. The effect of slip on viscosity using the Metzner–Reed power-law model is:

$$\eta_s = C_S \frac{\tau}{\dot{\gamma}} \quad (77)$$

where C_S is the slip coefficient, depending on the consistency index K . The slip coefficient decreases when K (thicker slurry) or the water content (less particles in the slurry) increases. Table 6 shows a summary of the existing viscosity relationships for cement.

2.2.3. Thixotropic Nature of Cement

Cement slurries can also behave as time-dependent non-Newtonian fluids with disperse particles of many different sizes (10 nm to 100 μm) [58,127,213,214]. In general, as discussed earlier, viscosity of cement depends on the shear rate, the application time, particle concentration, temperature and pressure, etc. Thixotropy and yield stress are two important concepts that need to be considered [215]. According to Barnes [216], the term “*thixotropy*”, first suggested by Freundlich [217], describes the reversible sol-gel transformation under isothermal conditions. This occurs when some of the chemically formed linkages between the cement particles break under shear (also known as structural breakdown). Thus, the process is shear rate dependent and time dependent. In thixotropic fluids, viscosity decreases with time for constant shear rate and the shear stress gradually reaches a steady value depending on the shear rate. This behavior is reversible when the system is in rest and the stress is removed [218]. “*Pseudoplasticity*” is also sometimes used to represent thixotropy with reference to shear rate dependency. For pseudoplastic fluids, viscosity decreases with the increasing of the shear rate. The opposite of “*thixotropy*” is “*antithixotropy*” [219] or “*rheopexy*”, which implies that the structure builds up under shear and breaks down at rest. Antithixotropy (shear-thickening) is the recovery process of thixotropy (shear-thinning), which is different from “*dilatancy*” (shear-thickening) of suspensions with high solid concentration under high shear rates [35]. Figure 18 shows the shear stress vs. shear rate response of different fluids for a constant shear rate test [125].

Table 6. Summary of viscosity relationships for cement.

Effect	Author(s)	Model	Equation No.
Effect of shear rate	Ostwald-de Waele (1929)	$\eta = \frac{\tau}{\dot{\gamma}} = K\dot{\gamma}^{n-1}$	(49)
	Robertson and Stiff (1976)	$\eta_{eff} = \frac{A(\dot{\gamma}_R + C)^B}{\dot{\gamma}_R}$	(50)
	Casson (1959)	$\eta = \frac{1}{\dot{\gamma}} \left[k_0 + k_1 \sqrt{\dot{\gamma}} \right]^2$	(51)
	Carreau–Yasuda (1997)	$\eta = \eta_\infty + (\eta_0 - \eta_\infty) \frac{1 + \ln(1 + k\dot{\gamma})}{1 + k\dot{\gamma}}$	(52)
Effect of volume fraction	Einstein (1906)	$\eta_r = \frac{\eta}{\eta_0} = 1 + \alpha\phi$	(53)
	Roscoe (1952)	$\eta_r = \frac{\eta}{\eta_0} = (1 - \phi)^{-2.5}$	(54)
	Mooney (1951)	$\eta_r = \frac{\eta}{\eta_0} = e^{\left[\frac{\alpha\phi}{(1 - \phi_m)} \right]}$	(55)
	Roscoe (1952)	$\eta_r = \frac{\eta}{\eta_0} = (1 - 1.35\phi)^{-2.5}$	(56)
	Krieger and Dougherty (1959)	$\eta_r = \frac{\eta}{\eta_0} = \left(1 - \frac{\phi}{\phi_m} \right)^{-\alpha\phi_m}$	(57)
	Chen and Lin (2017)	$\eta_r = \left(1 - \frac{\phi}{\phi_m} \right)^{-2.78} e^{0.073t}$	(58)
	Murata and Kikukawa (1973)	$\eta_r = \frac{\eta}{\eta_0} = B_0 e^{(K_1\phi + K_2)}$	(59)
	Sybertz and Reick (1991)	$\eta_0 = Q_1 \cdot e^{Q_2 \cdot \phi}$	(60)
	Mills (1985)	$\eta_r = \frac{\eta}{\eta_0} = \frac{(1 - \phi)}{\left(1 - \frac{\phi}{\phi_m} \right)^2}$	(61)
	Liu (2000)	$\eta_r = \frac{\eta}{\eta_0} = [a(\phi - \phi_m)]^{-n}$	(62)
Chong et al. (1971)	$\eta_r = \frac{\eta}{\eta_0} = \left(1 + \frac{0.75 \cdot \frac{\phi}{\phi_m}}{1 - \frac{\phi}{\phi_m}} \right)^2$	(63)	
Effects of temperature and pressure	Sercombe et al. (2000)	$\frac{1}{\eta_0} = \frac{1}{\eta_{0,0}} e^{\left[-\frac{H}{R} \left(\frac{1}{\theta} - \frac{1}{\theta_0} \right) \right]}$	(64)
		$\tilde{A}(\xi) = \dot{\xi} e^{\left(\frac{E_a}{R\theta} \right)}$	(65)
		$X \approx \frac{\pi}{3} O_v^B I_B G^3 t^4$	(66)
	Scherer et al. (2010)	$G(T, p) \approx G_0 e^{\left(-\frac{\Delta E_G + p\Delta V_G}{R\theta} \right)}$	(67)
		$I_B(T, p) \approx I_0 e^{\left(-\frac{\Delta E_I + p\Delta V_I}{R\theta} \right)}$	(68)
	Pang et al. (2013)	$\dot{\xi}(t) = \dot{\xi}_r(C(\theta, P), t)$	(69)
		$C = e^{\left[\frac{E_a}{R\left(\frac{1}{\theta} - \frac{1}{\theta_0} \right)} + \frac{\Delta V}{R} \left(\frac{P_r}{\theta} - \frac{P_0}{\theta_0} \right) \right]}$	(70)
	$\eta_c = \eta_r \cdot e^{\left[\frac{E}{R\theta_c} \right]}$	(71)	
	$\eta_c = \eta_{c0} + (1000 - \eta_{c0}) \cdot (t/t_v)^n$	(72)	
	$\eta_c = \eta_r \cdot e^{\left[\frac{E}{R\theta_{c0}} \right]} + (1000 - \eta_r \cdot e^{\left[\frac{E}{R\theta_{c0}} \right]}) \cdot (t/t_v)^n$	(73)	
Effect of additives/admixtures	Ivanov and Roshavelov (1990)	$\eta = -300.8 - 357.6X_1 - 553.4X_2 + 575.4X_3 - 80.8X_4 - 22.4X_5 + 293.7X_1X_2 - 329.4X_1X_3 + 14.7X_1X_4 + 57X_1X_5 - 528.4X_2X_3 + 48.9X_2X_4 + 21.2X_2X_5 - 151.1X_3X_4 - 29.3X_3X_5 + 175.2X_4X_5 + 114.4X_1^2 + 152.8X_2^2 + 664.6X_3^2 + 159.2X_4^2 + 213X_5^2$	(75)
	Sybertz and Reick (1991)	$\eta_0 = Q_1 \cdot e^{Q_2 \cdot \phi} \cdot (1 - \phi_f) + Q_3 \cdot e^{Q_4 \cdot \phi} \cdot \phi_f$	(76)
Effect of measurements (slip)	Bannister (1980)	$\eta_s = C_S \frac{\tau}{\dot{\gamma}}$	(77)

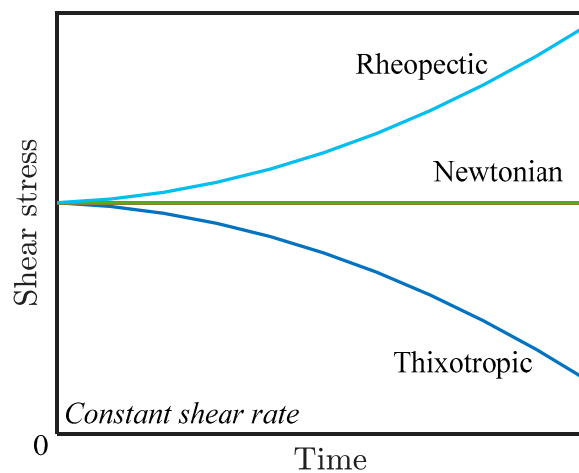


Figure 18. Effect of time on the behavior of various viscous fluids [125].

There are many ways to model the thixotropic effects in fluids. An excellent review is given by Barnes [216]. For a mathematical perspective of modeling thixotropic fluids with yield stress, we refer to [220–222]. An early formulation of suspensions with thixotropy was given by Fredrickson [223]. A more recent mathematical perspective is given by Renardy [224]. There have been other attempts to develop unified models to capture elasto-viscoplastic thixotropic yield stress fluids (see [225,226]).

The thixotropic aspect of cement is an indication that it can become a gel-like structure at rest which is unpumpable while it can be pumped again when stirred [200]. That is, thixotropy results in the development of gel strength and yield stress after the pumping has stopped. A high pressure is needed to restart the pumping. Thus, the thixotropy of cement and the static gel strength along with the yield stress affect the pumping and the restarting difficulties which can be of concern in cement safety (Wang et al. 2017). The thixotropic process (reversible) and the hydration process (irreversible) of cement usually occur simultaneously after the cement clinker is mixed with water. Initially, the thixotropic effect dominates and later the cement hydration process dominates [93]. Yuan et al. [75] assumed that in the intermediate period, only the thixotropic (reversible) process is important and the hydration (irreversible) process can be neglected.

As mentioned before, fresh cement pastes are initially thick colloidal suspensions consisting of cement particles dispersed in water [92]. The structure of suspensions is affected by water-to-cement ratio, particle size distribution, interparticle forces and attraction of the water to solid surfaces [35]. In the initial stages, just after mixing, the dispersed cement particles with high solid concentration coagulate and form a structure within the paste; this structure does not change in the next several hours until setting [97]. Interparticle forces in cement particles are attractive forces overcoming the repulsive forces between the particles, causing very small strains in the cement pastes (0.03%). When the interparticle forces dominate, cement pastes have poor flow properties [227]. Floccules are small clusters of cement particles formed in dilute cement suspensions and combine into large flocculent structures. Aggregations with non-uniformly distributed particles occur in the large flocculent structures, which are composed of high concentration flocs of particles. Flocculated particles form discrete aggregates or gels, as shown in Figure 19.

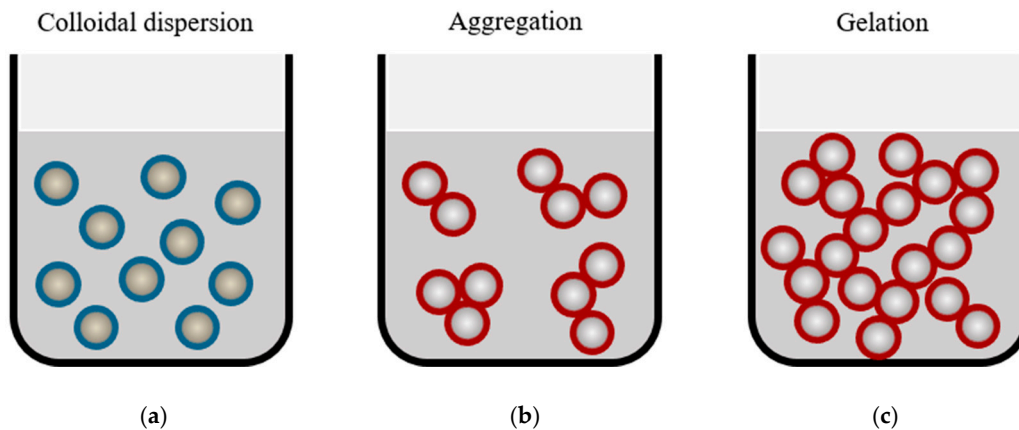


Figure 19. Microstructure of (a) dispersed particles; (b) aggregated particles; (c) gelled particles [228].

Thixotropic behavior is also related to coagulation (particle contacts), dispersion, and re-coagulation of cement particles [36]. The flocculated suspension behaves as viscoelastic solids with storage modulus (the ability to store energy related to deformation of the material) 14–24 kPa in low-strain linear-viscoelastic regions below yield [98]. As the strain increases to a critical value of 10^{-4} , the storage modulus decreases. With the increase of water-to-cement ratio, both the storage modulus and the critical strain decrease. The forces between the flocculated particles are weak and can be broken by shear force. Cement pastes show liquid-like behavior after the flocculated system is broken. During the mixing process, the aggregated cement particles become more uniformly distributed. Flocculent structure keeps breaking down because of the shear during the mixing, causing the thixotropic behavior of cement. At the same time, structural reconstruction occurs, and the flocculent structures rebuild when the shear force is stopped. Thus, cement pastes display two different states: liquid-like under shear conditions and a weak solid-like with a limited yield stress under static conditions. Accordingly, flocculation increases the yield stress and causes pseudoplastic/shear-thinning behavior. It has also been reported that early hydration reaction affects and changes the rheological behavior of fresh cement pastes/slurries from anti-thixotropic to thixotropic [42]. Effects of coagulation, dispersion, and re-coagulation of cement particles have been studied extensively. Cement particles can coagulate in a paste or a slurry; this is primarily caused by the surface attraction forces. Junctions are connections or contacts between the cement particles, consisting of reversible junctions (two particles can be separated) and permanent junctions (two particles cannot be separated).

The cement hydration process consists of a series of chemical reactions between the cement particles and water. From these reactions, the initial fluid-like suspension is transformed into a solid-like material. In general, the effect of cement hydration should be considered when studying rheological behavior of cement.

Hydration reactions result in structural changes, which affect the rheological behavior of cement [229]. The hydration process can cause an exponential increase in the yield stress [131]. Lapasin et al. [58] studied the time-dependent response of cement pastes. They noticed that the shear stresses reached a peak value with increasing age where hydration occurs during the initial stages of the flow (1 min) of the test and decaying to the equilibrium value and then increasing a little [229]. The steady-state flow curves of the cement pastes exhibit shear-thinning behavior and the presence of yield stress. The authors found partially-thixotropic phenomena for the time-dependent behavior of cement pastes. Before the shear rate reaches the initial shear rate value, the shear stress does not increase. At this stage, the kinetics of the structural rebuilding is much less than the kinetics of the structural break-down. After the steady-state conditions has been reached and as the shear rate begins to increase, further structural break-down could be detected because of the different aggregation state of the disperse system at different shear rates. Cement pastes are usually found partially thixotropic in

three stages: power-law shear-thinning fluid under low shear rate, a Newtonian plateau at high shear rates, and a shear-thickening paste [196].

Moore [41] introduced a structural parameter $\lambda(t)$ to describe the structural state of a thixotropic fluid, where λ indicates the degree of flocculation or aggregation (also known as the “degree of jamming”), describing the state of the material at a given time and giving the percentage of the particles in potential wells for colloidal fluids [92,214,230–233]. The value of λ is from 0 to 1. The slurry is considered to be dispersed when $\lambda = 0$, and fully flocculated when $\lambda = 1$. According to Feys and Asghari [234] and other references, λ decreases with time and increases with shear rate, that is,

$$\frac{d\lambda}{dt} = k_+(1 - \lambda) - k_-\dot{\gamma}\lambda \quad (78)$$

where k_+ and k_- represent the structural buildup and the structural breakdown coefficients. The structural parameter λ displays a characteristic relaxation time of t with the change of shear rate:

$$t = 1/(k_+ + k_-\dot{\gamma}) \quad (79)$$

Cheng and Evans [235] proposed a constitutive equation, including the structural parameter λ :

$$\tau = \eta(\lambda, \dot{\gamma})\dot{\gamma} \quad (80)$$

where the viscosity η is a function of shear rate $\dot{\gamma}$ and λ .

A rate-type equation gives the evolution of λ with time. In general, the rate at which the structure changes can be a function of the shear rate and the structural parameter. A rate equation for the structural parameter can be given [235]:

$$\frac{d\lambda}{dt} = g(\lambda, \dot{\gamma}) = K_1(\dot{\gamma})(1 - \lambda)^p - K_2(\dot{\gamma})\lambda^q \quad (81)$$

where $K_1(\dot{\gamma})$ and $K_2(\dot{\gamma})$ are rate constants related to the build-up and the break-down processes. In this equation, the effect of Brownian motion and the shear rate are also considered. The parameters p and q are indications of the orders of the two processes. Lapasin et al. [58] applied Cheng and Evans equation to cement pastes and suggested an alternative equation, where Equation (80) is replaced by:

$$\tau = f_0(\dot{\gamma}) + f_1(\dot{\gamma})\lambda \quad (82)$$

For fresh cement, the structural build-up can be negligible because of the partially thixotropic behavior [236]. Thus, Equation (81) becomes:

$$\frac{d\lambda}{dt} = -K_2(\dot{\gamma})\lambda^q \quad (83)$$

Hattori and Izumi [237] considered the effect of coagulation/junctions on the apparent viscosity at time t and shear rate $\dot{\gamma}$ by suggesting the following relationship for the viscosity:

$$\eta = B_3 \left[\frac{n_3 [U_0(\dot{\gamma}Ht^2 + 1) + Ht]}{(Ht + 1)(\dot{\gamma}t + 1)} \right]^{2/3} \quad (84)$$

where B_3 is the friction coefficient between the cement particles, n_3 is the number of uncoagulated particles in unit volume, U_0 is the initial degree of coagulation (percentage of junctions to total particles), H is the coagulation rate, which is related to particle attraction and cement hydration reactions.

De Kee and Chan Man Fong [71] suggested the following relationship for the viscosity:

$$\eta = \frac{\eta_0 k_c}{\alpha_0} \left[1 + (bf_1 - cf_2)e^{-\alpha_0 t} \right] \quad (85)$$

where

$$\alpha_0 = k_c(1 + bf_1 - cf_2) \quad (86)$$

where the parameters η_0 , k_c , b , c , f_1 and f_2 are functions of the shear rate. When $(bf_1 - cf_2) > 0$, the fluid behaves as a thixotropic model and when $(bf_1 - cf_2) < 0$, it is anti-thixotropic (or rheopectic). They also showed that if $(bf_1' - cf_2') > 0$, the fluid behaves as a shear-thinning fluid, and if $(bf_1' - cf_2') < 0$, as a shear-thickening fluid, where ' (the prime) denotes the derivative with respect to $\dot{\gamma}$. For further details about this model, see Carreau et al. [33] (p. 471).

Coussot et al. [92] suggested the following relationship between λ and $\dot{\gamma}$:

$$\frac{d\lambda}{dt} = \frac{1}{t_0} - \alpha\lambda\dot{\gamma} \quad (87)$$

where t_0 is the characteristic time of aging or rejuvenation, and α is a system-dependent constant.

The instantaneous viscosity based on Coussot's model is defined as a function of the flocculation parameter and the shear rate:

$$\eta = \eta_0 f(\lambda, \dot{\gamma}) = \eta_0(1 + \lambda^n) \quad (88)$$

where η_0 is the viscosity when the flow is not affected by the particle interactions ($\lambda = 0$), and n is a parameter indicating the effect of structural breakdown and reconstruction.

Coussot et al. [92] also proposed an equation (based on the experiment) that a stress ramp is applied after different times of rest. The dimensionless form of shear stress–shear rate relation when the cement is at rest is written as:

$$\tau_s = \dot{\gamma}_s \exp\left(\frac{1}{\dot{\gamma}_s} \left[1 + (\lambda_0 \dot{\gamma}_s - 1) \exp(-\dot{\gamma}_s \bar{t}_r) \right]\right) \quad (89)$$

where τ_s is the shear stress under steady state condition, $\tau_s = \tau\alpha T_0/\eta_0$, the shear rate is $\dot{\gamma}_s = \alpha T_0 \dot{\gamma}$, \bar{t}_r is the dimensionless time during which the cement is at rest for restructuring. This equation is able to describe the rheological behavior of fluids with thixotropy and yield stress.

A general form of a model based on the above ideas was given by Roussel [238,239]:

$$\tau = \tau_y(1 + \lambda) + k\dot{\gamma}^n \quad (90)$$

Roussel [214] suggested a viscosity that depends on the shear rate, as shown in Figure 20a:

$$\eta = \eta_\infty \left(1 + a^n \dot{\gamma}^{-n} \right) a = \frac{1}{\alpha t_r} \quad (91)$$

where n is an experimental parameter with positive value, η_∞ is the viscosity where the shear rate is infinite, α is a system-dependent constant, and t_r is the time during which the cement is at rest for restructuring, which is a constant. For transient flow, the rheological properties change with time. Roussel [214] also gave an evolution equation for the structural flocculation/jamming parameter λ , shown in Figure 20b.

$$\lambda(t) = \frac{a}{\dot{\gamma}} + \left(\lambda_0 - \frac{a}{\dot{\gamma}} \right) \exp\left(-\frac{\dot{\gamma}t}{\alpha t_r}\right) a = \frac{1}{\alpha t_r} \quad (92)$$

where λ_0 is the initial value of λ , α is a system-dependent constant and the applied strain rate $\dot{\gamma}$ is constant. The characteristic time t_c decreases with an increase in the strain rate, which makes reaching the steady state condition harder,

$$t_c = \frac{at_r}{\dot{\gamma}} = \frac{1}{\alpha\dot{\gamma}} \tag{93}$$

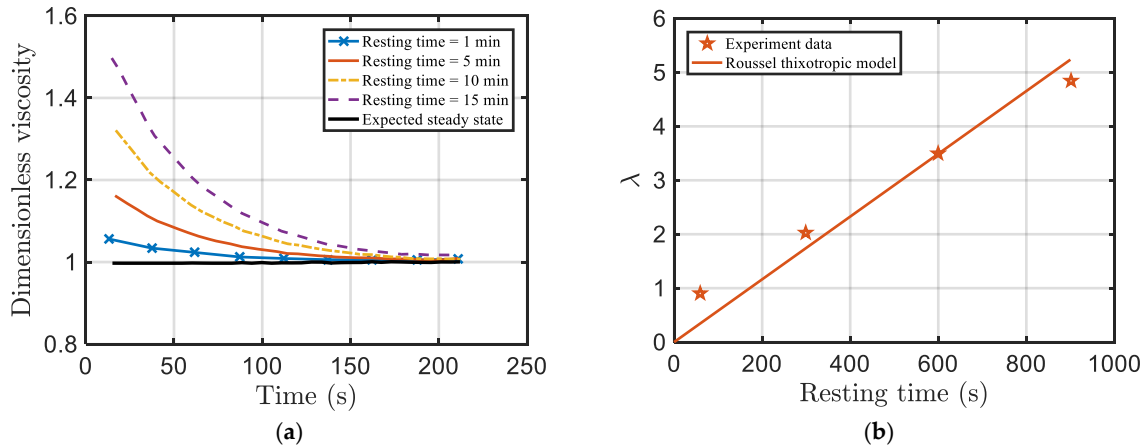


Figure 20. The thixotropic model of Roussel [238]: (a) Dimensionless viscosity at constant shear rate for various resting time; (b) state of flocculation λ vs. resting time.

Wallevik [36] suggested an equation for the shear viscosity that depends on a temporary shear viscosity η_{tmp} , where

$$\eta_s = \left(\eta_p + \frac{\tau_y}{\dot{\gamma}} \right) + \eta_{tmp} \tag{94}$$

where η_p is the plastic viscosity and τ_y is the yield stress; η_{tmp} is related to the number of reversible junctions J_t :

$$\eta_{tmp} = \tilde{\eta}_p + \frac{\tilde{\tau}_y}{\dot{\gamma}} = a_1 B_3 J_t^{2/3} + a_2 B_3 J_t^{2/3} / \dot{\gamma} \tag{95}$$

where $\tilde{\eta}_p$ and $\tilde{\tau}_y$ are the thixotropic counterparts of η_p and τ_y , B_3 is the friction coefficient between the cement particles, and a_1 and a_2 are the two empirical parameters.

Mewis and Wagner [240] provide a generalized thixotropic model for colloidal suspensions:

$$\eta(\dot{\gamma}, \lambda) = \lambda\tau_y + \lambda K_{st} \dot{\gamma}^n + K_\infty \dot{\gamma}^n \tag{96}$$

$$\frac{d\lambda}{dt} = -k_1 \dot{\gamma} \lambda + k_2 \dot{\gamma}^m (1 - \lambda) + k_3 (1 - \lambda) \tag{97}$$

In Equation (96), $\lambda\tau_y$ shows the effect of λ on the yield stress. No yield stress occurs when there is no flocculation. The term $\lambda K_{st} \dot{\gamma}^n$ indicates that the viscosity increases with λ .

Marchesini et al. [34] studied the irreversible time-dependent rheological behavior of cement slurries and presented a transient constitutive model considering the irreversible effect. The structural parameter is given by:

$$\frac{d\lambda}{dt} = \frac{1}{t_{eq}} \left\{ \left[1 - \lambda - (1 - \lambda_{final}) \zeta(t) \right]^a - (1 - \lambda_{eq})^a \left(\frac{\lambda - \lambda_{final} \zeta(t)}{\lambda_{eq}} \right)^b \right\} + \lambda_{final} \dot{\zeta}(t) \tag{98}$$

where t_{eq} and λ_{eq} are the characteristic time and the structural parameter for the thixotropic medium at equilibrium, λ_{final} is the structural parameter of the material at the final equilibrium state, $\zeta(t)$

is a function indicating the evolution of the irreversible processes at time t and a and b are the positive constants.

For an ideal thixotropic behavior, all irreversible processes are neglected, where the irreversible process function $\zeta(t) = 0$, and the structural parameter becomes:

$$\frac{d\lambda_{thixo}}{dt} = \frac{1}{t_{eq}} \left[(1 - \lambda_{thixo})^a - (1 - \lambda_{eq})^a \left(\frac{\lambda_{thixo}}{\lambda_{eq}} \right)^b \right] \quad (99)$$

The irreversible process function ζ_i could be written as a function of time and the structural parameter:

$$\zeta(t, \lambda_{eq}) = 1 - \frac{1}{\left[1 + \left(\frac{t}{t_{reac}} \right)^{1/\lambda_{eq}} \right]^{\frac{(1-m\lambda_{eq})\lambda_{eq}}{l}}} \quad (100)$$

where t_{reac} is the characteristic time for the hydration reactions, l and m are parameters related to the irreversible processes before and after t_{reac} is reached. In this approach, the viscosity function consists of a structural viscosity related to the structural parameter and a pure viscous part in the unstructured state [226,241].

Based on Marchesini et al.'s model, viscosity as a function of the structural parameter is given by:

$$\eta(\lambda) = \eta_{\infty} \left(\frac{1}{1 - \lambda_{thixo}} \right)^{\alpha} \left(\frac{\lambda_{final} - \lambda_{thixo}}{\lambda_{final} - \lambda} \right)^{\epsilon} \quad (101)$$

where η_{∞} is the viscosity of the complete unstructured state and α and ϵ are positive constants.

In this section, we have provided a review of the concept of the thixotropy in cements. A structural parameter λ is introduced to represent the degree of flocculation, which is related to the cement hydration process. Thus, the viscosity is a function of the structural parameter λ and a rate equation for λ (e.g., Equations (81), (97), and (98)) should be used along with the governing equations.

2.2.4. A New Model for Cement Slurry

We suggest that the total stress tensor T is defined as

$$T = T_y + T_v \quad (102)$$

where T_y is yield stress tensor and T_v is the viscous stress tensor. In general, the yield stress can be a function of many parameters, for example, volume fraction, w/c , etc.

$$T_y = T_y \left(\phi, \frac{w}{c}, \dots \right) \quad (103)$$

As mentioned earlier, one of the distinct features of some non-Newtonian fluids is the presence of normal stress effects (see [242]), which are manifestations of non-equal normal stresses when the fluid is sheared. In polymeric fluids, this phenomenon is usually observed as rod-climbing or die-swell; in fact, one of the earliest observations is due to Reynolds [243,244] related to the expansion of the voids in wet sands; he called this effect "dilatancy." Massoudi and Mehrabadi [245] discuss this concept along with the Mohr–Coulomb yield criterion. Later Reiner [246] developed a stress tensor model for wet sand; his theory was generalized by Massoudi [247] where the effects of density (volume fraction) gradient were included. Interestingly, in our review, we did not find any direct reference either to attempts at measuring the normal stress effects in cement or modeling them, despite the similarities between cement paste and wet sand. We propose a new constitutive model for the viscous stress tensor of the cement slurry, T_v , by generalizing the traditional second-grade fluid model [248,249].

$$T_v = -pI + \eta A_1 + \alpha_1 A_2 + \alpha_2 A_1^2 \quad (104)$$

where the viscosity can be a function of various parameters, $\eta = \eta(\dot{\gamma}, \phi, \theta, p, \lambda(t), w/c, \dots)$, α_1 and α_2 are the normal stress coefficients assumed to be constants, $\dot{\gamma}$ is the shear rate, ϕ is the volume fraction, θ is the temperature, p is the pressure, $\lambda(t)$ is the structural parameter describing the degree of flocculation or aggregation and w/c is the water-to-cement ratio. The kinematical tensors A_1 and A_2 are defined as:

$$A_1 = \text{grad}v + (\text{grad}v)^T \quad (105)$$

$$A_2 = \frac{dA_1}{dt} + A_1(\text{grad}v) + (\text{grad}v)^T A_1 \quad (106)$$

The general idea behind suggesting a new constitutive model for the viscous stress tensor T_v that would include the normal stress effects, is that many non-Newtonian fluids such as polymers, dense suspensions, drilling fluids, blood, granular materials, slags, etc. [123,250–255] have been shown to exhibit these non-linear effects. In our previous paper [11], we showed some preliminary results using the newly proposed viscous stress model where the effects of shear-rate dependent viscosity in cement slurries was studied. The Clausius–Duhem inequality shows [256] that for the classical second grade fluids:

$$\eta \geq 0 \alpha_1 \geq 0 \alpha_1 + \alpha_2 = 0 \quad (107)$$

As shown in this paper, for cement slurries/pastes, the viscosity depends on the shear-rate. In Section 2.1, we noticed that the power-law model, also known as the generalized Newtonian fluid (GNF) model [33] is one of the simplest models for shear-rate dependency of viscosity. Therefore, we use this idea and suggest a new model for T_v .

$$T_v = -pI + \mu_0 \left(1 - \frac{\phi}{\phi_m}\right)^{-\beta} (1 + \lambda^n) [1 + \text{tr}A_1^2]^m A_1 + \alpha_1 A_2 + \alpha_2 A_1^2 \quad (108)$$

$$\frac{d\lambda}{dt} = \frac{1}{t_0} - \kappa \lambda \dot{\gamma} \quad (109)$$

where we have used Krieger's idea for the volume fraction dependence of viscosity, η_0 is the (reference) coefficient of viscosity, tr is the trace operator, and m is the power-law exponent, a measure of non-linearity of the fluid, related to the shear-thinning effects (when $m < 0$) or shear-thickening effects (when $m > 0$). Equation (108), we believe, is a general expression for the viscous contribution of the stress tensor, T_v ; for cement slurries, this model potentially is capable of exhibiting normal stress effect, through the terms α_1 and α_2 , thixotropy effects because of the presence of the structural parameter λ , shear-rate dependent effects of the viscosity through the two parameters α and m (showing shear-thinning or shear-thickening effects), and the concentration dependency of viscosity through the two parameters ϕ_m and β . We do plan to use this equation in our future studies, and we do plan to develop/propose a yield stress model, T_y , for cement. A simplified version Equation (108) was used in our earlier study, Tao et al. [11,257].

Alternatively, in the absence of any experimental data related to the normal stress coefficients for the cement, we can suggest a more traditional formulation for the stress tensor T and use Macosko's formulation [31]:

$$T = 2\eta_p \mathbf{D} \quad \text{for } \Pi_{2D}^{1/2} \leq \dot{\gamma}_c$$

$$T = 2 \left[\frac{\tau_y}{|\Pi_{2D}|^{1/2}} + K |\Pi_{2D}|^{\frac{n-1}{2}} \right] \mathbf{D} \quad \text{for } \Pi_{2D}^{1/2} > \dot{\gamma}_c \quad (110)$$

where all the parameters are defined in Equation (8).

By using one of the correlations given for τ_y in Table 4, namely

$$\tau_y(\phi, w/c) = m_1 \frac{\phi^2(\phi - \phi_{perc})}{\phi_m(\phi_m - \phi)} \times (-175w/c + 137) \quad (111)$$

and substituting it in (110), we can obtain a three-dimensional form for the stress tensor considering different effects. Therefore, we assume

$$T_y = 2 \left[\begin{array}{l} T = 2\eta_p \mathbf{D} \\ \frac{m_1 \frac{\phi^2(\phi - \phi_{perc})}{\phi_m(\phi_m - \phi)} \times (-175w/c + 137)}{|\Pi_{2D}|^{1/2}} + K |\Pi_{2D}|^{\frac{n-1}{2}} \end{array} \right] \mathbf{D} \quad \begin{array}{l} \text{for } \Pi_{2D}^{1/2} \leq \dot{\gamma}_c \\ \text{for } \Pi_{2D}^{1/2} > \dot{\gamma}_c \end{array} \quad (112)$$

We can also assume that K could depend on volume fraction, temperature, etc.

3. Concluding Remarks

Rheological behavior of cement is important in cement, concrete, and petroleum engineering industries. In this article, we have provided a comprehensive review of the rheological models used for cement slurries. We have looked at the models describing the total stress tensor for cement as well as the yield stress models and models focusing on the viscous stress tensor. Different effects such as changing the cement concentration, the water-to-cement ratio, the additives/admixtures, the shear rate, the temperature and pressure, the mixing method and the thixotropic nature of cement are taken into consideration. We also propose a new constitutive model where the traditional second-grade fluid model is generalized to include the contributions from variable shear viscosity, concentration, thixotropy, etc.

Author Contributions: M.M. developed the framework of the paper and C.T. did most of the literature review and writing (with help from M.M.). All authors (C.T., B.G.K., E.R. and M.M.) contributed to the editing of the paper. All authors have read and agreed to the published version of the manuscript.

Funding: This research was supported by the U.S. Department of Energy, National Energy Technology Laboratory.

Acknowledgments: This paper is supported by an appointment to the U.S. Department of Energy Postgraduate Research Program for C.T. at the National Energy Technology Laboratory, administrated by the Oak Ridge Institute for Science and Education.

Conflicts of Interest: The authors declare no conflict of interest.

Disclaimer: This report was prepared as an account of work sponsored by an agency of the United States Government. Neither the United States Government nor any agency thereof, nor any of their employees, makes any warranty, express or implied, or assumes any legal liability or responsibility for the accuracy, completeness, or usefulness of any information, apparatus, product, or process disclosed, or represents that its use would not infringe privately owned rights. Reference herein to any specific commercial product, process, or service by trade name, trademark, manufacturer, or otherwise does not necessarily constitute or imply its endorsement, recommendation, or favoring by the United States Government or any agency thereof. The views and opinions of authors expressed herein do not necessarily state or reflect those of the United States Government or any agency thereof.

Appendix A. Cement Chemistry

Figure A1 shows the microstructure of the anhydrous cement powder for silicate phase, aluminate phase, and gypsum.

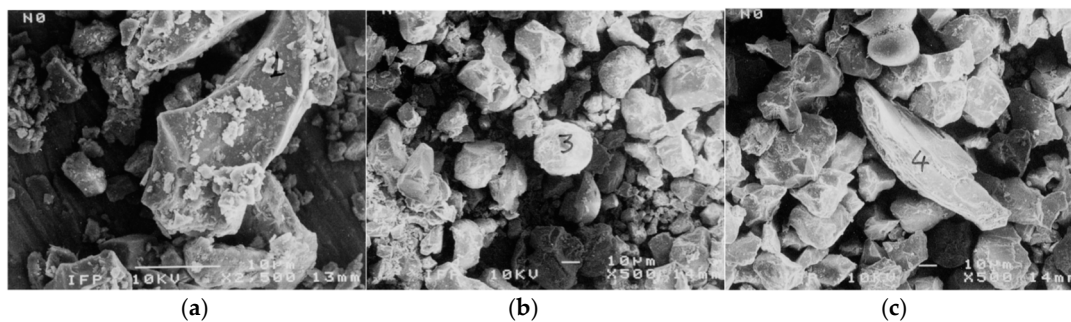


Figure A1. Dry cement image under scanning electron microscope (SEM): (a) silicate phase; (b) aluminate phase; (c) gypsum particle [19].

A cement particle contains: alite (C_3S), belite (C_2S), aluminate phase (C_3A), ferrite phase (C_3AF), alkali sulfate, free lime and gypsum [12,258]. Alite, tricalcium silicate (Ca_3SiO_5), accounts for 40–70% mass of a clinker. It displays a hexagonal crystal behavior with the size up to 150 μm . It reacts with water in a short time and to a large extent determines the strengths at the early age (within 28 day). Belite, dicalcium silicate (Ca_2SiO_4), accounts for 15–45% mass of a clinker. It displays a rounded grain habit with size 5–40 μm [259]. It is less reactive with water than alite and determines the strengths at later age (after 28 days). Alite and belite generate well-crystallized calcium hydroxide and poorly-crystallized calcium silicate hydrate (C-S-H). Tricalcium aluminate ($Ca_3Al_2O_6$), accounts for 1–15% mass of a clinker. It displays lath-like or irregular behavior with size 1–60 μm . It is also reactive with water. *American Petroleum Institute* standards limits the tricalcium aluminate content of a class G cement to lower than 3% [2]. Ferrite is tetracalcium aluminoferrite (Ca_2AlO_5 , Ca_2FeO_5) that accounts for 0–18% mass of a clinker. It displays crystal behavior. Aluminate and ferrite phases are interstitial/matrix phases to bind the silicate crystals. Periclase (MgO) displays crystal behavior with the size up to 30 μm and free lime (CaO) behavior as rounded crystals is isolated or joined with other phases. Both periclase and free lime have less quantities but affect the performance. Alkali sulfates and calcium sulfates are also found in clinker which affect the hydration rates and strength development [259,260]. Besides cement phase composition, surface area of each phase also affects the cement performance. Surface area is affected by the texture of clinker and the grinding conditions.

Increasing the content of C_3S and C_3A is considered to be an effective way to obtain high-initial-strength cement and concrete. However, in modern cement and concrete application, researchers have found lower water-to-cement ratio to also play an important role. It is the closeness of the cement particles and cement concentration that determine the compressive strength of cement and concrete [157]. It is reasonably easy to control rheological properties such as viscosity and yield stress for cements without too much C_3S and C_3A content. For sustainable purpose, Aitcin [157] suggests more mineral components to be added with clinker to lower the water-to-cement ratio and to increase the life cycle of cement and concrete structures and extend the effect of hydraulic binders and aggregates. When mixed with water, the reactions generate calcium silicate and aluminate ions in the solution. Cement hydration consists of three stages: (1) an initial reaction after mixing (at least 15 min); (2) a dormant period during which only weak chemical reactions occur; (3) an actual cement hydration [40]. Among the cement hydrates generated, calcium-silicate-hydrate (C-S-H) and calcium hydroxide (portandite) are two of the most important hydrates. The dissolution-diffusion precipitation process changes anhydrous material into hydrates, which decrease the porosity of the cement [261]. Through the hydration process, cement develops strength in two steps: gelation and setting. Gelation occurs almost immediately after cement is mixed with water. The coagulated system develops some strength, which could easily be broken by mixing. It is not possible to measure the yield stress because of the weakness of the network. Setting starts a few hours after the coagulation/flocculation. During the time between coagulation and setting, also called the dormant period, hydrates nucleate and growth occur. Shear modulus is developed to the GPa range until setting.

Appendix B. Governing Equations of Motion and Heat Transfer

Cement slurries could be mathematically described using the method of continuum mechanics. It is possible to model these slurries using either a single-phase (component) approach or a multi-phase (component) approach. We provide a summary of the governing equations for these two approaches.

Appendix B.1. Single Component Approach

The governing equations of motion include the conservation of mass, linear momentum, angular momentum, convection-diffusion equation [262,263], the energy equation and the entropy inequality. When the slurry is assumed to behave as a non-homogeneous and possibly a (non-linear) fluid, then we have:

- Conservation of mass

$$\frac{\partial \rho}{\partial t} + \operatorname{div}(\rho v) = 0 \quad (\text{A1})$$

where $\partial/\partial t$ is the partial derivative with respect to time, div is the divergence operator, and v is the velocity vector, ρ is the density of the slurry.

- Conservation of linear momentum

$$\rho \frac{dv}{dt} = \operatorname{div} T + \rho b \quad (\text{A2})$$

where b is the body force vector, T is the Cauchy stress tensor, and d/dt is the total time derivative, given by $d(\cdot)/dt = \partial(\cdot)/\partial t + [\operatorname{grad}(\cdot)]v$.

- Conservation of angular momentum

$$T = T^T \quad (\text{A3})$$

This equation indicates that in the absence of couple stresses the stress tensor is symmetric.

- Convection-diffusion equation for the particles

$$\frac{\partial \phi}{\partial t} + \operatorname{div}(\phi v) = -\operatorname{div} N \quad (\text{A4})$$

where N is the particle flux, and ϕ is the particle volume fraction function or volume distribution (related to concentration), which is a continuous function of position, and time, where $0 \leq \phi(x, t) \leq \phi_{max} < 1$. In reality, $\phi = 1$ at a particle and $\phi = 0$ at a void space (fluid).

- Conservation of energy

$$\rho \frac{d\varepsilon}{dt} = T : L - \operatorname{div} q + \rho r \quad (\text{A5})$$

where ε is the specific internal energy, L is the gradient of velocity, q is the heat flux vector, and r is the specific radiant energy. For complete thermodynamical considerations, the application of the second law of thermodynamics (or the entropy inequality), is also needed [264,265]:

$$\rho \dot{\eta} + \operatorname{div} \varphi - \rho s \geq 0 \quad (\text{A6})$$

where $\eta(x, t)$ is the specific entropy density, $\varphi(x, t)$ is the entropy flux, and s is the entropy supply density from external sources, and $\dot{\eta}$ means the material time derivative of η . If we assume that $\varphi = \frac{q}{\theta}$, and $s = \frac{r}{\theta}$, where θ is the absolute temperature, Equation (A6) reduces to the more familiar form of the Clausius–Duhem inequality:

$$\rho \dot{\eta} + \operatorname{div} \frac{q}{\theta} - \rho \frac{r}{\theta} \geq 0 \quad (\text{A7})$$

In this approach, constitutive relations for T , N , q , ε and r are needed in order to achieve “closure” for the governing equations. In this paper, we have followed this approach and we have focused on modeling T .

Appendix B.2. Multi-Phase (Component) Flow Approach

Many researchers have considered cement slurries to behave as multi-phase fluids; in this case the governing equations should be given for all the components [266,267]. In general, two distinct approaches have been used for multi-component flows: (1) “dilute phase approach,” or the Lagrangian approach; (2) “dense phase approach,” or the Eulerian approach. It is the latter approach that is often used for cement. Here we present a summary of this approach using the mixture theory, also known as theory of interacting continua systems [268–270]. The details of mixture theory are provided in the books [271,272]. Conservation laws are written for each component taking into account interaction with other constituents. Constitutive relations are required to achieve “closure.” The mixture theory equations for a multi-component system are as follows [269,270]:

- Conservation of mass:

$$\frac{D^{(\alpha)}\rho_\alpha}{Dt} + \rho_\alpha \operatorname{div} \mathbf{v}^{(\alpha)} = m_\alpha \quad (\text{A8})$$

where $\alpha = 1, 2$.

- Conservation of linear momentum

$$\rho_\alpha \frac{D^{(\alpha)}\mathbf{v}}{Dt} = \operatorname{div} \mathbf{T}^{(\alpha)} + \boldsymbol{\pi}^{(\alpha)} - m_\alpha (\mathbf{v}^{(\alpha)} - \mathbf{J}^{(\alpha)}) + \rho_\alpha \mathbf{F}^\alpha \quad (\text{A9})$$

- Conservation of angular momentum

$$\mathbf{T}_s^{(\alpha)} = \boldsymbol{\lambda}^{(\alpha)} \quad (\text{A10})$$

- Conservation of energy

$$\rho_\alpha \frac{D^{(\alpha)}U_\alpha}{Dt} = \rho_\alpha r_\alpha - \operatorname{div} \mathbf{q}^{(\alpha)} + \psi_\alpha + \operatorname{tr}(\mathbf{T}_s^{(\alpha)} \mathbf{D}^{(\alpha)}) - m_\alpha \left[U_\alpha + \left(\mathbf{J}^\alpha - \frac{1}{2} \mathbf{v}^{(\alpha)} \right) \cdot \mathbf{v}^{(\alpha)} - G_\alpha \right] \quad (\text{A11})$$

- Entropy

$$\sum_\alpha \left[\rho_\alpha \frac{D^{(\alpha)}S_\alpha}{Dt} + m_\alpha S_\alpha + \operatorname{div} \left(\frac{\mathbf{q}^{(\alpha)}}{\theta_\alpha} \right) - \frac{\rho_\alpha r_\alpha}{\theta_\alpha} \right] \geq 0 \quad (\text{A12})$$

where

$$\rho \mathbf{v} = \sum_\alpha \rho_\alpha \mathbf{v}^{(\alpha)} \quad (\text{A13})$$

$$\frac{D^{(\alpha)}\beta}{Dt} = \frac{\partial \beta}{\partial t} + \mathbf{v}^{(\alpha)} \cdot \operatorname{grad} \beta \quad (\text{A14})$$

for any scalar β , and

$$\frac{D^{(\alpha)}\mathbf{w}}{Dt} = \frac{\partial \mathbf{w}}{\partial t} + (\operatorname{grad} \mathbf{w}) \mathbf{v}^{(\alpha)} \quad (\text{A15})$$

for any vector \mathbf{w} , where

$$\sum_\alpha m_\alpha = 0 \quad (\text{A16})$$

$$\sum_\alpha (\boldsymbol{\pi}^{(\alpha)} + m_\alpha \mathbf{J}^{(\alpha)}) = 0 \quad (\text{A17})$$

The entropy inequality becomes:

$$\sum_{\alpha} \eta_{\alpha} \geq 0 \quad (\text{A18})$$

where

$$\eta_{\alpha} = -\rho_{\alpha} \frac{D^{(\alpha)} A_{\alpha}}{Dt} - \rho_{\alpha} S_{\alpha} \frac{D^{(\alpha)} \theta_{\alpha}}{Dt} - m_{\alpha} \left[A_{\alpha} + \left(\mathbf{J}^{(\alpha)} - \frac{1}{2} \mathbf{v}^{(\alpha)} \cdot \mathbf{v}^{(\alpha)} - G_{\alpha} \right) + \psi_{\alpha} \right. \\ \left. + \text{tr} \left(\mathbf{T}_s^{(\alpha)} \mathbf{D}^{(\alpha)} \right) - \frac{\mathbf{q}^{\alpha} \cdot \text{grad} \theta_{\alpha}}{\theta_{\alpha}} \right] \quad (\text{A19})$$

where ρ_{α} is the density of the α component, \mathbf{v} is the velocity vector, \mathbf{D} is the symmetric part of the velocity gradient, \mathbf{T} is the stress tensor, $\boldsymbol{\pi}$ represents the interaction forces, θ is the temperature, U is the internal energy, r is the radiant heating, A_{α} is the Helmholtz free energy $A_{\alpha} = U_{\alpha} - \theta_{\alpha} S_{\alpha}$, S_{α} is the entropy per unit mass, \mathbf{q} is the heat flux vector, and ψ_{α} , m_{α} , and G_{α} are the supply terms. $\mathbf{T}_s^{(\alpha)}$ is the symmetric part of the partial stress tensor $\mathbf{T}^{(\alpha)}$, and $\boldsymbol{\lambda}^{(\alpha)}$ is an anti-symmetric second-order tensor. The entropy inequality is used to impose certain restrictions on the types of motions and processes. Constitutive relations are required for A_{α} , S_{α} , $\boldsymbol{\pi}$, \mathbf{q} , and $\mathbf{T}^{(\alpha)}$.

In reactive flows, for example those encountered in cement slurries, a series of hydration reactions happen after the components are mixed with water. Some researchers have applied a finite rate model, using the eddy dissipation concept [273]. For cement, the volumetric reaction model and the eddy dissipation model were applied for hydration reactions and interaction between turbulence and chemical reactions [274,275].

Appendix C. Computational Fluid Dynamics Studies

Wallevik [36,276] developed a computational fluid dynamics (CFD) software called viscometric-visco-plastic-flow (VVPF) to study the steady-state and transient flows. Visco-plastic materials with yield stress and thixotropic behavior such as fresh concrete, mortar, and cement paste were studied using the Bingham fluid model. Finite difference method based on alternating direction implicit technique was applied in this software. Moyers-Gonzalez and Frigaard [277] investigated the kinematic instabilities in two-layer eccentric annular flows during oil and gas well cementing process. A non-Newtonian fluid model with shear-thinning and yield stress, namely the Herschel–Bulkley model, was used. Manzar and Shah [278] applied FLUENT for the CFD analysis of slurries used in petroleum industry in different pipes. Lootens et al. [48] used a 3D Bingham fluid model to study the visco-plastic flow of cement pastes under penetrometer test using the Flow3D solver [279]. Malekmohammadi et al. [266] studied the buoyancy-driven flow of non-Newtonian fluids in a horizontal pipe and solved the multi-phase momentum conservation equations using the finite volume method and volume of fluid method (VOF) [280]. Cremonesi et al. [281] simulated the transient flow of non-Newtonian fresh cement suspensions by using the Lagrangian formulation of the Navier–Stokes equations based on the particle finite element approach. The governing equations including the momentum and the mass conservation for the Bingham model are solved using FLUENT software. Aranha et al. [282] developed an in-house software to simulate the annular fluid displacement in vertical and directional offshore wells for Newtonian and non-Newtonian fluids. Wu et al. [155] developed a mathematical model for fresh cement pastes using the numerical software COMSOL (“Heat Transfer in Fluids” model), considering the effects of temperature and cement hydration. Bu et al. [283] modeled the flow characteristics of cement slurry in an eccentric annulus for laminar conditions. The authors used the Herschel–Bulkley model and obtained numerical solution using ANSYS FLUENT. Zulqarnain and Tyagi [284] studied the fluid displacements in the casing-formation annulus to predict the final cement volume fraction in the annulus for different operating conditions. Zhao et al. [285] applied Lattice Boltzmann method (LBM) to investigate the behavior of shear-thinning fluids in a cementing operation in a horizontal eccentric annulus. A 2D flow model was used along with ANSYS FLUENT solver. Anglade et al. [286] analyzed the flow of fresh cement suspensions using the finite element method, where both shear-thinning and shear-thickening behavior are considered. Wu et al. [287] applied a modified LBM for Herschel–Bulkley fluids for more stable and accurate

simulations. This modified Herschel–Bulkley model was used to study the flow between parallel plates and flow in the screw extruder in cement 3D printing. Bao et al. [288] used the Bingham and the power-law fluid models in porous media to study the flow between parallel plates with discrete fracture modeling (DFM) by applying the open-source MATLAB Reservoir Simulation Toolbox (MRST). Tardy and Bittleston [289,290] solved the flow in 2D and 3D axial-azimuthal-radial space and annular displacement of wellbore completion by considering Newtonian fluids with CAFFA and ANSYS FLUENT CFD software. Zhou et al. [291] developed a new model to look at gas migration in non-Newtonian fluids with yield stress and the factors affecting the wellhead pressure change by the analysis of variance (ANOVA). Naccache et al. [292] performed a numerical simulation to study the displacement of two fluids (e.g., cement slurries and drilling fluids) in vertical annular pipe in the cementing operation in the petroleum industry. For the multiphase fluid problem, the governing equations were solved by using the ANSYS FLUENT. A generalized Newtonian fluid (GNF) was used and the regularized Herschel–Bulkley equation was applied for the viscosity of viscoplastic fluids. Foroushan et al. [293] modeled the instability of interface and fluid mixing of cement slurry and drilling mud during cementing operations in oil and gas wells in 3D using ANSYS FLUENT. Skadsem et al. [294] studied the flow of non-Newtonian fluid in an inclined wellbore with concentric and eccentric configurations numerically and experimentally. The 3D flow model for the two fluids was solved with biviscosity approach and finite element simulation in OpenFOAM. Liu et al. [273] modeled the multi-phase pipe flow considering the hydration effects of cemented paste backfill slurry by using a CFD model with ANSYS FLUENT. Murphy et al. [295] simulated the shear flow of two Bingham plastic cement slurries containing Portland cement and fly ash particles by applying fast lubrication dynamics-discrete element model with LAMMPS. Rosenbaum et al. [296] studied the influence of bubbles on foamed cement viscosity using an Extended Stokesian Dynamics Approach with LAMMPS.

Many optimization algorithms are also used in the cement industry. For example, Ohen and Blick [297] used the golden section search method to determine the parameters in the Robertson–Stiff non-Newtonian fluid model. Shahriar and Nehdi applied an artificial neural network (ANN) [298], multiple regression analysis (MRA) [299] and factorial design approach [300] to predict the shear flow and rheological properties (Bingham parameters including yield stress and plastic viscosity) of oil well cement slurries by comparing and validating with the experimental database. The rheological properties with this ANN model were sensitive to the effect of temperature and admixture content of oil well cement. Velayati et al. [4] optimized the cement formulations based on a series of criteria to evaluate the performance of cement slurry under gas migration. The optimization plan was verified by fluid migration analysis (FMA) test. Optimization algorithms including the deterministic simplex method and the stochastic genetic method were applied to determine the parameters in the Herschel–Bulkley model for fresh cement suspensions [9]. Multi-objective optimization methods, such as support vector regression (SVR), model tress (MT), M5 model rules, mix and design approach, particle swarm optimizations (PSO) and response surface method (RSM) are also used in cement chemistry and hydration processes to obtain optimal chemical combination and proportion for better cement performance, workability, and energy consumptions [201,301–304].

References

1. Sabins, F.; Wiggins, M.L. Parametric study of gas entry into cemented wellbores. *Oceanogr. Lit. Rev.* **1998**, *1*, 182.
2. Lootens, D.; Hébraud, P.; Lécolier, E.; Van Damme, H. Gelation, Shear-Thinning and Shear-Thickening in Cement Slurries. *Oil Gas Sci. Technol.* **2004**, *59*, 31–40. [[CrossRef](#)]
3. Banfill, P.F. The rheology of fresh cement and concrete—a review. In Proceedings of the 11th International Cement Chemistry Congress, Durban, South Africa, 11–16 May 2003; Volume 1, pp. 50–62.
4. Velayati, A.; Tokhmechi, B.; Soltanian, H.; Kazemzadeh, E. Cement slurry optimization and assessment of additives according to a proposed plan. *J. Nat. Gas Sci. Eng.* **2015**, *23*, 165–170. [[CrossRef](#)]

5. Hodne, H.; Saasen, A.; O'Hagan, A.B.; Wick, S.O. Effects of time and shear energy on the rheological behaviour of oilwell cement slurries. *Cem. Concr. Res.* **2000**, *30*, 1759–1766. [CrossRef]
6. Sabins, F.; Childs, J.D. Method of Using Thixotropic Cements for Combating Gas Migration Problems. U.S. Patent 4524828, 25 June 1985.
7. Shahin, G.T., Jr. Method for Monitoring Well Cementing Operations. U.S. Patents 6125935, 3 October 2000.
8. Vuk, T.; Ljubičić-Mlakar, T.; Gabrovsšek, R.; Kaucičič, V. Tertiary gelation of oilwell cement. *Cem. Concr. Res.* **2000**, *30*, 1709–1713. [CrossRef]
9. Li, Z.; Vandenbossche, J.; Iannacchione, A.; Brigham, J.; Kutchko, B. Theory-Based Review of Limitations with Static Gel Strength in Cement/Matrix Characterization. *SPE Drill. Complet.* **2016**, *31*, 145–158. [CrossRef]
10. Prohaska, M.; Ogbe, D.O.; Economides, M.J. Determining wellbore pressures in cement slurry columns. In Proceedings of the SPE Western Regional Meeting, Anchorage, AK, USA, 26–28 May 1993.
11. Tao, C.; Kutchko, B.G.; Rosenbaum, E.; Wu, W.-T.; Massoudi, M. Steady Flow of a Cement Slurry. *Energies* **2019**, *12*, 2604. [CrossRef]
12. Taylor, H.F. *Cement Chemistry*; Thomas Telford: London, UK, 1997; ISBN 0-7277-2592-0.
13. Brothers, L.E.; Palmer, A.V. Cementing in Deep Water Offshore Wells. U.S. Patents 6835243, 28 December 2004.
14. Scherer, G.W.; Funkhouser, G.P.; Peethamparan, S. Effect of pressure on early hydration of class H and white cement. *Cem. Concr. Res.* **2010**, *40*, 845–850. [CrossRef]
15. American Petroleum Institute (API). *10B Recommended Practice for Testing Oil Well Cements and Cement Additives*; American Petroleum Institute: Washington, DC, USA, 1997.
16. Kumar, S.; Singh, C.J.; Singh, R.P.; Kachari, J. Microfine cement: Special superfine Portland cement. In Proceedings of the 7th NCB International Seminar, New Delhi, India, 30 April 2002.
17. Saasen, A.; Rafoss, E.; Behzadi, A. Experimental investigation of rheology and thickening time of class G oil well cement slurries containing glycerin. *Cem. Concr. Res.* **1991**, *21*, 911–916. [CrossRef]
18. Mindess, S.; Young, J.F. *Concrete*; Prentice Hall: Englewood, NJ, USA, 1981.
19. Vlachou, P.-V.; Piau, J.-M. Physicochemical study of the hydration process of an oil well cement slurry before setting. *Cem. Concr. Res.* **1999**, *29*, 27–36. [CrossRef]
20. Frigaard, I.A.; Paso, K.G.; de Souza Mendes, P.R. Bingham's model in the oil and gas industry. *Rheol. Acta* **2017**, *56*, 259–282. [CrossRef]
21. Banfill, P.F.G. Rheology of fresh cement paste. In *Annual Transactions of The Nordic Rheology Society*; 1997; Available online: <https://researchportal.hw.ac.uk/en/publications/rheology-of-fresh-cement-paste> (accessed on 23 January 2020).
22. Shahriar, A. Investigation on Rheology of Oil Well Cement Slurries. Ph.D. Dissertation, University of Western Ontario, London, ON, Canada, 2011.
23. Rice, J.A.; Gu, C.; Li, C.; Guan, S. A radar-based sensor network for bridge displacement measurements. In Proceedings of the Sensors and Smart Structures Technologies for Civil, Mechanical, and Aerospace Systems 2012, San Diego, CA, USA, 11–15 March 2012; Volume 8345, p. 83450I.
24. Guan, S.; Rice, J.A.; Li, C.; Gu, C. Automated DC offset calibration strategy for structural health monitoring based on portable CW radar sensor. *IEEE Trans. Instrum. Meas.* **2014**, *63*, 3111–3118. [CrossRef]
25. Guan, S.; Rice, J.A.; Li, C.; Li, Y.; Wang, G. Dynamic and static structural displacement measurement using backscattering DC coupled radar. *Smart Struct. Syst.* **2015**, *16*, 521–535. [CrossRef]
26. Guan, S.; Rice, J.A.; Li, C.; Li, Y.; Wang, G. Structural displacement measurements using DC coupled radar with active transponder. *Struct. Control Health Monit.* **2017**, *24*, e1909. [CrossRef]
27. Helsel, M.A.; Ferraris, C.F.; Bentz, D. Comparative study of methods to measure the density of Cementitious powders. *J. Test. Eval.* **2015**, *44*, 2147–2154. [CrossRef]
28. Bentz, D.P.; Garboczi, E.J.; Haecker, C.J.; Jensen, O.M. Effects of cement particle size distribution on performance properties of Portland cement-based materials. *Cem. Concr. Res.* **1999**, *29*, 1663–1671. [CrossRef]
29. Chindaprasirt, P.; Jaturapitakkul, C.; Sinsiri, T. Effect of fly ash fineness on compressive strength and pore size of blended cement paste. *Cem. Concr. Compos.* **2005**, *27*, 425–428. [CrossRef]
30. Schowalter, W.R. *Mechanics of Non-Newtonian Fluids*; Pergamon Press: Oxford, UK, 1978; ISBN 0-08-021778-8.
31. Macosko, C.W.; Larson, R.G. *Rheology: Principles, Measurements, and Applications*; Wiley: Hoboken, NJ, USA, 1994.
32. Bird, R.B.; Armstrong, R.C.; Hassager, O. Dynamics of Polymeric Liquids. Volume 1: Fluid Mechanics. 1987. Available online: https://inis.iaea.org/search/search.aspx?orig_q=RN:18088690 (accessed on 23 January 2020).

33. Carreau, P.J.; De Kee, D.C.R.; Chhabra, R.P. *Rheology of Polymeric Systems: Principles and Applications*; Hanser Publishers: New York, NY, USA, 1997.
34. Marchesini, F.H.; Oliveira, R.M.; Althoff, H.; de Souza Mendes, P.R. Irreversible time-dependent rheological behavior of cement slurries: Constitutive model and experiments. *J. Rheol.* **2019**, *63*, 247–262. [[CrossRef](#)]
35. Shaughnessy, R.; Clark, P.E. The rheological behavior of fresh cement pastes. *Cem. Concr. Res.* **1988**, *18*, 327–341. [[CrossRef](#)]
36. Wallevik, J.E. Thixotropic investigation on cement paste: Experimental and numerical approach. *J. Non-Newton. Fluid Mech.* **2005**, *132*, 86–99. [[CrossRef](#)]
37. Rubio-Hernández, F.-J. Rheological Behavior of Fresh Cement Pastes. *Fluids* **2018**, *3*, 106. [[CrossRef](#)]
38. Lapasin, R.; Papo, A.; Rajgelj, S. Flow behavior of fresh cement pastes. A comparison of different rheological instruments and techniques. *Cem. Concr. Res.* **1983**, *13*, 349–356. [[CrossRef](#)]
39. Asaga, K.; Roy, D.M. Rheological properties of cement mixes: IV. Effects of superplasticizers on viscosity and yield stress. *Cem. Concr. Res.* **1980**, *10*, 287–295. [[CrossRef](#)]
40. Barbic, L.; Tinta, V.; Lozar, B.; Marinkovic, V. Effect of Storage Time on the Rheological Behavior of Oil Well Cement Slurries. *J. Am. Ceram. Soc.* **1991**, *74*, 945–949. [[CrossRef](#)]
41. Moore, F. The rheology of ceramic slip and bodies. *Trans. Brit. Ceram. Soc.* **1959**, *58*, 470–492.
42. Ish-Shalom, M.; Greenberg, S.A. The Rheology of Fresh Portland Cement Pastes. 1960. Available online: <https://trid.trb.org/view/102102> (accessed on 23 January 2020).
43. Odler, I. Hydration, setting and hardening of Portland cement. *LEA's Chem. Cem. Concr.* **1998**, *4*, 241–297.
44. Bingham, E.C. *Fluidity and Plasticity*; McGraw-Hill: New York City, NY, USA, 1922; Volume 2.
45. Atzeni, C.; Massidda, L.; Sanna, U. Comparison between rheological models for portland cement pastes. *Cem. Concr. Res.* **1985**, *15*, 511–519. [[CrossRef](#)]
46. Robertson, R.E.; Stiff, H.A., Jr. An improved mathematical model for relating shear stress to shear rate in drilling fluids and cement slurries. *Soc. Pet. Eng. J.* **1976**, *16*, 31–36. [[CrossRef](#)]
47. Macosko, C.W.; Krieger, I.M. Rheology: Principles, Measurements, and Applications. *J. Colloid Interface Sci.* **1996**, *178*, 382.
48. Lootens, D.; Jousset, P.; Martinie, L.; Roussel, N.; Flatt, R.J. Yield stress during setting of cement pastes from penetration tests. *Cem. Concr. Res.* **2009**, *39*, 401–408. [[CrossRef](#)]
49. Denn, M.M. *Polymer Melt Processing: Foundations in Fluid Mechanics and Heat Transfer*; Cambridge University Press: Cambridge, UK, 2008; ISBN 1-316-58314-7.
50. White, J.L. Approximate constitutive equations for slow flow of rigid plastic viscoelastic fluids. *J. Non-Newton. Fluid Mech.* **1981**, *8*, 195–202. [[CrossRef](#)]
51. Lipscomb, G.G.; Denn, M.M. Flow of Bingham fluids in complex geometries. *J. Non-Newton. Fluid Mech.* **1984**, *14*, 337–346. [[CrossRef](#)]
52. Mendes, P.R.S.; Dutra, E.S. Viscosity function for yield-stress liquids. *Appl. Rheol.* **2004**, *14*, 296–302. [[CrossRef](#)]
53. Herschel, W.H.; Bulkley, R. Measurement of consistency as applied to rubber-benzene solutions. *Am. Soc. Test. Mater.* **1926**, *26*, 621–633.
54. Jones, T.E.R.; Taylor, S. A mathematical model relating the flow curve of a cement paste to its water/cement ratio. *Mag. Concr. Res.* **1977**, *29*, 207–212. [[CrossRef](#)]
55. Choi, M.; Prud'homme, R.K.; Scherer, G. Rheological evaluation of compatibility in oil well cementing. *Appl. Rheol.* **2017**, *27*, 43354.
56. Ostwald, W. Ueber die rechnerische Darstellung des Strukturgebietes der Viskosität. *Colloid Polym. Sci.* **1929**, *47*, 176–187. [[CrossRef](#)]
57. Williamson, R.V. The flow of pseudoplastic materials. *Ind. Eng. Chem.* **1929**, *21*, 1108–1111. [[CrossRef](#)]
58. Lapasin, R.; Papo, A.; Rajgelj, S. The phenomenological description of the thixotropic behaviour of fresh cement pastes. *Rheol. Acta* **1983**, *22*, 410–416. [[CrossRef](#)]
59. Eyring, H. Viscosity, plasticity, and diffusion as examples of absolute reaction rates. *J. Chem. Phys.* **1936**, *4*, 283–291. [[CrossRef](#)]
60. Sisko, A.W. The flow of lubricating greases. *Ind. Eng. Chem.* **1958**, *50*, 1789–1792. [[CrossRef](#)]
61. Papo, A. Rheological models for cement pastes. *Mater. Struct.* **1988**, *21*, 41–46. [[CrossRef](#)]
62. Casson, N. Rheology of disperse systems. In *Proceedings of a Conference Organized by the British Society of Rheology*; Pergamon Press: New York, NY, USA, 1959.

63. Kok, M.V.; Karakaya, G. Fluid migration and rheological properties of different origin G-class cements in oil well drilling applications. *Int. J. Oil Gas Coal Technol.* **2018**, *19*, 449–457. [[CrossRef](#)]
64. Shangraw, R.; Grim, W.; Mattocks, A.M. An Equation for Non-Newtonian Flow. *Trans. Soc. Rheol.* **1961**, *5*, 247–260. [[CrossRef](#)]
65. Beirute, R.M.; Flumerfelt, R.W. An Evaluation of the Robertson-Stiff Model Describing Rheological Properties of Drilling Fluids and Cement Slurries. *Soc. Pet. Eng. J.* **1977**, *17*, 97–100. [[CrossRef](#)]
66. Batra, R.L.; Parthasarathy, H. Flow of a Robertson-Stiff Fluid Between Two Approaching Disks. *Polym. Plast. Technol. Eng.* **1996**, *35*, 497–516. [[CrossRef](#)]
67. Vom Berg, W. Influence of specific surface and concentration of solids upon the flow behaviour of cement pastes. *Mag. Concr. Res.* **1979**, *31*, 211–216. [[CrossRef](#)]
68. Lapasin, R.; Longo, V.; Rajgelj, S. Thixotropic behaviour of cement pastes. *Cem. Concr. Res.* **1979**, *9*, 309–318. [[CrossRef](#)]
69. Billberg, P. Development of SCC static yield stress at rest and its effect on the lateral form pressure. In *SCC 2005, Combining the Second North American Conference on the Design and Use of Self-Consolidating Concrete and the Fourth International RILEM Symposium on Self-Compacting Concrete*; 2005; pp. 583–589. Available online: <http://www.diva-portal.org/smash/record.jsf?pid=diva2%3A343052&dsid=4012> (accessed on 23 January 2020).
70. Quemada, D. Models for rheological behavior of concentrated disperse media under shear. *Adv. Rheol.* **1984**, *2*, 571–582.
71. De Kee, D.; Chan Man Fong, C.F. Rheological properties of structured fluids. *Polym. Eng. Sci.* **1994**, *34*, 438–445. [[CrossRef](#)]
72. Yahia, A.; Khayat, K.H. Applicability of rheological models to high-performance grouts containing supplementary cementitious materials and viscosity enhancing admixture. *Mater. Struct.* **2003**, *36*, 402–412. [[CrossRef](#)]
73. Yahia, A.; Khayat, K. Analytical models for estimating yield stress of high-performance pseudoplastic grout. *Cem. Concr. Res.* **2001**, *31*, 731–738. [[CrossRef](#)]
74. Vipulanandan, C.; Heidari, M.; Qu, Q.; Farzam, H.; Pappas, J.M. Behavior of piezoresistive smart cement contaminated with oil based drilling mud. In *Proceedings of the Offshore Technology Conference*, Houston, TX, USA, 5–8 May 2014.
75. Yuan, B.; Yang, Y.; Tang, X.; Xie, Y. A starting pressure prediction of thixotropic cement slurry: Theory, model and example. *J. Pet. Sci. Eng.* **2015**, *133*, 108–113. [[CrossRef](#)]
76. Tattersall, G.H.; Banfill, P.F. *The Rheology of Fresh Concrete*; The National Academies of Sciences, Engineering, and Medicine: Washington, DC, USA, 1983; ISBN 0-273-08558-1. Available online: <https://trid.trb.org/view/199391> (accessed on 23 January 2020).
77. Barnes, H.A.; Walters, K. The yield stress myth? *Rheol. Acta* **1985**, *24*, 323–326. [[CrossRef](#)]
78. Barnes, H.A. The ‘yield stress myth’? paper—21 years on. *Appl. Rheol.* **2007**, *17*, 43110-1–43110-5. [[CrossRef](#)]
79. Barnes, H.A. The yield stress—A review or ‘παντα ρει’—Everything flows? *J. Non-Newton. Fluid Mech.* **1999**, *81*, 133–178. [[CrossRef](#)]
80. Hartnett, J.P.; Hu, R.Y. The yield stress—An engineering reality. *J. Rheol.* **1989**, *33*, 671–679. [[CrossRef](#)]
81. Astarita, G. Letter to the Editor: The engineering reality of the yield stress. *J. Rheol.* **1990**, *34*, 275–277. [[CrossRef](#)]
82. Evans, I.D. Letter to the editor: On the nature of the yield stress. *J. Rheol.* **1992**, *36*, 1313–1318. [[CrossRef](#)]
83. Papanastasiou, T.C. Flows of materials with yield. *J. Rheol.* **1987**, *31*, 385–404. [[CrossRef](#)]
84. Bonn, D.; Denn, M.M. Yield stress fluids slowly yield to analysis. *Science* **2009**, *324*, 1401–1402. [[CrossRef](#)]
85. Denn, M.M.; Bonn, D. Issues in the flow of yield-stress liquids. *Rheol. Acta* **2011**, *50*, 307–315. [[CrossRef](#)]
86. Moller, P.; Fall, A.; Chikkadi, V.; Derks, D.; Bonn, D. An attempt to categorize yield stress fluid behaviour. *Philos. Trans. Royal Soc. A Math. Phys. Eng. Sci.* **2009**, *367*, 5139–5155. [[CrossRef](#)] [[PubMed](#)]
87. Bird, R.B.; Dai, G.C.; Yarusso, B.J. The rheology and flow of viscoplastic materials. *Rev. Chem. Eng.* **1983**, *1*, 1–70. [[CrossRef](#)]
88. Møller, P.C.; Mewis, J.; Bonn, D. Yield stress and thixotropy: On the difficulty of measuring yield stresses in practice. *Soft Matter* **2006**, *2*, 274–283. [[CrossRef](#)]
89. Dinkgreve, M.; Paredes, J.; Denn, M.M.; Bonn, D. On different ways of measuring “the” yield stress. *J. Non-Newton. Fluid Mech.* **2016**, *238*, 233–241. [[CrossRef](#)]

90. Nguyen, Q.D.; Boger, D.V. Measuring the flow properties of yield stress fluids. *Annu. Rev. Fluid Mech.* **1992**, *24*, 47–88. [[CrossRef](#)]
91. Coussot, P. Yield stress fluid flows: A review of experimental data. *J. Non-Newton. Fluid Mech.* **2014**, *211*, 31–49. [[CrossRef](#)]
92. Coussot, P.; Nguyen, Q.D.; Huynh, H.T.; Bonn, D. Viscosity bifurcation in thixotropic, yielding fluids. *J. Rheol.* **2002**, *46*, 573–589. [[CrossRef](#)]
93. Jarny, S.; Roussel, N.; Rodts, S.; Bertrand, F.; Le Roy, R.; Coussot, P. Rheological behavior of cement pastes from MRI velocimetry. *Cem. Concr. Res.* **2005**, *35*, 1873–1881. [[CrossRef](#)]
94. Roussel, N.; Ovarlez, G.; Garrault, S.; Brumaud, C. The origins of thixotropy of fresh cement pastes. *Cem. Concr. Res.* **2012**, *42*, 148–157. [[CrossRef](#)]
95. Mahaut, F.; Mokéddem, S.; Chateau, X.; Roussel, N.; Ovarlez, G. Effect of coarse particle volume fraction on the yield stress and thixotropy of cementitious materials. *Cem. Concr. Res.* **2008**, *38*, 1276–1285. [[CrossRef](#)]
96. Schmidt, G.; Schlegel, E. Rheological characterization of CSH phases–water suspensions. *Cem. Concr. Res.* **2002**, *32*, 593–599. [[CrossRef](#)]
97. Nachbaur, L.; Mutin, J.C.; Nonat, A.; Choplin, L. Dynamic mode rheology of cement and tricalcium silicate pastes from mixing to setting. *Cem. Concr. Res.* **2001**, *31*, 183–192. [[CrossRef](#)]
98. Schultz, M.A.; Struble, L.J. Use of oscillatory shear to study flow behavior of fresh cement paste. *Cem. Concr. Res.* **1993**, *23*, 273–282. [[CrossRef](#)]
99. Perrot, A.; Lecompte, T.; Khelifi, H.; Brumaud, C.; Hot, J.; Roussel, N. Yield stress and bleeding of fresh cement pastes. *Cem. Concr. Res.* **2012**, *42*, 937–944. [[CrossRef](#)]
100. Assaad, J.J.; Harb, J.; Maalouf, Y. Effect of vane configuration on yield stress measurements of cement pastes. *J. Non-Newton. Fluid Mech.* **2016**, *230*, 31–42. [[CrossRef](#)]
101. Qian, Y.; Kawashima, S. Distinguishing dynamic and static yield stress of fresh cement mortars through thixotropy. *Cem. Concr. Res.* **2018**, *86*, 288–296. [[CrossRef](#)]
102. Michaux, M.; Defosse, C. Oil well cement slurries I. Microstructural approach of their rheology. *Cem. Concr. Res.* **1986**, *16*, 23–30. [[CrossRef](#)]
103. Vance, K.; Kumar, A.; Sant, G.; Neithalath, N. The rheological properties of ternary binders containing Portland cement, limestone, and metakaolin or fly ash. *Cem. Concr. Res.* **2013**, *52*, 196–207. [[CrossRef](#)]
104. Struble, L.; Sun, G.-K. Viscosity of Portland cement paste as a function of concentration. *Adv. Cem. Based Mater.* **1995**, *2*, 62–69. [[CrossRef](#)]
105. Legrand, C. Rheologie Des Melanges De Ciment Ou De Sable et d’eau. *Rev. Mater Constr. Trav. Publics Cim. Beton* **1970**.
106. Kurdowski, W. *Cement and Concrete Chemistry*; Springer Science & Business: Berlin/Heidelberg, Germany, 2014; ISBN 94-007-7945-3.
107. Sybertz, F.; Reick, P. Effect of fly as on the rheological properties of cement paste. *Rheol. Fresh Cem. Concr.* **1991**, 13–22.
108. Zhou, Z.; Solomon, M.J.; Scales, P.J.; Boger, D.V. The yield stress of concentrated flocculated suspensions of size distributed particles. *J. Rheol.* **1999**, *43*, 651–671. [[CrossRef](#)]
109. Flatt, R.J.; Bowen, P. Yield Stress of Multimodal Powder Suspensions: An Extension of the YODEL (Yield Stress mODEL). *J. Am. Ceram. Soc.* **2007**, *90*, 1038–1044. [[CrossRef](#)]
110. Hamaker, H.C. The London—van der Waals attraction between spherical particles. *Physica* **1937**, *4*, 1058–1072. [[CrossRef](#)]
111. Flatt, R.J.; Bowen, P. Yodel: A Yield Stress Model for Suspensions. *J. Am. Ceram. Soc.* **2006**, *89*, 1244–1256. [[CrossRef](#)]
112. Ma, S.; Kawashima, S. A rheological approach to study the early-age hydration of oil well cement: Effect of temperature, pressure and nanoclay. *Constr. Build. Mater.* **2019**, *215*, 119–127. [[CrossRef](#)]
113. Chateau, X.; Ovarlez, G.; Trung, K.L. Homogenization approach to the behavior of suspensions of noncolloidal particles in yield stress fluids. *J. Rheol.* **2008**, *52*, 489–506. [[CrossRef](#)]
114. Chougnet, A.; Palermo, T.; Audibert, A.; Moan, M. Rheological behaviour of cement and silica suspensions: Particle aggregation modelling. *Cem. Concr. Res.* **2008**, *38*, 1297–1301. [[CrossRef](#)]
115. Ivanov, Y.P.; Roshavelov, T.T. The effect of condensed silica fume on the rheological behaviour of cement pastes. In *Rheology of Fresh Cement and Concrete: Proceedings of an International Conference, Liverpool, 1990*; CRC Press: Boca Raton, FL, USA, 1990; pp. 23–26.

116. Rosquoët, F.; Alexis, A.; Khelidj, A.; Phelipot, A. Experimental study of cement grout. *Cem. Concr. Res.* **2003**, *33*, 713–722. [[CrossRef](#)]
117. Lobanov, V.P. The visco-plastic properties of building mortars. *Kolloidn. Zhurnal* **1950**, *12*, 352–358.
118. Bombled, J.P. Influence of sulphates on the rheological behaviour of cement pastes and their evolution. In *Proceedings of the 7th International Congress on the Chemistry of Cement: Paris*; Cement Research Institute of India: New Delhi, India, 1980; pp. 164–169.
119. Roy, D.M.; Asaga, K. Rheological properties of cement mixes: V. The effects of time on viscometric properties of mixes containing superplasticizers; conclusions. *Cem. Concr. Res.* **1980**, *10*, 387–394. [[CrossRef](#)]
120. Ivanov, Y.; Stanoeva, E. Influence of cement composition and other factors on the rheological behavior of cement pastes. *Silic. Ind.* **1979**, *44*, 199–203.
121. Ivanov, Y.; Zacharieva, S. Influence of fly ash on the rheology of cement pastes. In *Proceedings of the 7th International Congress on the Chemistry of Cement: Paris*; Cement Research Institute of India: New Delhi, India, 1980; pp. 103–107.
122. Chen, X.; Wu, S.; Zhou, J. Experimental and modeling study of dynamic mechanical properties of cement paste, mortar and concrete. *Constr. Build. Mater.* **2013**, *47*, 419–430. [[CrossRef](#)]
123. Massoudi, M.; Wang, P. Slag behavior in gasifiers. Part II: Constitutive modeling of slag. *Energies* **2013**, *6*, 807–838. [[CrossRef](#)]
124. Fredrickson, A.G. *Principles and Applications of Rheology*; Prentice-Hall: Upper Saddle River, NJ, USA, 1964.
125. White, F.M. *Fluid Mechanics fourth edition*; McGraw and Hill: Singapore, 1994.
126. Einstein, A. Eine neue bestimmung der moleküldimensionen. *Ann. Der Phys.* **1906**, *324*, 289–306. [[CrossRef](#)]
127. Roussel, N.; Lemaître, A.; Flatt, R.J.; Coussot, P. Steady state flow of cement suspensions: A micromechanical state of the art. *Cem. Concr. Res.* **2010**, *40*, 77–84. [[CrossRef](#)]
128. Roscoe, R. The viscosity of suspensions of rigid spheres. *Br. J. Appl. Phys.* **1952**, *3*, 267. [[CrossRef](#)]
129. Mooney, M. The viscosity of a concentrated suspension of spherical particles. *J. Colloid Sci.* **1951**, *6*, 162–170. [[CrossRef](#)]
130. Krieger, I.M.; Dougherty, T.J. A mechanism for non-Newtonian flow in suspensions of rigid spheres. *Trans. Soc. Rheol.* **1959**, *3*, 137–152. [[CrossRef](#)]
131. Struble, L.; Szecsy, R.; Lei, W.-G.; Sun, G.-K. Rheology of cement paste and concrete. *Cem. Concr. Aggreg.* **1998**, *20*, 269–277.
132. Mansoutre, S.; Colombet, P.; Damme, H.V. Water retention and granular rheological behavior of fresh C3S paste as a function of concentration. *Cem. Concr. Res.* **1999**, *29*, 1441–1453.
133. Justnes, H.; Vikan, H. Viscosity of cement slurries as a function of solids content. *Ann. Trans. Nordic Rheol. Soc.* **2005**, *13*, 75–82.
134. Bonen, D.; Shah, S.P. Fresh and hardened properties of self-consolidating concrete. *Prog. Struct. Eng. Mater.* **2005**, *7*, 14–26. [[CrossRef](#)]
135. Hendrickx, R.; Rezeau, M.; Van Balen, K.; Van Gemert, D. Mortar and paste rheology: Concentration, polydispersity and air entrapment at high solid fraction. *Appl. Rheol.* **2009**, *19*. [[CrossRef](#)]
136. Tregger, N.A.; Pakula, M.E.; Shah, S.P. Influence of clays on the rheology of cement pastes. *Cem. Concr. Res.* **2010**, *40*, 384–391. [[CrossRef](#)]
137. Bentz, D.P.; Ferraris, C.F.; Galler, M.A.; Hansen, A.S.; Guynn, J.M. Influence of particle size distributions on yield stress and viscosity of cement–fly ash pastes. *Cem. Concr. Res.* **2012**, *42*, 404–409. [[CrossRef](#)]
138. Ouyang, J.; Tan, Y. Rheology of fresh cement asphalt emulsion pastes. *Constr. Build. Mater.* **2015**, *80*, 236–243. [[CrossRef](#)]
139. O’Neill, R.; McCarthy, H.O.; Montufar, E.B.; Ginebra, M.-P.; Wilson, D.I.; Lennon, A.; Dunne, N. Critical review: Injectability of calcium phosphate pastes and cements. *Acta Biomater.* **2017**, *50*, 1–19. [[CrossRef](#)]
140. Chen, C.-T.; Lin, C.-W. Stiffening Behaviors of Cement Pastes Measured by a Vibrational Viscometer. *Adv. Civ. Eng. Mater.* **2017**, *6*, 20160061. [[CrossRef](#)]
141. Murata, J.; Kikukawa, H. Studies on rheological analysis of fresh concrete. In *Proceedings of the RILEM Seminar: Fresh Concrete*; RILEM: Paris, France, 1973.
142. Mills, P. Non-Newtonian behaviour of flocculated suspensions. *J. De Phys. Lett.* **1985**, *46*, 301–309. [[CrossRef](#)]
143. Liu, D.-M. Particle packing and rheological property of highly-concentrated ceramic suspensions: ϕ_m determination and viscosity prediction. *J. Mater. Sci.* **2000**, *35*, 5503–5507. [[CrossRef](#)]

144. Chong, J.S.; Christiansen, E.B.; Baer, A.D. Rheology of concentrated suspensions. *J. Appl. Polym. Sci.* **1971**, *15*, 2007–2021. [[CrossRef](#)]
145. Aiad, I.; El-Sabbagh, A.M.; Adawy, A.I.; Shafek, S.H.; Abo-EL-Enein, S.A. Effect of some prepared superplasticizers on the rheological properties of oil well cement slurries. *Egypt. J. Pet.* **2018**, *27*, 1061–1066. [[CrossRef](#)]
146. Vipulanandan, C.; Mohammed, A. Smart cement rheological and piezoresistive behavior for oil well applications. *J. Pet. Sci. Eng.* **2015**, *135*, 50–58. [[CrossRef](#)]
147. Kim, J.H.; Kwon, S.H.; Kawashima, S.; Yim, H.J. Rheology of cement paste under high pressure. *Cem. Concr. Compos.* **2017**, *77*, 60–67. [[CrossRef](#)]
148. Ravi, K.M.; Sutton, D.L. New rheological correlation for cement slurries as a function of temperature. In Proceedings of the SPE Annual Technical Conference and Exhibition, New Orleans, LA, USA, 23–26 September 1990.
149. Sercombe, J.; Hellmich, C.; Ulm, F.-J.; Mang, H. Modeling of Early-Age Creep of Shotcrete. I: Model and Model Parameters. *J. Eng. Mech.* **2000**, *126*, 284–291. [[CrossRef](#)]
150. Bazant, Z.P. Creep and damage in concrete. *Mater. Sci. Concr. IV* **1995**, 355–389. Available online: http://cee.northwestern.edu/people/bazant/PDFs/Papers%20-%20Backup%202_20_2013/331.pdf (accessed on 23 January 2020).
151. Ulm, F.-J.; Coussy, O. Strength growth as chemo-plastic hardening in early age concrete. *J. Eng. Mech.* **1996**, *122*, 1123–1132. [[CrossRef](#)]
152. Avrami, M. Kinetics of phase change. I General theory. *J. Chem. Phys.* **1939**, *7*, 1103–1112. [[CrossRef](#)]
153. Pang, X.; Meyer, C.; Darbe, R.; Funkhouser, G.P. Modeling the effect of curing temperature and pressure on cement hydration kinetics. *ACI Mater. J.* **2013**, *110*, 137.
154. Wu, D.; Cai, S.; Huang, G. Coupled effect of cement hydration and temperature on rheological properties of fresh cemented tailings backfill slurry. *Trans. Nonferrous Metals Soc. China* **2014**, *24*, 2954–2963. [[CrossRef](#)]
155. Wu, D.; Fall, M.; Cai, S.J. Coupling temperature, cement hydration and rheological behaviour of fresh cemented paste backfill. *Miner. Eng.* **2013**, *42*, 76–87. [[CrossRef](#)]
156. Papo, A.; Caufin, B. A study of the hydration process of cement pastes by means of oscillatory rheological techniques. *Cem. Concr. Res.* **1991**, *21*, 1111–1117. [[CrossRef](#)]
157. Aïtcin, P.-C. Cements of yesterday and today: Concrete of tomorrow. *Cem. Concr. Res.* **2000**, *30*, 1349–1359. [[CrossRef](#)]
158. Jayasree, C.; Murali Krishnan, J.; Gettu, R. Influence of superplasticizer on the non-Newtonian characteristics of cement paste. *Mater. Struct.* **2011**, *44*, 929–942. [[CrossRef](#)]
159. Ma, G.; Wang, L. A critical review of preparation design and workability measurement of concrete material for largescale 3D printing. *Front. Struct. Civ. Eng.* **2018**, *12*, 382–400. [[CrossRef](#)]
160. Bellotto, M. Cement paste prior to setting: A rheological approach. *Cem. Concr. Res.* **2013**, *52*, 161–168. [[CrossRef](#)]
161. Mikanovic, N.; Jolicoeur, C. Influence of superplasticizers on the rheology and stability of limestone and cement pastes. *Cem. Concr. Res.* **2008**, *38*, 907–919. [[CrossRef](#)]
162. Daukšys, M.; Skripkiūnas, G.; Janavičius, E. Complex influence of plasticizing admixtures and sodium silicate solution on rheological properties of Portland cement paste. *Mater. Sci.* **2009**, *15*, 349–355.
163. Rehman, S.K.U.; Ibrahim, Z.; Jameel, M.; Memon, S.A.; Javed, M.F.; Aslam, M.; Mehmood, K.; Nazar, S. Assessment of Rheological and Piezoresistive Properties of Graphene based Cement Composites. *Int. J. Concr. Struct. Mater.* **2018**, *12*, 64. [[CrossRef](#)]
164. Sanfelix, S.G.; Santacruz, I.; Szczotok, A.M.; Belloc, L.M.O.; De la Torre, A.G.; Kjøniksen, A.-L. Effect of microencapsulated phase change materials on the flow behavior of cement composites. *Constr. Build. Mater.* **2019**, *202*, 353–362. [[CrossRef](#)]
165. Khayat, K.H.; Yahia, A. Effect of welan gum-high-range water reducer combinations on rheology of cement grout. *Mater. J.* **1997**, *94*, 365–372.
166. Cyr, M.; Legrand, C.; Mouret, M. Study of the shear thickening effect of superplasticizers on the rheological behaviour of cement pastes containing or not mineral additives. *Cem. Concr. Res.* **2000**, *30*, 1477–1483. [[CrossRef](#)]
167. Nehdi, M.; Mindess, S.; Aïtcin, P.-C. Rheology of High-Performance Concrete: Effect of Ultrafine Particles. *Cem. Concr. Res.* **1998**, *28*, 687–697. [[CrossRef](#)]

168. Gołaszewski, J.; Szwabowski, J. Influence of superplasticizers on rheological behaviour of fresh cement mortars. *Cem. Concr. Res.* **2004**, *34*, 235–248. [[CrossRef](#)]
169. Aiad, I. Influence of time addition of superplasticizers on the rheological properties of fresh cement pastes. *Cem. Concr. Res.* **2003**, *33*, 1229–1234. [[CrossRef](#)]
170. Puertas, F.; Santos, H.; Palacios, M.; Martinez-Ramirez, S. Polycarboxylate superplasticiser admixtures: Effect on hydration, microstructure and rheological behaviour in cement pastes. *Adv. Cem. Res.* **2005**, *17*, 77–89. [[CrossRef](#)]
171. Zingg, A.; Winnefeld, F.; Holzer, L.; Pakusch, J.; Becker, S.; Gauckler, L. Adsorption of polyelectrolytes and its influence on the rheology, zeta potential, and microstructure of various cement and hydrate phases. *J. Colloid Interface Sci.* **2008**, *323*, 301–312. [[CrossRef](#)]
172. Wong, H.H.C.; Kwan, A.K.H. Rheology of Cement Paste: Role of Excess Water to Solid Surface Area Ratio. *J. Mater. Civ. Eng.* **2008**, *20*, 189–197. [[CrossRef](#)]
173. Abbas, G.; Irawan, S.; Kumar, S.; Memon, R.K.; Khalwar, S.A. Characteristics of Oil Well Cement Slurry using Hydroxypropylmethylcellulose. *J. Appl. Sci.* **2014**, *14*, 1154–1160. [[CrossRef](#)]
174. Zhang, X.; Han, J. The effect of ultra-fine admixture on the rheological property of cement paste. *Cem. Concr. Res.* **2000**, *30*, 827–830. [[CrossRef](#)]
175. Park, C.K.; Noh, M.H.; Park, T.H. Rheological properties of cementitious materials containing mineral admixtures. *Cem. Concr. Res.* **2005**, *35*, 842–849. [[CrossRef](#)]
176. Vikan, H.; Justnes, H. Rheology of cementitious paste with silica fume or limestone. *Cem. Concr. Res.* **2007**, *37*, 1512–1517. [[CrossRef](#)]
177. Stryczek, S.; Brylicki, W.; Małolepszy, J.; Gonet, A.; Wiśniowski, R.; Kotwica, Ł. Potential use of fly ash from fluidal combustion of brown coal in cementing slurries for drilling and geotechnical works. *Arch. Min. Sci.* **2009**, *54*, 775–786.
178. Baldino, N.; Gabriele, D.; Lupi, F.R.; Seta, L.; Zinno, R. Rheological behaviour of fresh cement pastes: Influence of synthetic zeolites, limestone and silica fume. *Cem. Concr. Res.* **2014**, *63*, 38–45. [[CrossRef](#)]
179. Li, D.; Wang, D.; Ren, C.; Rui, Y. Investigation of rheological properties of fresh cement paste containing ultrafine circulating fluidized bed fly ash. *Constr. Build. Mater.* **2018**, *188*, 1007–1013. [[CrossRef](#)]
180. Burroughs, J.F.; Weiss, J.; Haddock, J.E. Influence of high volumes of silica fume on the rheological behavior of oil well cement pastes. *Constr. Build. Mater.* **2019**, *203*, 401–407. [[CrossRef](#)]
181. Laskar, A.I.; Talukdar, S. Rheological behavior of high performance concrete with mineral admixtures and their blending. *Constr. Build. Mater.* **2008**, *22*, 2345–2354. [[CrossRef](#)]
182. Provis, J.L.; Duxson, P.; van Deventer, J.S.J. The role of particle technology in developing sustainable construction materials. *Adv. Powder Technol.* **2010**, *21*, 2–7. [[CrossRef](#)]
183. Hou, J.; Liu, Z. Synthesizing Dispersant for MTC Design and Its Effect on Slurry Rheology. *SPE Drill. Complet.* **2000**, *15*, 31–36. [[CrossRef](#)]
184. Nehdi, M. Why some carbonate fillers cause rapid increases of viscosity in dispersed cement-based materials. *Cem. Concr. Res.* **2000**, *30*, 1663–1669. [[CrossRef](#)]
185. Hodne, H.; Saasen, A.; Strand, S. Rheological properties of high temperature oil well cement slurries. *Annu. Trans. Nordi. Rheol. Soc.* **2001**, *8*, 31–38.
186. Kaufmann, J.; Winnefeld, F.; Hesselbarth, D. Effect of the addition of ultrafine cement and short fiber reinforcement on shrinkage, rheological and mechanical properties of Portland cement pastes. *Cem. Concr. Compos.* **2004**, *26*, 541–549. [[CrossRef](#)]
187. Sonebi, M.; Svermova, L.; Bartos, P.J.M. Factorial Design of Cement Slurries Containing Limestone Powder for Self-Consolidating Slurry-Infiltrated Fiber Concrete. *ACI Mater. J.* **2004**, *101*, 136–145.
188. Senff, L.; Hotza, D.; Lucas, S.; Ferreira, V.M.; Labrincha, J.A. Effect of nano-SiO₂ and nano-TiO₂ addition on the rheological behavior and the hardened properties of cement mortars. *Mater. Sci. Eng. A* **2012**, *532*, 354–361. [[CrossRef](#)]
189. Soltanian, H.; Khalokakaie, R.; Ataei, M.; Kazemzadeh, E. Fe₂O₃ nanoparticles improve the physical properties of heavy-weight wellbore cements: A laboratory study. *J. Nat. Gas Sci. Eng.* **2015**, *26*, 695–701. [[CrossRef](#)]
190. Sun, X.; Wu, Q.; Lee, S.; Qing, Y.; Wu, Y. Cellulose Nanofibers as a Modifier for Rheology, Curing and Mechanical Performance of Oil Well Cement. *Sci. Rep.* **2016**, *6*, 31654. [[CrossRef](#)]

191. Tang, Z.; Huang, R.; Mei, C.; Sun, X.; Zhou, D.; Zhang, X.; Wu, Q. Influence of Cellulose Nanoparticles on Rheological Behavior of Oil Well Cement-Water Slurries. *Materials* **2019**, *12*, 291. [[CrossRef](#)]
192. Colombo, A.; Geiker, M.R.; Justnes, H.; Lauten, R.A.; De Weerd, K. On the effect of calcium lignosulfonate on the rheology and setting time of cement paste. *Cem. Concr. Res.* **2017**, *100*, 435–444. [[CrossRef](#)]
193. Senff, L.; Labrincha, J.A.; Ferreira, V.M.; Hotza, D.; Repette, W.L. Effect of nano-silica on rheology and fresh properties of cement pastes and mortars. *Constr. Build. Mater.* **2009**, *23*, 2487–2491. [[CrossRef](#)]
194. Quercia, G.; Brouwers, H.J.H.; Garnier, A.; Luke, K. Influence of olivine nano-silica on hydration and performance of oil-well cement slurries. *Mater. Des.* **2016**, *96*, 162–170. [[CrossRef](#)]
195. Wang, W.; Taleghani, A.D. Three-dimensional analysis of cement sheath integrity around Wellbores. *J. Pet. Sci. Eng.* **2014**, *121*, 38–51. [[CrossRef](#)]
196. Phan, T.H.; Chaouche, M.; Moranville, M. Influence of organic admixtures on the rheological behaviour of cement pastes. *Cem. Concr. Res.* **2006**, *36*, 1807–1813. [[CrossRef](#)]
197. Emoto, T.; Bier, T.A. Rheological behavior as influenced by plasticizers and hydration kinetics. *Cem. Concr. Res.* **2007**, *37*, 647–654. [[CrossRef](#)]
198. Lu, H.; Xie, C.; Gao, Y.; Li, L.; Zhu, H. Cement Slurries with Rheological Properties Unaffected by Temperature. *SPE Drill. Complet.* **2016**, *30*, 316–321. [[CrossRef](#)]
199. Velayati, A.; Soltanian, H.; Pourmazaheri, Y.; Aghajafari, A.H.; Kazemzadeh, E.; Barati, P. Investigation of Cassia fistula fruit dry extract effect on the oil and gas well cement properties. *J. Nat. Gas Sci. Eng.* **2016**, *36*, 298–304. [[CrossRef](#)]
200. Wang, C.; Chen, X.; Wang, R. Do chlorides qualify as accelerators for the cement of deepwater oil wells at low temperature? *Constr. Build. Mater.* **2017**, *133*, 482–494. [[CrossRef](#)]
201. Tao, C.; Watts, B.; Ferraro, C.C.; Masters, F.J. A Multivariate Computational Framework to Characterize and Rate Virtual Portland Cements. *Comput. Aided Civ. Infrastruct. Eng.* **2019**, *34*, 266–278. [[CrossRef](#)]
202. Tao, C. Optimization of Cement Production and Hydration for Improved Performance, Energy Conservation, and Cost. Ph.D. Dissertation, University of Florida, Gainesville, FL, USA, 2017.
203. Stryczek, S.; Wiśniowski, R.; Gonet, A.; Złotkowski, A.; Ziaja, J. Influence of Polycarboxylate Superplasticizers on Rheological Properties of Cement Slurries Used in Drilling Technologies/Wpływ Superplastyfikatorów Z Grupy Polikarboksylianów Na Właściwości Reologiczne Zaczynów Cementowych Stosowanych W Technologiach Wiertniczych. *Arch. Min. Sci.* **2013**, *58*, 719–728.
204. Massidda, L.; Sanna, U. *Rheological Behaviour of Portland Cement Pastes Containing Fly Ash*; Il Cemento: Milano, Roma, 1982.
205. Yang, M.; Jennings, H.M. Influences of mixing methods on the microstructure and rheological behavior of cement paste. *Adv. Cem. Based Mater.* **1995**, *2*, 70–78. [[CrossRef](#)]
206. Williams, D.A.; Saak, A.W.; Jennings, H.M. The influence of mixing on the rheology of fresh cement paste. *Cem. Concr. Res.* **1999**, *29*, 1491–1496. [[CrossRef](#)]
207. Orban, J.; Parcevaux, P.; Guillot, D. Influence of shear history on the rheological properties of oil well cement slurries. In Proceedings of the 8th International Congress on the Chemistry of Cement, Rio de Janeiro, Brazil, 22–27 September 1986; Volume 6, pp. 243–247.
208. Saleh, F.K.; Salehi, S.; Teodoriu, C. Experimental investigation of mixing energy of well cements: The gap between laboratory and field mixing. *J. Nat. Gas Sci. Eng.* **2019**, *63*, 47–57. [[CrossRef](#)]
209. Han, D.; Ferron, R.D. Effect of mixing method on microstructure and rheology of cement paste. *Constr. Build. Mater.* **2015**, *93*, 278–288. [[CrossRef](#)]
210. Saleh, F.K.; Teodoriu, C. The mechanism of mixing and mixing energy for oil and gas wells cement slurries: A literature review and benchmarking of the findings. *J. Nat. Gas Sci. Eng.* **2017**, *38*, 388–401. [[CrossRef](#)]
211. Mannheimer, R.J. Laminar and turbulent flow of cement slurries in large diameter pipe: A comparison with laboratory viscometers. *J. Rheol.* **1991**, *35*, 113–133. [[CrossRef](#)]
212. Saak, A.W.; Jennings, H.M.; Shah, S.P. The influence of wall slip on yield stress and viscoelastic measurements of cement paste. *Cem. Concr. Res.* **2001**, *31*, 205–212. [[CrossRef](#)]
213. Bannister, C.E. Rheological evaluation of cement slurries: Methods and models. In Proceedings of the SPE Annual Technical Conference and Exhibition, Dallas, TX, USA, 21–24 September 1980.
214. Roussel, N. Steady and transient flow behaviour of fresh cement pastes. *Cem. Concr. Res.* **2005**, *35*, 1656–1664. [[CrossRef](#)]
215. Mewis, J. Thixotropy—a general review. *J. Non-Newton. Fluid Mech.* **1979**, *6*, 1–20. [[CrossRef](#)]

216. Barnes, H.A. Thixotropy—A review. *J. Non-Newton. Fluid Mech.* **1997**, *70*, 1–33. [[CrossRef](#)]
217. Freundlich, H. *Thixotropy*; Hermann & Cie: Paris, France, 1935; Volume 1.
218. Barnes, H.A.; Hutton, J.F.; Walters, K. *An Introduction to Rheology*; Elsevier: Edinburgh, London, UK, 1989; ISBN 0-08-093369-6.
219. Hartley, G.S. Negative thixotropy. *Nature* **1938**, *142*, 161. [[CrossRef](#)]
220. Renardy, M.; Wang, X. Boundary layers for the upper convected Maxwell fluid. *J. Non-Newton. Fluid Mech.* **2012**, *189*, 14–18. [[CrossRef](#)]
221. Renardy, M.; Renardy, Y. Thixotropy in yield stress fluids as a limit of viscoelasticity. *IMA J. Appl. Math.* **2016**, *81*, 522–537. [[CrossRef](#)]
222. Larson, R.G. A constitutive equation for polymer melts based on partially extending strand convection. *J. Rheol.* **1984**, *28*, 545–571. [[CrossRef](#)]
223. Fredrickson, A.G. A model for the thixotropy of suspensions. *AIChE J.* **1970**, *16*, 436–441. [[CrossRef](#)]
224. Renardy, M. The mathematics of myth: Yield stress behavior as a limit of non-monotone constitutive theories. *J. Non-Newton. Fluid Mech.* **2010**, *165*, 519–526. [[CrossRef](#)]
225. de Souza Mendes, P.R.; Thompson, R.L. A unified approach to model elasto-viscoplastic thixotropic yield-stress materials and apparent yield-stress fluids. *Rheol. Acta* **2013**, *52*, 673–694. [[CrossRef](#)]
226. de Souza Mendes, P.R. Thixotropic elasto-viscoplastic model for structured fluids. *Soft Matter* **2011**, *7*, 2471–2483. [[CrossRef](#)]
227. Chappuis, J. Rheological measurements with cement pastes in viscometers: A comprehensive approach. In *Proceedings of Fresh Cement and Concrete*; Taylor & Francis: London, UK, 1990; pp. 3–12.
228. Al Ghanami, R.C.; Saunders, B.R.; Bosquillon, C.; Shakesheff, K.M.; Alexander, C. Responsive particulate dispersions for reversible building and deconstruction of 3D cell environments. *Soft Matter* **2010**, *6*, 5037–5044. [[CrossRef](#)]
229. Sant, G.; Ferraris, C.F.; Weiss, J. Rheological properties of cement pastes: A discussion of structure formation and mechanical property development. *Cem. Concr. Res.* **2008**, *38*, 1286–1296. [[CrossRef](#)]
230. Tsenoglou, C. Scaling concepts in suspension rheology. *J. Rheol.* **1990**, *34*, 15–24. [[CrossRef](#)]
231. Usui, H. A thixotropy model for coal-water mixtures. *J. Non-Newton. Fluid Mech.* **1995**, *60*, 259–275. [[CrossRef](#)]
232. Potanin, A.A.; De Rooij, R.; Van den Ende, D.; Mellema, J. Microrheological modeling of weakly aggregated dispersions. *J. Chem. Phys.* **1995**, *102*, 5845–5853. [[CrossRef](#)]
233. Quemada, D. Rheological modelling of complex fluids: IV: Thixotropic and “thixoelastic” behaviour. Start-up and stress relaxation, creep tests and hysteresis cycles. *Eur. Phys. J. Appl. Phys.* **1999**, *5*, 191–207. [[CrossRef](#)]
234. Feys, D.; Asghari, A. Influence of maximum applied shear rate on the measured rheological properties of flowable cement pastes. *Cem. Concr. Res.* **2019**, *117*, 69–81. [[CrossRef](#)]
235. Cheng, D.C.; Evans, F. Phenomenological characterization of the rheological behaviour of inelastic reversible thixotropic and antithixotropic fluids. *B. J. Appl. Phys.* **1965**, *16*, 1599. [[CrossRef](#)]
236. Legrand, C. Contribution à l’étude de la rhéologie du béton frais. *Mater. Constr.* **1972**, *5*, 275–295. [[CrossRef](#)]
237. Hattori, K.; Izumi, K. A rheological expression of coagulation rate theory. *J. Dispers. Sci. Technol.* **1982**, *3*, 129–145. [[CrossRef](#)]
238. Roussel, N. A thixotropy model for fresh fluid concretes: Theory, validation and applications. *Cem. Concr. Res.* **2006**, *36*, 1797–1806. [[CrossRef](#)]
239. Roussel, N. Rheology of fresh concrete: From measurements to predictions of casting processes. *Mater. Struct.* **2007**, *40*, 1001–1012. [[CrossRef](#)]
240. Mewis, J.; Wagner, N.J. *Colloidal Suspension Rheology*; Cambridge University Press: Cambridge, UK, 2012; ISBN 0-521-51599-8.
241. de Souza Mendes, P.R. Modeling the thixotropic behavior of structured fluids. *J. Non-Newton. Fluid Mech.* **2009**, *164*, 66–75. [[CrossRef](#)]
242. Truesdell, C.; Noll, W. *The Non-linear Field Theories of Mechanics*; Springer: Berlin, Germany, 1992.
243. Reynolds, O. LVII. On the dilatancy of media composed of rigid particles in contact. With experimental illustrations. *Lond. Edinb. Dublin Philos. Mag. J. Sci.* **1885**, *20*, 469–481. [[CrossRef](#)]
244. Reynolds, O. IV. On the theory of lubrication and its application to Mr. Beauchamp tower’s experiments, including an experimental determination of the viscosity of olive oil. *Philos. Trans. Royal Soc. Lond.* **1886**, *1*, 157–234.

245. Massoudi, M.; Mehrabadi, M.M. A continuum model for granular materials: Considering dilatancy and the Mohr-Coulomb criterion. *Acta Mech.* **2001**, *152*, 121–138. [[CrossRef](#)]
246. Reiner, M. A mathematical theory of dilatancy. *Am. J. Math.* **1945**, *67*, 350–362. [[CrossRef](#)]
247. Massoudi, M. A generalization of Reiner's mathematical model for wet sand. *Mech. Res. Commun.* **2011**, *38*, 378–381. [[CrossRef](#)]
248. Man, C.-S. Nonsteady channel flow of ice as a modified second-order fluid with power-law viscosity. *Arch. Ration. Mech. Anal.* **1992**, *119*, 35–57. [[CrossRef](#)]
249. Man, C.-S.; Sun, Q.-X. On the significance of normal stress effects in the flow of glaciers. *J. Glaciol.* **1987**, *33*, 268–273. [[CrossRef](#)]
250. Gupta, G.; Massoudi, M. Flow of a generalized second grade fluid between heated plates. *Acta Mech.* **1993**, *99*, 21–33. [[CrossRef](#)]
251. Massoudi, M. Heat transfer in complex fluids. In *Two Phase Flow, Phase Change and Numerical Modeling*; No. NETL-PUB-234; National Energy Technology Lab (NETL): Pittsburgh, PA, USA; In-house Research; Morgantown, WV, USA, 2012.
252. Wu, W.-T.; Aubry, N.; Massoudi, M.; Kim, J.; Antaki, J.F. A numerical study of blood flow using mixture theory. *Int. J. Eng. Sci.* **2014**, *76*, 56–72. [[CrossRef](#)] [[PubMed](#)]
253. Miao, L.; Massoudi, M. Heat transfer analysis and flow of a slag-type fluid: Effects of variable thermal conductivity and viscosity. *Int. J. Non-Linear Mech.* **2015**, *76*, 8–19. [[CrossRef](#)]
254. Wu, W.-T.; Aubry, N.; Antaki, J.F.; Massoudi, M. Normal stress effects in the gravity driven flow of granular materials. *Int. J. Non-Linear Mech.* **2017**, *92*, 84–91. [[CrossRef](#)]
255. Wu, W.-T.; Aubry, N.; Antaki, J.; Massoudi, M. Flow of a Dense Suspension Modeled as a Modified Second Grade Fluid. *Fluids* **2018**, *3*, 55. [[CrossRef](#)]
256. Dunn, J.E.; Fosdick, R.L. Thermodynamics, stability, and boundedness of fluids of complexity 2 and fluids of second grade. *Arch. Ration. Mech. Anal.* **1974**, *56*, 191–252. [[CrossRef](#)]
257. Tao, C.; Rosenbaum, E.; Kutchko, B.G.; Massoudi, M. *Effects of Shear-rate Dependent Viscosity on the Flow of A Cement Slurry*; NETL-PUB-22169; National Energy Technology Lab (NETL): Pittsburgh, PA, USA, 2018.
258. Hanehara, S.; Yamada, K. Interaction between cement and chemical admixture from the point of cement hydration, absorption behaviour of admixture, and paste rheology. *Cem. Concr. Res.* **1999**, *29*, 1159–1165. [[CrossRef](#)]
259. Stutzman, P. Scanning electron microscopy imaging of hydraulic cement microstructure. *Cem. Concr. Compos.* **2004**, *26*, 957–966. [[CrossRef](#)]
260. Gebauer, J.; Kristmann, M. The influence of the composition of industrial clinker on cement and concrete properties. *World Cem. Technol.* **1979**, *10*, 46–51.
261. Powers, T.C. Structure and physical properties of hardened Portland cement paste. *J. Am. Ceram. Soc.* **1958**, *41*, 1–6. [[CrossRef](#)]
262. Slattery, J.C. *Advanced Transport Phenomena*; Cambridge University Press: Cambridge, UK, 1999; ISBN 1-316-58390-2.
263. Probstein, R.F. *Physicochemical Hydrodynamics: An Introduction*; John Wiley & Sons: Hoboken, NJ, USA, 2005; ISBN 0-471-72512-9.
264. Liu, I.-S. *Continuum Mechanics*; Springer Science & Business Media: Berlin/Heidelberg, Germany, 2013; ISBN 3-662-05056-0.
265. Ziegler, H. *An introduction to Thermomechanics*; Elsevier: Amsterdam, The Netherlands, 2012; Volume 21, ISBN 0-444-59893-6.
266. Malekmohammadi, S.; Naccache, M.F.; Frigaard, I.A.; Martinez, D.M. Buoyancy driven slump flows of non-Newtonian fluids in pipes. *J. Pet. Sci. Eng.* **2010**, *72*, 236–243. [[CrossRef](#)]
267. Aranha, P.E.; Miranda, C.R.; Magalhães, J.V.M.; Campos, G.; Martins, A.L. Dynamic Aspects Governing Cement-Plug Placement in Deepwater Wells. *SPE Drill. Complet.* **2011**, *26*, 341–351. [[CrossRef](#)]
268. Atkin, R.J.; Craine, R.E. Continuum theories of mixtures: Applications. *IMA J. Appl. Math.* **1976**, *17*, 153–207. [[CrossRef](#)]
269. Atkin, R.J.; Craine, R.E. Continuum theories of mixtures: Basic theory and historical development. *Q. J. Mech. Appl. Math.* **1976**, *29*, 209–244. [[CrossRef](#)]
270. Bowen, R.M. Theory of mixtures in continuum physics. In *Mixtures and Electromagnetic Field Theories*; Academic Press: New York, NY, USA, 1976.

271. Truesdell, C. Thermodynamics of diffusion. In *Rational Thermodynamics*; Springer: Berlin/Heidelberg, Germany, 1984; pp. 219–236.
272. Rajagopal, K.R.; Tao, L. Mechanics of mixtures. *J. Fluid Mech.* **1996**, *323*, 410.
273. Liu, L.; Fang, Z.; Qi, C.; Zhang, B.; Guo, L.; Song, K.I.-I.L. Numerical study on the pipe flow characteristics of the cemented paste backfill slurry considering hydration effects. *Powder Technol.* **2019**, *343*, 454–464. [[CrossRef](#)]
274. Rohani, B.; Wahid, M.A.; Sies, M.M.; Saqr, K.M. Comparison of Eddy Dissipation Model and Presumed Probability Density Function Model for Temperature Prediction in a Non-Premixed Turbulent Methane Flame. In *AIP Conference Proceedings*; AIP Publishing LLC: Melville, NY, USA, 2012; Volume 1440, pp. 384–391. Available online: <https://doi.org/10.1063/1.4704240> (accessed on 23 January 2020).
275. Wang, P. The model constant A of the eddy dissipation model. *Prog. Comput. Fluid Dyn. Int. J.* **2016**, *16*, 118–125. [[CrossRef](#)]
276. Wallevik, J.E. *Rheology of Particle Suspensions: Fresh Concrete, Mortar and Cement Paste with Various Types of Lignosulfonates*; Fakultet for Ingeniørvitenskap og Teknologi: Trondheim, Norway, 2003; ISBN 82-471-5566-4. Available online: <http://hdl.handle.net/11250/236410> (accessed on 23 January 2020).
277. Moyers-Gonzalez, M.A.; Frigaard, I.A. Kinematic instabilities in two-layer eccentric annular flows, part 2: Shear-thinning and yield-stress effects. *J. Eng. Math.* **2009**, *65*, 25–52. [[CrossRef](#)]
278. Manzar, M.A.; Shah, S.N. Particle Distribution and Erosion During the Flow of Newtonian and Non-Newtonian Slurries in Straight and Coiled Pipes. *Eng. Appl. Comput. Fluid Mech.* **2009**, *3*, 296–320. [[CrossRef](#)]
279. Lootens, D. Ciments et Suspensions concentrées Modèles. Écoulement, Encombrement et Flocculation. Ph.D. Dissertation, Université Pierre et Marie Curie-Paris VI, Paris, France, 2004. Available online: <https://pastel.archives-ouvertes.fr/tel-00007217/> (accessed on 23 January 2020).
280. Patankar, S. *Numerical Heat Transfer and Fluid Flow*; CRC Press: Boca Raton, FL, USA, 1980; ISBN 1-4822-3421-1.
281. Cremonesi, M.; Ferrara, L.; Frangi, A.; Perego, U. Simulation of the flow of fresh cement suspensions by a Lagrangian finite element approach. *J. Non-Newton. Fluid Mech.* **2010**, *165*, 1555–1563. [[CrossRef](#)]
282. Aranha, P.E.; Miranda, C.; Cardoso, W.; Campos, G.; Martins, A.; Gomes, F.C.; de Araujo, S.B.; Carvalho, M. A comprehensive theoretical and experimental study on fluid displacement for oilwell-cementing operations. *SPE Drill. Complet.* **2012**, *27*, 596–603. [[CrossRef](#)]
283. Bu, Y.; Li, Z.; Wan, C.; Li, H.A. Determination of optimal density difference for improving cement displacement efficiency in deviated wells. *J. Nat. Gas Sci. Eng.* **2016**, *31*, 119–128. [[CrossRef](#)]
284. Zulqarnain, M.; Tyagi, M. Development of simulations based correlations to predict the cement volume fraction in annular geometries after fluid displacements during primary cementing. *J. Pet. Sci. Eng.* **2016**, *145*, 1–10. [[CrossRef](#)]
285. Zhao, Y.; Wang, Z.; Zeng, Q.; Li, J.; Guo, X. Lattice Boltzmann simulation for steady displacement interface in cementing horizontal wells with eccentric annuli. *J. Pet. Sci. Eng.* **2016**, *145*, 213–221. [[CrossRef](#)]
286. Anglade, C.; Papon, A.; Mouret, M. Constitutive parameter identification: An application of inverse analysis to the flow of cement-based suspensions in the fresh state from synthetic data. *J. Non-Newton. Fluid Mech.* **2017**, *241*, 14–25.
287. Wu, W.; Huang, X.; Li, Y.; Fang, C.; Jiang, X. A modified LBM for non-Newtonian effect of cement paste flow in 3D printing. *Rapid Prototyp. J.* **2019**, *25*, 22–29. [[CrossRef](#)]
288. Bao, K.; Lavrov, A.; Nilsen, H.M. Numerical modeling of non-Newtonian fluid flow in fractures and porous media. *Comput. Geosci.* **2017**, *21*, 1313–1324. [[CrossRef](#)]
289. Tardy, P.M.J. A 3D model for annular displacements of wellbore completion fluids with casing movement. *J. Pet. Sci. Eng.* **2018**, *162*, 114–136. [[CrossRef](#)]
290. Tardy, P.M.J.; Bittleston, S.H. A model for annular displacements of wellbore completion fluids involving casing movement. *J. Pet. Sci. Eng.* **2015**, *126*, 105–123. [[CrossRef](#)]
291. Zhou, Y.; Wojtanowicz, A.K.; Li, X.; Miao, Y. Analysis of gas migration in Sustained-Casing-Pressure annulus by employing improved numerical model. *J. Pet. Sci. Eng.* **2018**, *169*, 58–68. [[CrossRef](#)]
292. Naccache, M.F.; Pinto, H.A.M.; Abdu, A. Flow displacement in eroded regions inside annular ducts. *J. Braz. Soc. Mech. Sci. Eng.* **2018**, *40*, 420. [[CrossRef](#)]
293. Foroushan, H.K.; Ozbayoglu, E.M.; Miska, S.Z.; Yu, M.; Gomes, P.J. On the Instability of the Cement/Fluid Interface and Fluid Mixing (includes associated erratum). *SPE Drill. Complet.* **2018**, *33*, 063–076. [[CrossRef](#)]

294. Skadsem, H.J.; Kragset, S.; Lund, B.; Ytrehus, J.D.; Taghipour, A. Annular displacement in a highly inclined irregular wellbore: Experimental and three-dimensional numerical simulations. *J. Pet. Sci. Eng.* **2019**, *172*, 998–1013. [[CrossRef](#)]
295. Murphy, E.; Lomboy, G.; Wang, K.; Sundararajan, S.; Subramaniam, S. The rheology of slurries of athermal cohesive micro-particles immersed in fluid: A computational and experimental comparison. *Chem. Eng. Sci.* **2019**, *193*, 411–420. [[CrossRef](#)]
296. Rosenbaum, E.; Massoudi, M.; Dayal, K. The Influence of Bubbles on Foamed Cement Viscosity Using an Extended Stokesian Dynamics Approach. *Fluids* **2019**, *4*, 166. [[CrossRef](#)]
297. Ohen, H.A.; Blick, E.F. Golden section search method for determining parameters in Robertson-Stiff non-Newtonian fluid model. *J. Pet. Sci. Eng.* **1990**, *4*, 309–316. [[CrossRef](#)]
298. Shahriar, A.; Nehdi, M.L. Artificial intelligence model for rheological properties of oil well cement slurries incorporating SCMs. *Adv. Cem. Res.* **2012**, *24*, 173–185. [[CrossRef](#)]
299. Shahriar, A.; Nehdi, M. Modeling Rheological Properties of Oil Well Cement Slurries Using Multiple Regression Analysis and Artificial Neural Networks. *Int. J. Mater. Sci.* **2013**, *3*, 13.
300. Shahriar, A.; Nehdi, M.L. Optimization of rheological properties of oil well cement slurries using experimental design. *Mater. Struct.* **2012**, *45*, 1403–1423. [[CrossRef](#)]
301. Bassioni, G.; Ali, M.M.; Almansoori, A.; Raudaschl-Sieber, G.; Kühn, F.E. Rapid determination of complex oil well cement properties using mathematical models. *RSC Adv.* **2017**, *7*, 5148–5157. [[CrossRef](#)]
302. el Mahdi Safhi, A.; Benzerzour, M.; Rivard, P.; Abriak, N.-E. Feasibility of using marine sediments in SCC pastes as supplementary cementitious materials. *Powder Technol.* **2019**, *344*, 730–740. [[CrossRef](#)]
303. Watts, B.; Tao, C.; Ferraro, C.; Masters, F. Proficiency analysis of VCCTL results for heat of hydration and mortar cube strength. *Constr. Build. Mater.* **2018**, *161*, 606–617. [[CrossRef](#)]
304. Ferraro, C.C.; Watts, B.; Tao, C.; Masters, F. *Advanced Analysis, Validation and Optimization of Virtual Cement and Concrete Testing*; Florida Department of Transportation: Tallahassee, FL, USA, 2017; Available online: <https://trid.trb.org/view/1569681> (accessed on 23 January 2020).



© 2020 by the authors. Licensee MDPI, Basel, Switzerland. This article is an open access article distributed under the terms and conditions of the Creative Commons Attribution (CC BY) license (<http://creativecommons.org/licenses/by/4.0/>).